THE UNIVERSITY OF MICHIGAN

COLLEGE OF ENGINEERING

DEPARTMENT OF ELECTRICAL ENGINEERING

Radiation Laboratory

1969-4-Q = RL-2041

DOPPLER RADIATION STUDY

First Interim Report to Modification No. 1
(22 December 1969 - 22 March 1970)

By
Chiao-Min Chu, Soon K. Cho and Joseph E. Ferris

May 1970

Contract N62269-68-C-0715

Technical Monitor - Mr. Edward Rickner

Prepared for:
Naval Air Development Center
Warminster, PA 18974

Ann Arbor, Michigan

FOREWORD

This report was prepared by The University of Michigan Radiation Laboratory, Department of Electrical Engineering, Ann Arbor, Michigan. This is the First Interim Report to Modification No. 1 of Contract N62269-68-C-0715, "Doppler Radiation Study," and covers the period 22 December 1969 to 22 March 1970. The research was carried out under the direction of Professor Ralph E. Hiatt, Head of the Radiation Laboratory; the Principal Investigator was Professor Chiao-Min Chu. The sponsor of this research is the U. S. Naval Air Development Center, Warminster, Pennsylvania and the Technical Monitor is Mr. Edward Rickner.

ABSTRACT

In order to extend our understanding of the reflection characteristics of the moderately rough ocean surface, the scattering cross section was computed and analyzed for various sea states with plane wave incidence. The use of the results of the cross section analysis makes it feasible, in principle, to predict qualitatively the order of the maximum reflected radiation intensity and its angular distribution for various receiving points for a given transmitting antenna pattern. The result of the cross section analysis also indicated that the assumption of the infinite conductivity for the sea water introduces errors no greater than 2 dB for the purely horizontally and vertically polarized incidences, indicating the relative fairness of the usual assumption of infinite conductivity for the sea water at 13 GHz.

TABLE OF CONTENTS

NOMENCLATURE

$a_{\ell m}, b_{\ell m}, c_{\ell m}$	Parameters associated with the polarization of the wave and the reflection coefficients of the surface.
A_o, B_o	Dimensionless parameters: The ratios of (scale length)^2 to mean-square height of a sea surface in x and y directions, respectively.
dB	Decibel.
F_{2M}	Normalized maximum reflected radiation power density per unit solid angle for a sea surface.
L_1, L_2, L_3 M_1, M_2, M_3	The parameters defined in connections with $\left[a_{\ell m} q_z - b_{\ell m} q_x - c_{\ell m} q_y\right]^2$.
q_x, q_y, z_z	The parameters associated with the phase of the radiation in x, y, and z directions
$R_\perp$, $R_{\parallel}$	Fresnel's reflection coefficients for perpendicular and parallel wave components.
U	Wind speed.
X, Y	The normalized rectangular coordinates.
α	A parameters defined as q_x/q_z .
β	A parameter defined as q_y/z_z .
θ	Latitude angle in spherical coordinates.
θ_1, θ_2	θ-coordinates of incident and reflected waves.
θ_{1M}	θ-coordinate of an incident wave for which the reflected radiation intensity is maximum.
$\sigma(\hat{\Omega}_2, \hat{\Omega}_1)$	Scattering cross section.
σ_{hh}	Scattering cross section of a horizontally polarized reflected component wave for a horizontally polarized incident wave.

σ_{vh}	Scattering cross section of a vertically polarized reflected component wave for a horizontally polarized incident wave.
σ_{hv}	Scattering cross section of a horizontally polarized reflected component wave for a vertically polarized incident wave.
σ_{vv}	Scattering cross section of a vertically polarized reflected component wave for a vertically polarized incident wave.
σ_h	Total scattering cross section for a horizontally polarized incident wave.
σ_v	Total scattering cross section for a vertically polarized incident wave.
$(\sigma_h)_c$	Total scattering cross section for a horizontally polarized incident wave when the reflecting surface is assumed to have infinite conductivity.
$(\sigma_v)_c$	Total scattering cross section for a vertically polarized incident wave when the reflecting surface is assumed to have infinite conductivity.
$(\frac{\sigma_{hh}}{\sigma_{vh}})_c$	Ratio of σ_{hh} to σ_{vh} for a reflecting surface of infinite conductivity.
ϕ	Azimuth angle in spherical coordinates.
ϕ_1, ϕ_2	ϕ-coordinates of incident and reflected waves.
ϕ_{1M}	ϕ-coordinate of the incident wave for which the reflected radiation intensity is maximum.
ψ	Wind direction.
$\hat{\Omega}_1, \hat{\Omega}_2$	Unit vectors for the directions of incident and reflected waves.

I

INTRODUCTION AND SUMMARY

In the theoretical phase of this work, a refinement was made on the physical optics model for the electromagnetic wave scattering of a moderately rough ocean surface by removing the infinite-conductivity assumption for the sea water. The results are summarized in Appendix A. Based on the refined model, an attempt has been made in Section II to show the reflection characteristics of a moderately rough ocean surface by means of the scattering cross section for several sea states. It is concluded that in the frequency range of our interest, the finite conductivity of the sea water may change the scattering cross section by as much as 2dB. For all practical purposes, the essential characteristics of the angular distribution of the scattered radiation remains the same as obtained where infinite conductivity was assumed for sea water. The maximum reflected radiation intensity and its direction of arrival were computed for various sea states and receiving points; these results are presented in Section III.

In the experimental phase of this work, a fly-by test was conducted for the low angle forward scattered radiation. The description of this test and some preliminary discussions of the findings are presented in Section IV. A detailed analysis and interpretation of the data is in progress and will be reported in the next period.

Cognizant of the inadequacies of the physical optics method for describing the scattering property near grazing angles, an effort has been made to develop a theoretical model making use of experimental results in order to find the most effective remedy for the aforementioned defect in the physical optics model. As a result of the careful considerations, it appears that the multiple scattering, rather than the surface wave approach, as we initially

anticipated, may provide a most promising method in compensating for the shortcomings of the physical optics approach. This phase of the work will be continued in the next period.

The diversity of the variation of the ground surface is in general much more extensive than that of the ocean surface and the analytical study of the reflection from the ground is proportionately more difficult to deal with. Therefore, we have limited ourselves to the kinds of ground surface which are more amenable to a theoretical analysis and will focus our attention on moderately rough terrain. For this type of surface, it seems reasonable to adopt the theoretical result of the bistatic cross section derived for open developed sea (Appendix A, Eqs. (A.4) - (A.5)). In applying that expression to obtain the reflected radiation intensity from terrain, the essential problem is to find the appropriate A_0 and B_0 for a given state of the ground surface, since these quantities depend on the roughness of the reflecting surface.

A large number of experimental studies of the radar return from terrain have been reported. Among these is a report on measurements of the bistatic cross section at X-band (S. Cost, 1965) for a few varieties of ground surface; these include smooth sand, bare loam, green and dried soybean plants and green grass. The radar return from other types of ground surface such as concrete, asphalt and gravel, was investigated by W. Peake et al (1960) . A careful study of the above experimental work as well as others related to our objective would enable us to determine the proper set of values for A_0 and B_0 for different ground surfaces. To aid us in this regard, we have planned a limited number of controlled experiments to be performed here in the near future.

II

BEHAVIOR OF REFLECTION OF A MODERATELY ROUGH SEA SURFACE

In Chu et al (1969, Vol. I), the objective was to find the maximum reflected radiation intensity and its direction of arrival at each receiving point when the sea surface was illuminated by the doppler antenna AN/APN-153. In so doing, the following procedure was adopted.

a) The moderately rough surface is normally distributed and spatially homogeneous with its correlation function of the form

$$H(\tau_x, \tau_y) = H(0,0) \exp\left[-\left(-\frac{\tau_x^2}{\ell_x^2} + \frac{\tau_y^2}{\ell_y^2}\right)\right] .$$

Based on these assumptions, the general formula was derived for the bistatic cross section.

b) By employing the Neumann spectrum, the correlation function was obtained for the open developed sea on the assumption that the stochastic process of such a sea state is stationary.

c) Thereupon, the formula of the reflected radiation intensity was derived, and numerical values were obtained for various sea states by assuming that the conductivity of the sea water is infinite.

In this section some calculations have been made in an effort to improve our understanding of the reflection property of the open developed sea. Scattering cross sections* have been calculated for a variety of sea states and incident latitude angles for plane wave illumination of the sea surface at an operating frequency of 13.2 GHz. To see the effect of the conductivity on the reflection at this frequency, both the finite and infinitely conducting surfaces were considered. The numerical results show that the cross sections obtained under the infinite-conductivity assumption is at most 2 dB higher than those obtained with the consideration of the finite conductivity. This suggests that, at and above 13 GHz

*For a definition of the scattering cross section, see Eq. (2.17), 1969-1-F, Vol. I Phase I Report (Chu et al, Dec. 1969).

the assumption of infinite conductivity is a fair one for the sea water. It should be emphasized that this observation on the behavior of the sea surface is based on the open developed sea and the physical optics method in which the scattering matrix was linearized in the surface slopes.

Based on the above observation, one would conjecture, then, that at the frequency level of 13.2 GHz, it is the state of the reflecting surface and the incident latitude angle that are of dominant influence on the reflection from the moderately rough sea surface, the conductivity being only of secondary importance.

Figures 2-1 and 2-2 show the variation of σ_h and σ_v for the finite conducing surface and $(\sigma_h)_c$ for the infinitely conducting surface when the incident latitude* and azimuth angles are 20^o and 180^o respectively, for a wind speed of 4m/sec in the down-wind and cross-wind directions. See Fig. 2-0 for the coordinate system employed. Figures 2-3 and 2-4 show similar curves for an incident latitude angle of 50^o , and Figures 2-5 through 2-8 are for a wind speed of 1.5 m/sec. It should be pointed out that the cross sections are symmetric about the azimuth angle $\phi_2 = 0^o$ and that, in the case of the infinitely conducting surface, the cross section is independent of the incident polarization (see Appendix A). Figures 2-9 and 2-10 show the dependence of the cross section on the incident latitude angle θ_1 in the plane of incidence. As seen from these figures, the shape of the cross section pattern remains more or less the same, but merely rotates about the center of the chart as the incident latitude angles changes with the maximum cross section occurring consistently in the specular direction.

It may be of interest to note that the result of our bistatic cross section analysis enables us to see the existence of so-called "critical angles"** in the sea return measurement. Based on our analysis, it will be seen that it is closely tied with the sea state which determines the pattern, or the shape,

*Latitude angle is equivalent to elevation angle.

**Katzin (1955) recognized the "critical angle" in backscattering from a rough sea surface.

of the cross section on a given azimuth plane and the phenomenon of dependence of the cross section on the incident latitude angle, i.e. the simple rotation of the cross section pattern according as the incident latitude angle changes, with the maximum cross section occurring in the specular direction.

In Figs. 2-9 and 2-10, it is observed that, on a given azimuth plane, the cross section pattern is broader for a higher wind speed, indicating that the reflection from the sea becomes more diffuse as the wind speed increases (up to the upper wind speed limit of about 5 m/sec, beyond which a linear analysis such as ours would be suspect due to increasing nonlinear effects. cf. footnote on pg.107, Vol.I, Phase I Report, 1969-1-F, Chu et al, December 1969). For instance, at the wind speed of 1.5 m/sec ($\simeq$ 3 knots/hr), the shape of the cross section somewhat resembles an inflated balloon; that is, it is mostly contained within the half-wedge $\Delta\theta_2 \simeq 15^o$ about the maximum point (i.e., the specular point): beyond 15^o from the maximum point on the cross section, the rate of decrease in the cross section is increasingly steep. Recognizing this and the dependence of the cross section on the incident latitude angle in the form of the rotation as previously discussed, one can see that the backscattering is significant in the case of down-wind speed 1.5m/sec, up to the incident latitude angle $\theta_1 = 15^o$, say, and for $\theta_1 > 15^o$, the backscattering cross section decreases rather sharply, so that the critical angle is about 15^o in this case. Since the shape of the cross section for the cross wind is somewhat narrower than that for the down wind, the corresponding critical angle is less than 15^o.

For the sea state corresponding to the wind speed of 4m/sec ($\simeq$ 8 knots/hr), referring to Figs. 2-10, the cross section is seen to be broader, so that the critical angle should increase. It is in the neighborhood of 30^o - 35^o in this case. Figures 2-11 through 2-14 show similar curves on different azimuthal planes.

From these numerical results the following observations can be summarized for bistatic cross sections for the open developed sea:

a) The smaller the incident latitude angle, the wider the azimuth range and the narrower the latitude range in which the cross section is significant.

b) The higher the wind speed (up to the limit, say, 6m/sec $\simeq$ 11.6 knots/hr), the lower the maximum cross section, but the wider the azimuth range in which the cross section is significant.

c) The cross section pattern does not change to all practical purposes, but merely rotates about the center of the polar chart as the incident latitude angle changes.

d) The cross section is maximum in the plane of incidence.

e) The variation of the cross section tends to be slightly more uniform in the azimuth plane for the cross-wind case than for the down-wind case.

f) The effect of the infinite conductivity assumption on the cross section is slight, justifying such an assumption.

Based on the definition of the polarization vectors (Chu et al, 1969, Eqs.A.4 - A.6, Vol.I), it is shown in the Appendix A to this present report that there is no depolarization of the incident wave either in the backscattering or specular directions*, while the maximum depolarization occurs near $\phi_2 = 80^o$ for both horizontally and vertically polarized incident waves. Figures 2-15 and 2-16 show the variations of σ_{vh}/σ_{hh}, σ_{hv}/σ_{vv} and $(\sigma_{vh}/\sigma_{hh})_c = (\sigma_{hv}/\sigma_{vv})_c$ for the down-wind and cross-wind speed of 4m/sec for the incident latitude angle $\theta_1 = 20^o$.

The cross sections in the backscattering direction are tabulated in Table II-1 for a few different incident latitude angles and sea states. It is observed that the backscattering cross section is not insignificant for a small latitude angle θ_1, while for a large θ_1 the backscatter is negligible.

---

*The absence of depolarizations in the backscattering, as indicated in this report, is believed to be the consequence of the physical optics method and is contrary to some experimental observations.

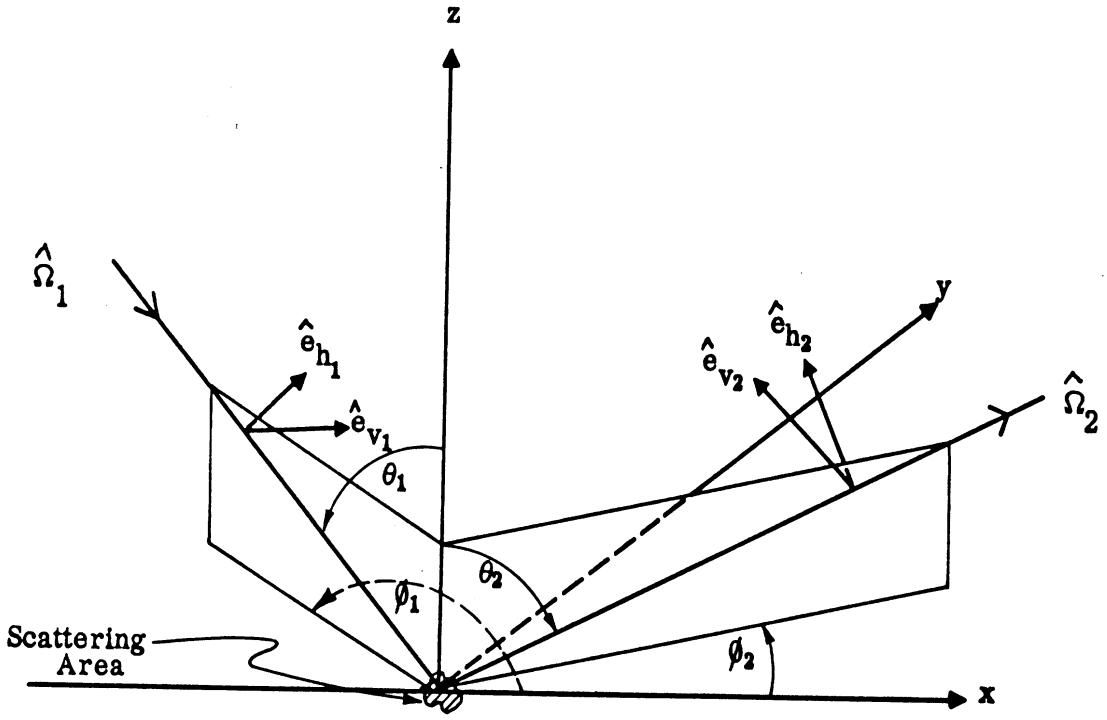

FIG. 2-0 : Coordinate System and Direction of Polarization

It has been found that experimental measurements of the bistatic cross section for ocean surfaces, with which to compare our theoretical results, are scarce in the frequency range of our interest. Therefore, comparison of our theoretical results will be limited to the backscattering case for which a few experimental observations have been reported by various investigators. Before we proceed to do so, however, it is felt that a point should be made in connection with the use of experimental sea return data. In a majority of the experimental work reported on sea return, the author seems to imply that the state of the sea is more or less specified when the local wind velocity and the "average" wave height are given. There is a danger in this simple description of the sea state and hence the data accompanied by such a description may be rendered a misinterpretation because it is more than likely that the ocean surface wave height measured at the time of the experiment is not closely correlated to the local wind velocity alone. Usually, it is not only the local wind velocity, but also (sometimes to a significant degree) the history of the sea state originating far away from the site of the experiment that affects the local wave height. The oceanographer is well aware of this fact. This seems to be one of the difficulties which confront experimental efforts of sea surface scattering. Nevertheless, one should be on guard in comparing a set of experimental data with other experimental or theoretical data and avoid relying only on the local wind velocity and the average wave height. Such a description of the sea state may not provide a valid ground for comparison because the wave height and the local wind speed cannot be viewed, in general, in terms of the causality in a meaningful sense. In this regard, the "open developed sea" is exceptional in that there exists a one-to-one correspondence in the statistical sense between the surface height and the local wind velocity. Recall that the Neumann spectrum (Chu et al, 1969, Vol. I, Eq. A. 109) is a function of the wind velocity.

Our theoretical results for the backscattering cross section are compared with experimental findings reported by various investigations and summarized as follows:

a) Polarization Dependence — $\sigma_h > \sigma_v$ holds for all sea states at 13.2 GHz considered in our cross section analysis, even though the difference is less than 1 dB for most cases. It can be said, then, that to all practical purposes, the polarization dependence of the cross section at the operating frequency of 13.2 GHz is negligible. For X-band, MacDonald (1956) reported σ_v greater than σ_h by several dB. The local wind speed and the average wave height were 14 mph ($\simeq$ 6.2 m/sec) and 5.6 ft ($\simeq$ 168 cm), respectively. For the open developed sea, the rms wave height corresponding to the wind speed of 6.2 m/sec is about 23 cm (see Chu et al, 1969, Vol.I, Fig. A-4). In the report by MacDonald (1956), a wind speed of 6 mph was recorded, while the wave height was 6.2 ft, which shows that the local wind speed cannot be reliably correlated, in general, to the wave height. Beckmann and Spizzichino (1963) give a summary of various reports on the dependence on polarization which indicates that at our frequency, there is no appreciable difference between σ_h and σ_v.

b) Dependence on Wind Direction — $\sigma_{\text{down wind}} > \sigma_{\text{cross wind}}$ was indicated in our theoretical result for all sea states considered. MacDonald (1956) reported $\sigma_{\text{upwind}} > \sigma_{\text{down wind}} > \sigma_{\text{cross wind}}$. Because of the form of the correlation function which we adopted in our theoretical work, i.e.

$$H(\tau_x, \tau_y) = H(0,0)\exp\left[-\left(\frac{\tau_x^2}{\ell_x^2} + \frac{\tau_y^2}{\ell_y^2}\right)\right] ,$$

we would find no difference between the cross section of the down-wind and the up-wind cases.

c) Dependence on Incident Latitude Angle — As previously discussed in detail, our theoretical result indicates that the backscattering cross section becomes increasingly small as the incident latitude angle increases (or as the incident depression angle decreases), indicating a possible existence of the critical angle in transition as the incident latitude angle increases from zero for a given sea state. Katzin (1955) indicated the existence of such an angle in his experimental report.

TABLE II-1: BACKSCATTERING CROSS SECTIONS ($\phi_1=\phi_2=180^o$) in dB .

θ (deg.)	Down Wind ----- Wind Speed 1.5 m/sec ----- Cross Wind					
	σ_h	σ_v	$(\sigma_h)_c$	σ_h	σ_v	$(\sigma_h)_c$
2	18.93	18.92	20.9	18.5	18.49	20.4
5	16.13	16.1	18.0	13.36	13.34	15.3
7	12.9	12.87	14.8	7.44	7.41	9.36
10	5.9	5.85	7.8	-5.3	-5.4	-3.4
20	-38.3	-38.5	-36.5	-86.2	-86.5	-84.4
30	-126	-126.7	-124.5	*	*	*
40	*	*	*	*	*	*
50	*	*	*	*	*	*
60	*	*	*	*	*	*
70	*	*	*	*	*	*
80	*	*	*	**	**	**
	----- Wind Speed 4 m/sec -----					
2	15.23	15.2	17.2	15.1	15.08	17.0
5	14.15	14.1	16.0	13.16	13.14	15.1
7	12.83	12.80	14.75	10.94	10.90	12.9
10	10.0	9.9	12.0	6.2	6.1	8.1
20	-7.6	-7.9	-5.8	-24.2	-24.5	-22.4
30	-42.9	-43.4	-41.2	-84.6	-85.4	-83.0
40	-108.5	-110	-107	-196.6	-197.6	-195.0
50	*	*	*	*	*	*
60	*	*	*	*	*	*
70	*	*	*	*	*	*
80	*	*	*	*	*	*

* Indicates a number of -200 or less

** Indicates insignificant cross section (- ∞)

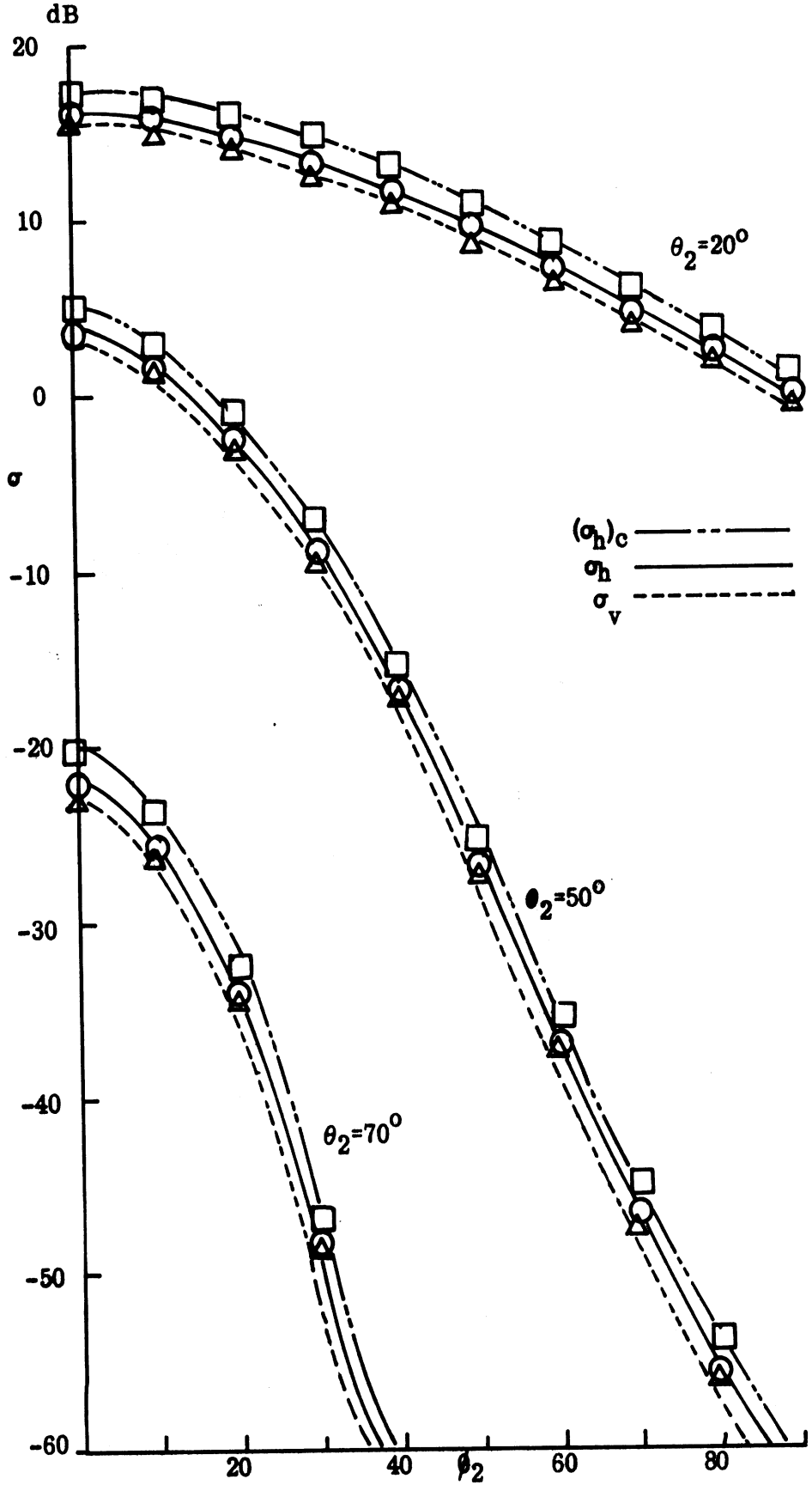

FIG. 2-1: σ_h, σ_v and $(\sigma_h)_c$ for Down Wind Speed at 4m/sec; θ_1=20°, ϕ_1=180°

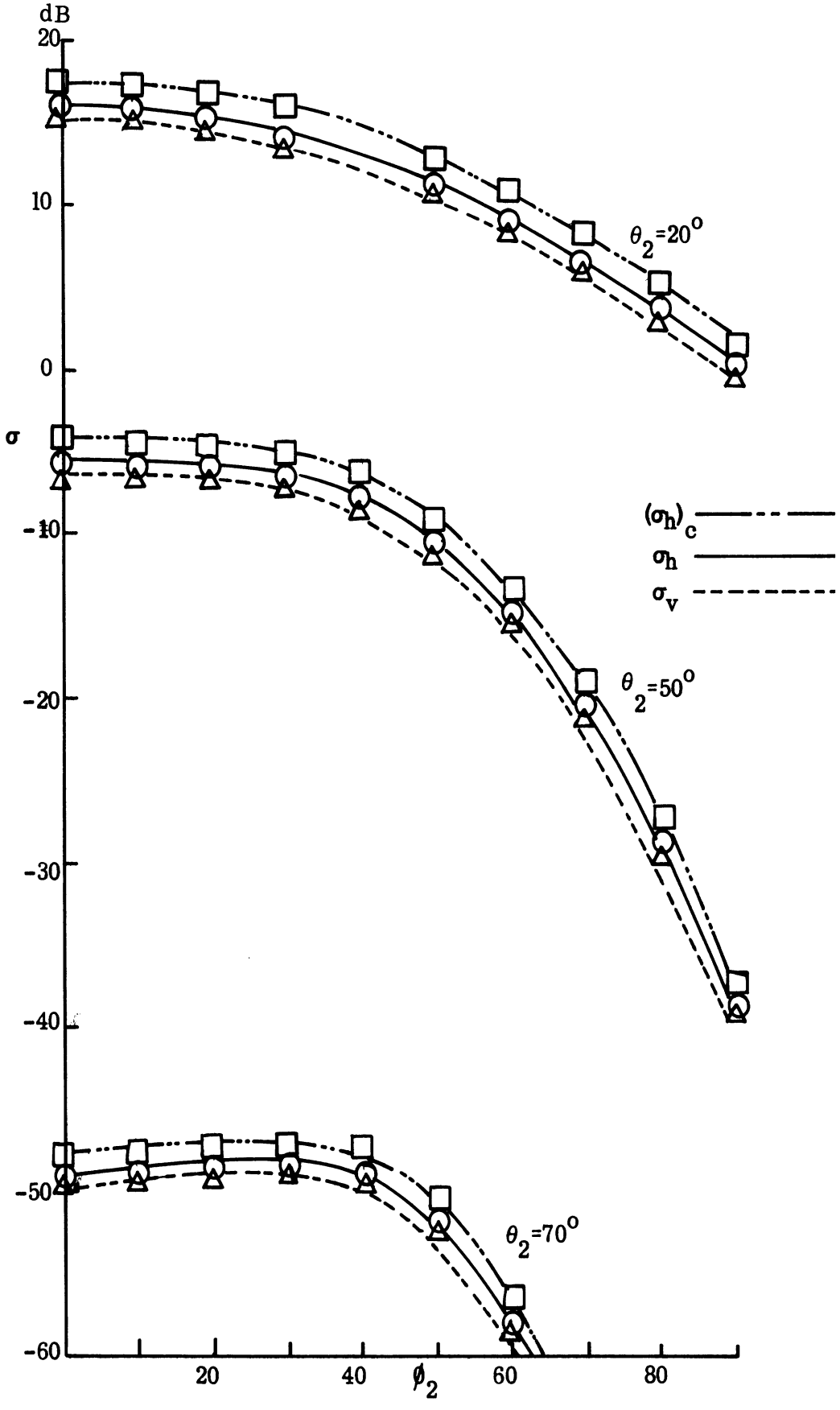

FIG. 2-2: σ_h, σ_v and $(\sigma_h)_c$ for Cross Wind Speed at 4m/sec; θ_1=20°, ϕ_1=180°.

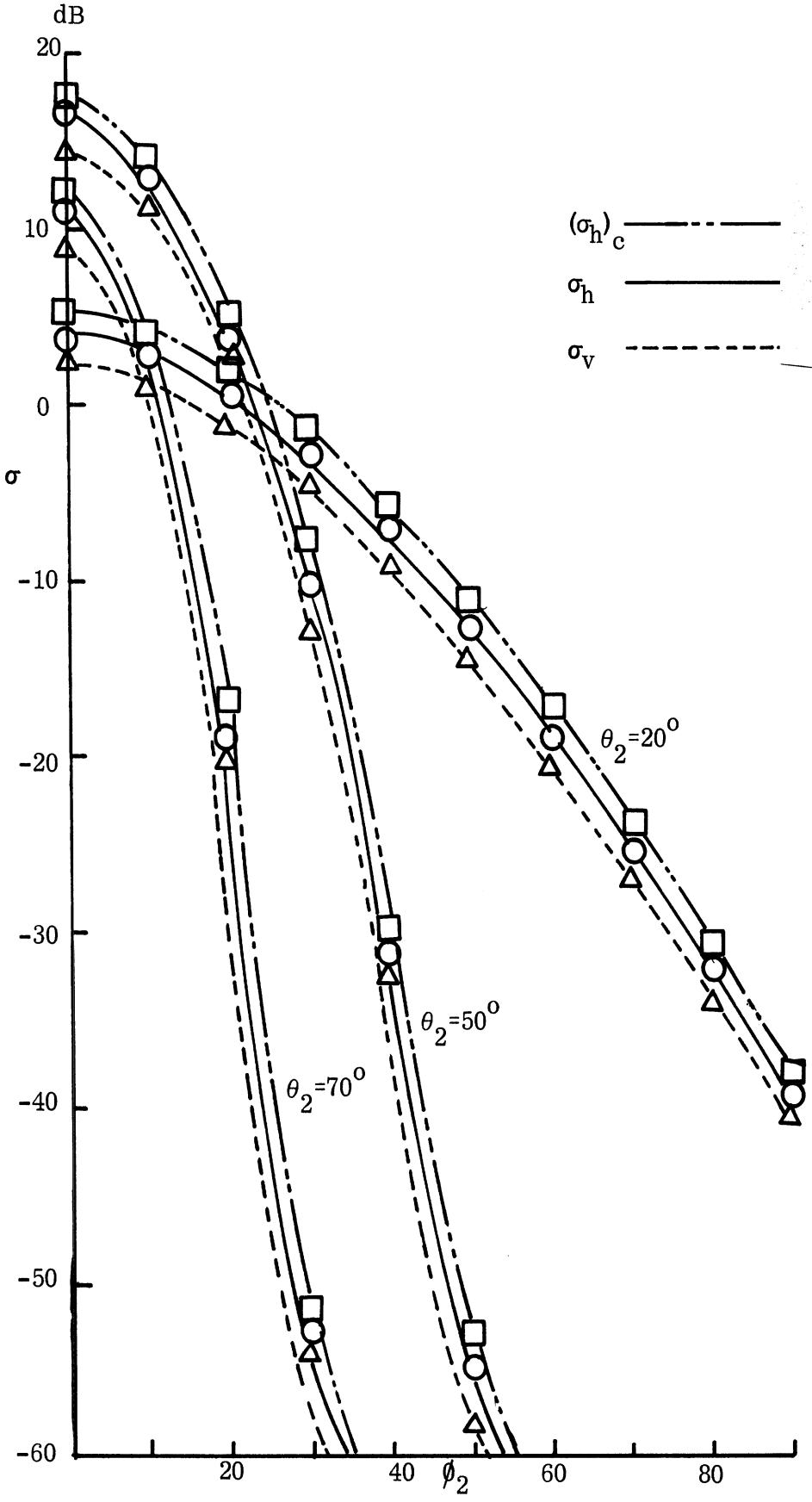

FIG. 2-3: σ_h, σ_v and $(\sigma_h)_c$ for Down Wind Speed at 4m/sec; θ_1=50°, ϕ_1=180°.

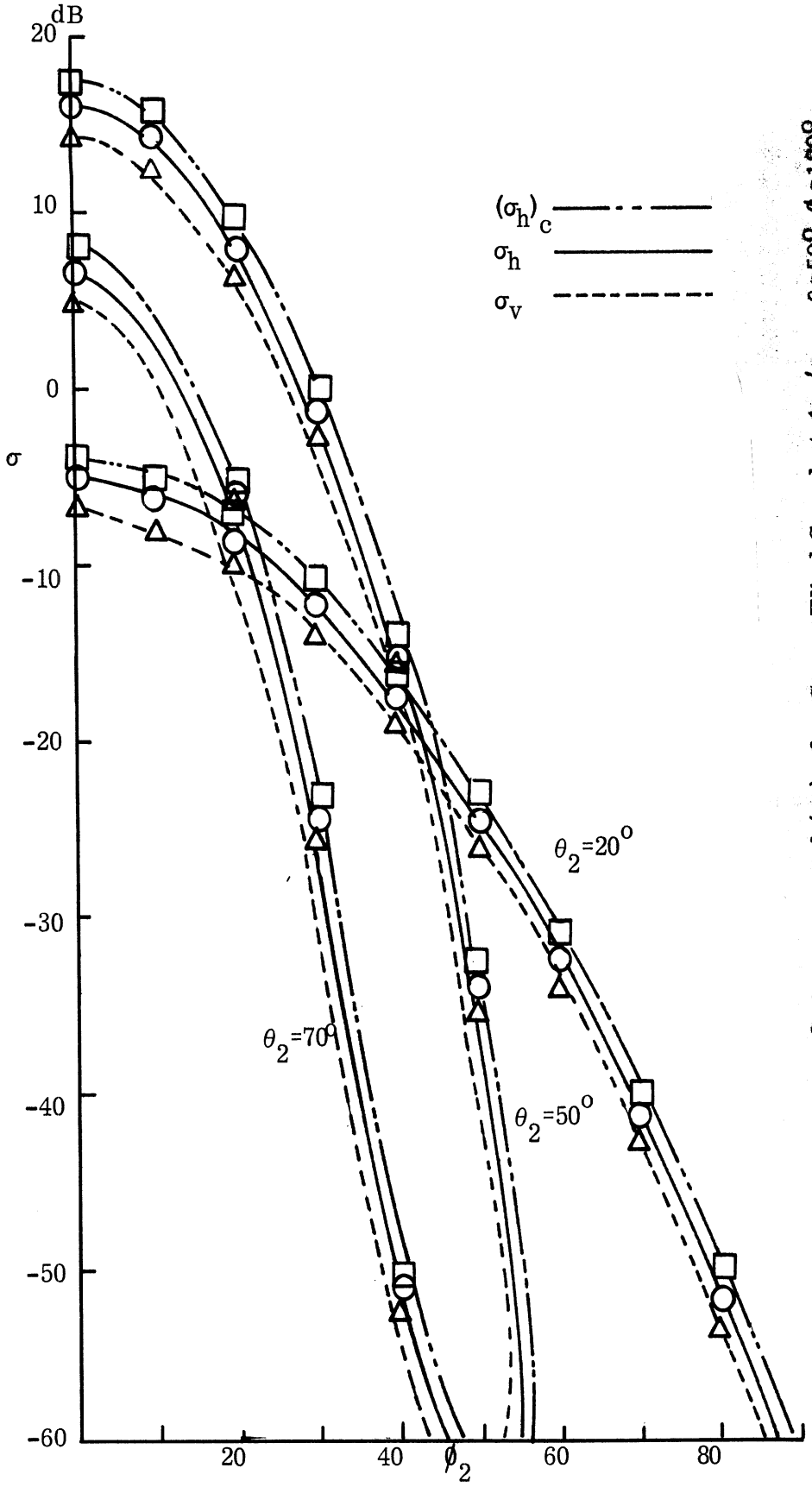

FIG. 2-4: σ_h, σ_v and $(\sigma_h)_c$ for Cross Wind Speed at 4m/sec; θ_1=50°, ϕ_1=180°.

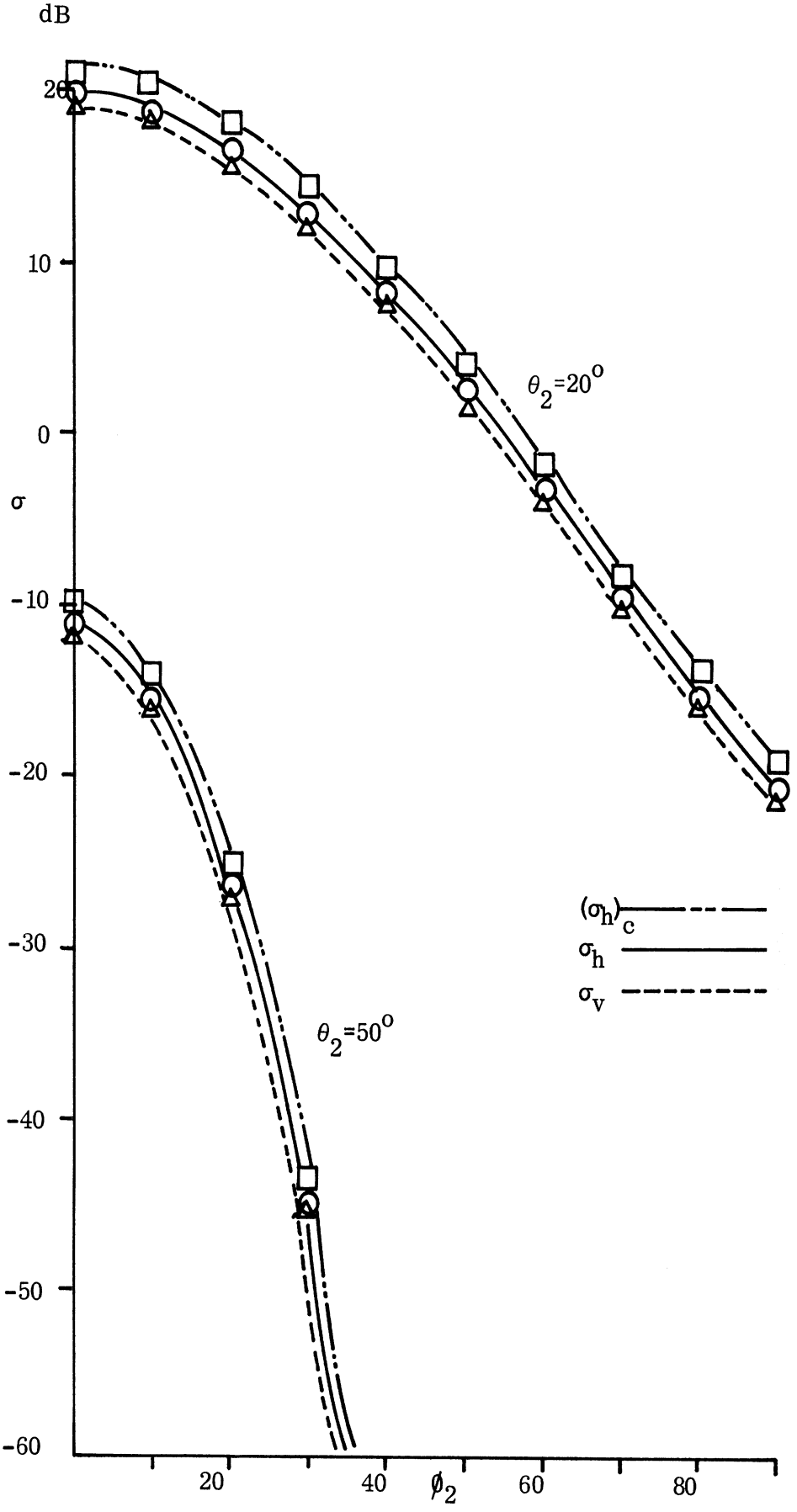

FIG. 2-5: σ_h, σ_v and $(\sigma_h)_c$ for Down Wind Speed at 1.5m/sec; θ_1=20°, ϕ_1=180°.

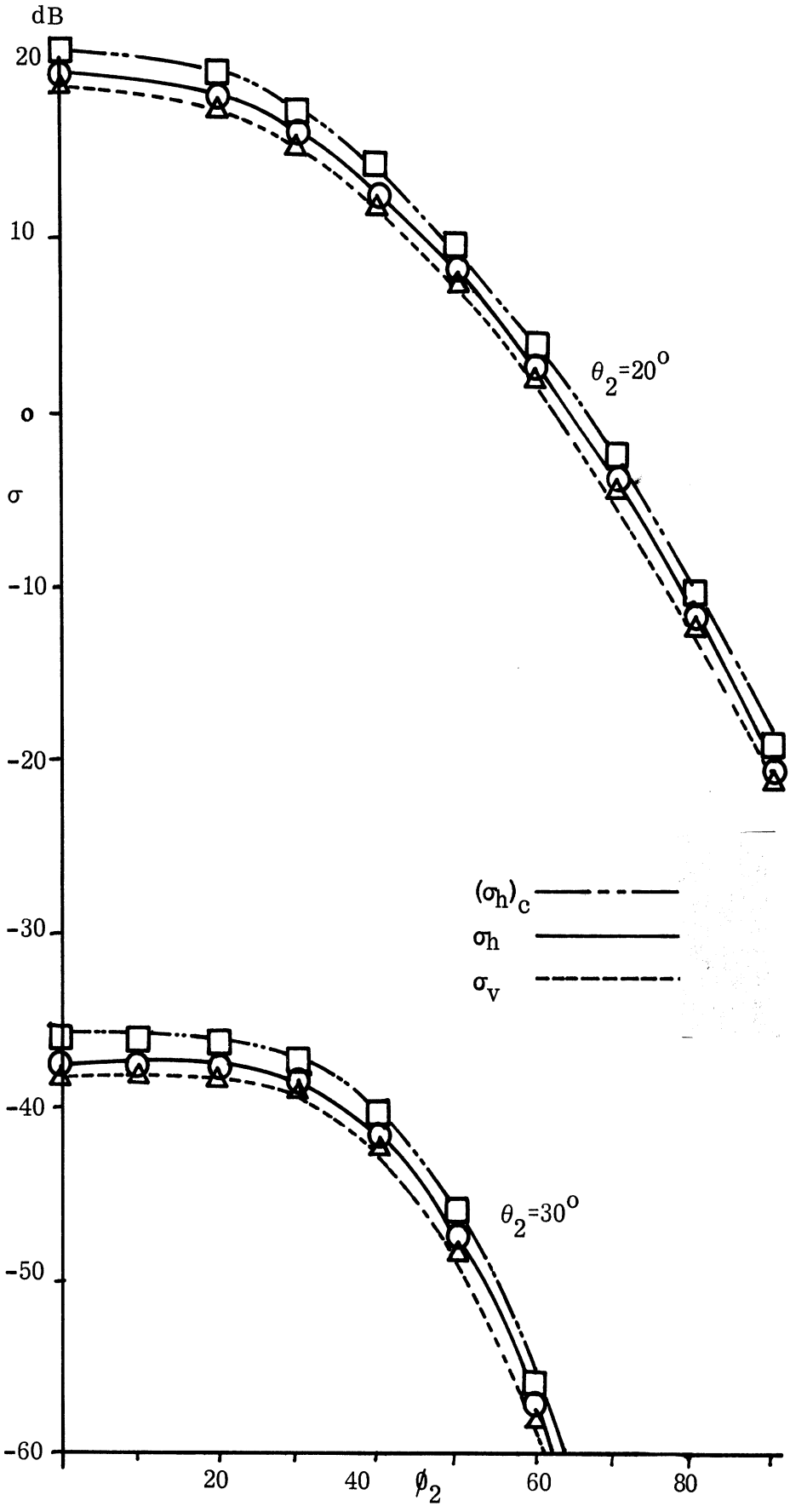

FIG. 2-6: σ_h, σ_v and $(\sigma_h)_c$ for Cross Wind Speed at 1.5m/sec; θ_1=20°, ϕ_1=180°.

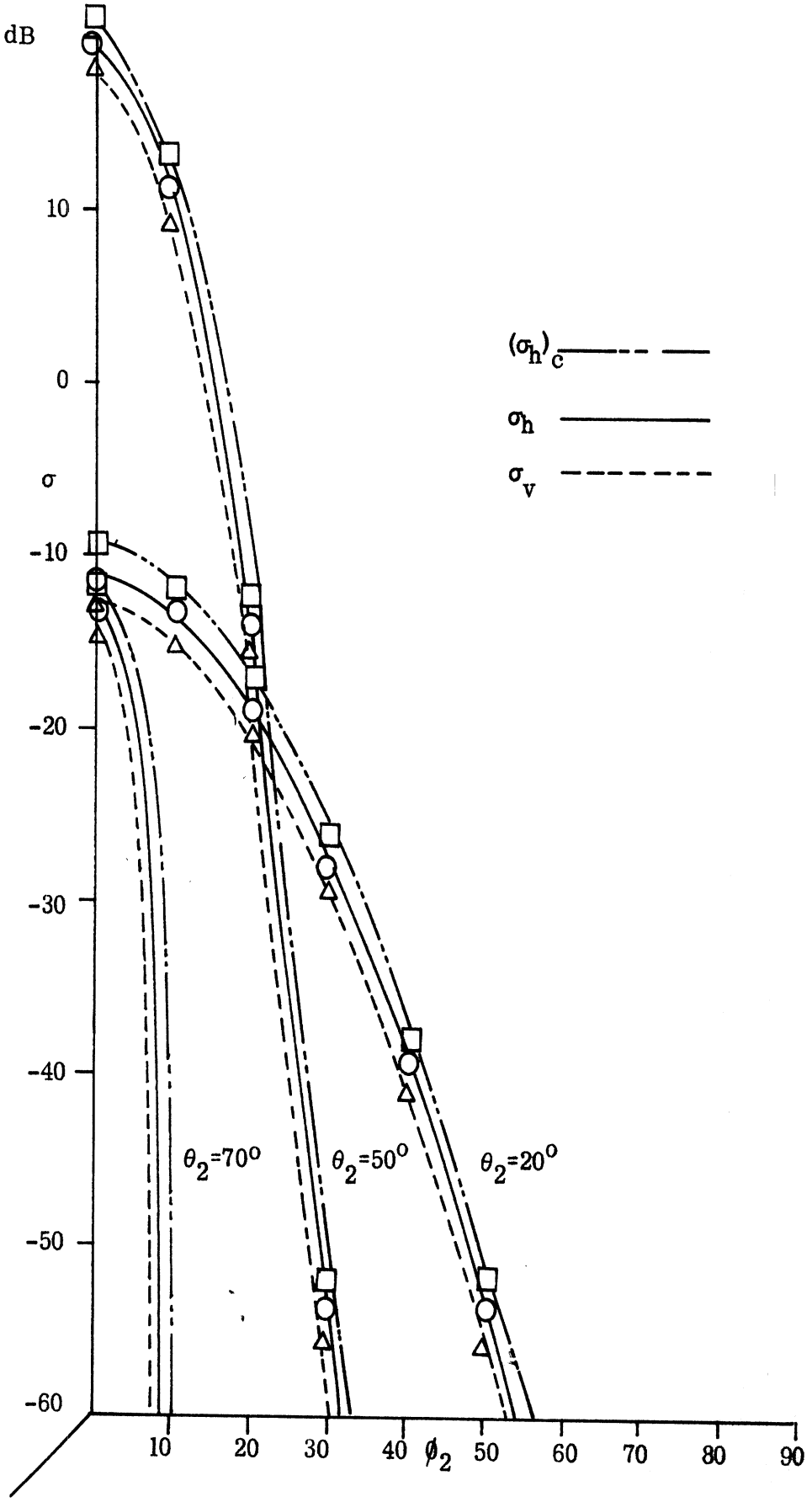

FIG. 2-7: σ_h, σ_v and $(\sigma_h)_c$ for Down Wind Speed at 1.5m/sec; θ_1=50°, ϕ_1=180°.

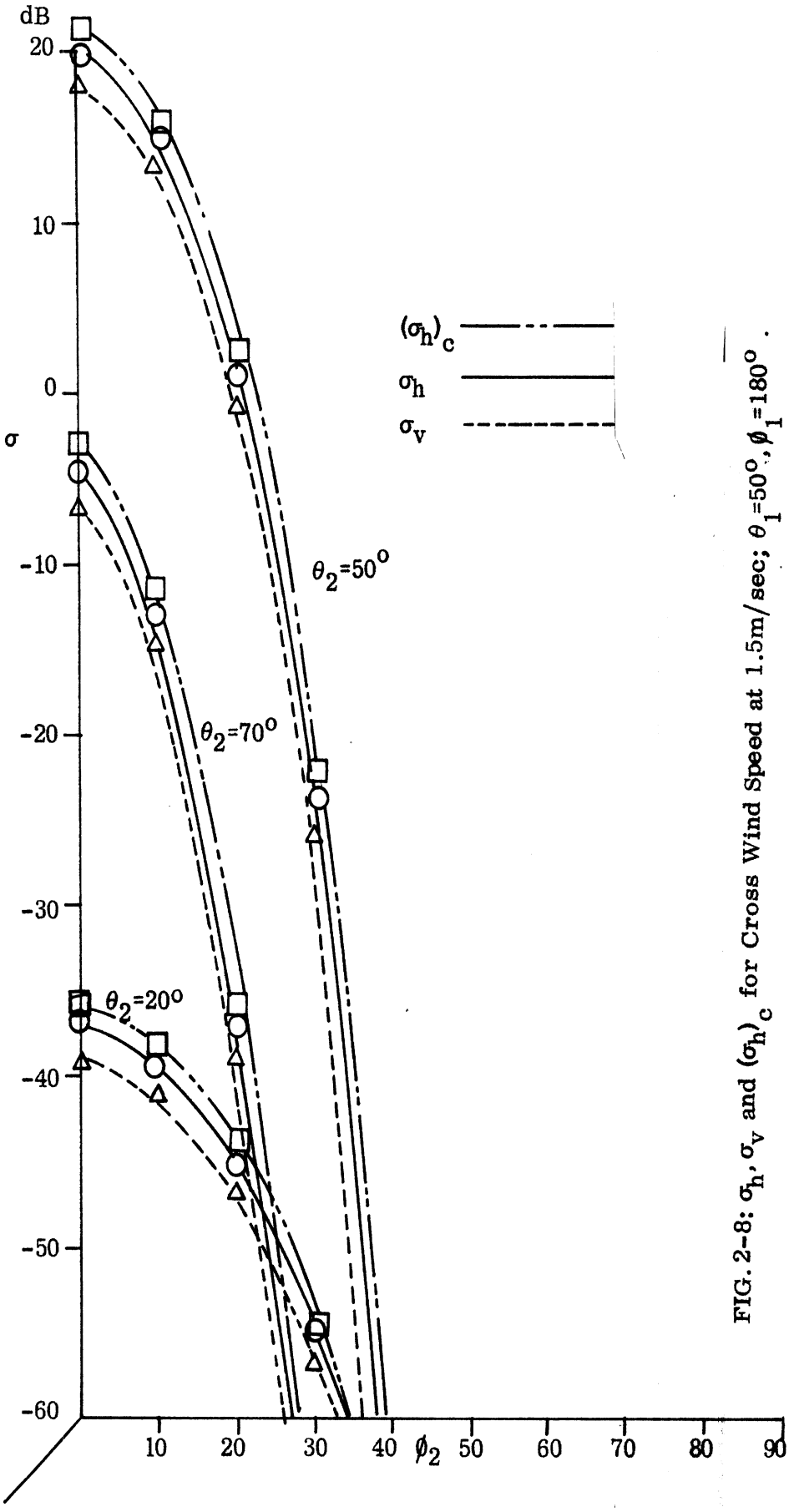

FIG. 2-8: σ_h, σ_v and $(\sigma_h)_c$ for Cross Wind Speed at 1.5m/sec; θ_1=50°, ϕ_1=180°.

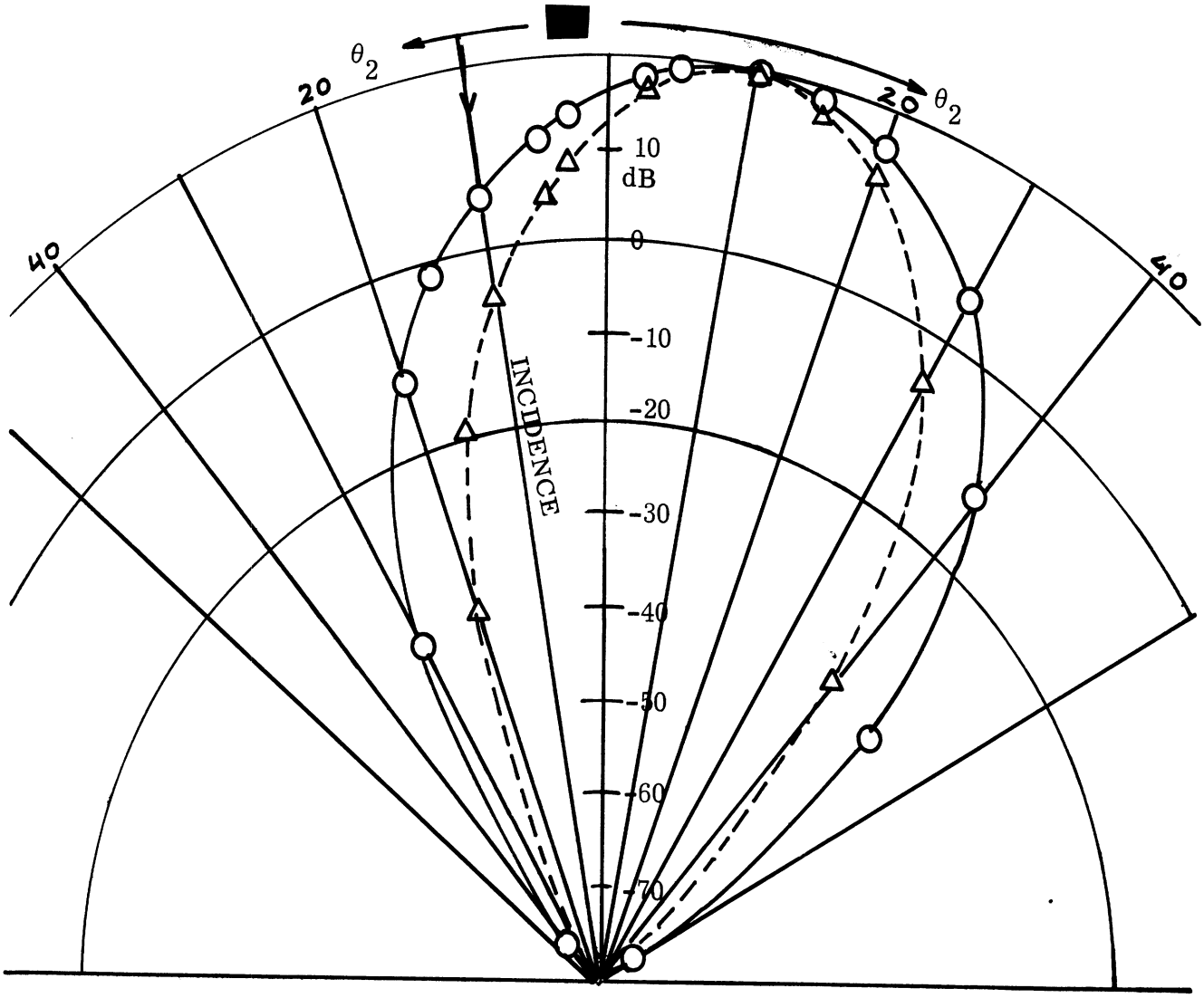

FIG. 2-9a: Variation of σ_h in Plane of Incidence ($\phi_1 = 180^o$) When Incident Latitude Angle $\theta_1 = 10^o$ and Wind Speed = 1.5 m/sec.

—— Down Wind
---- Cross Wind

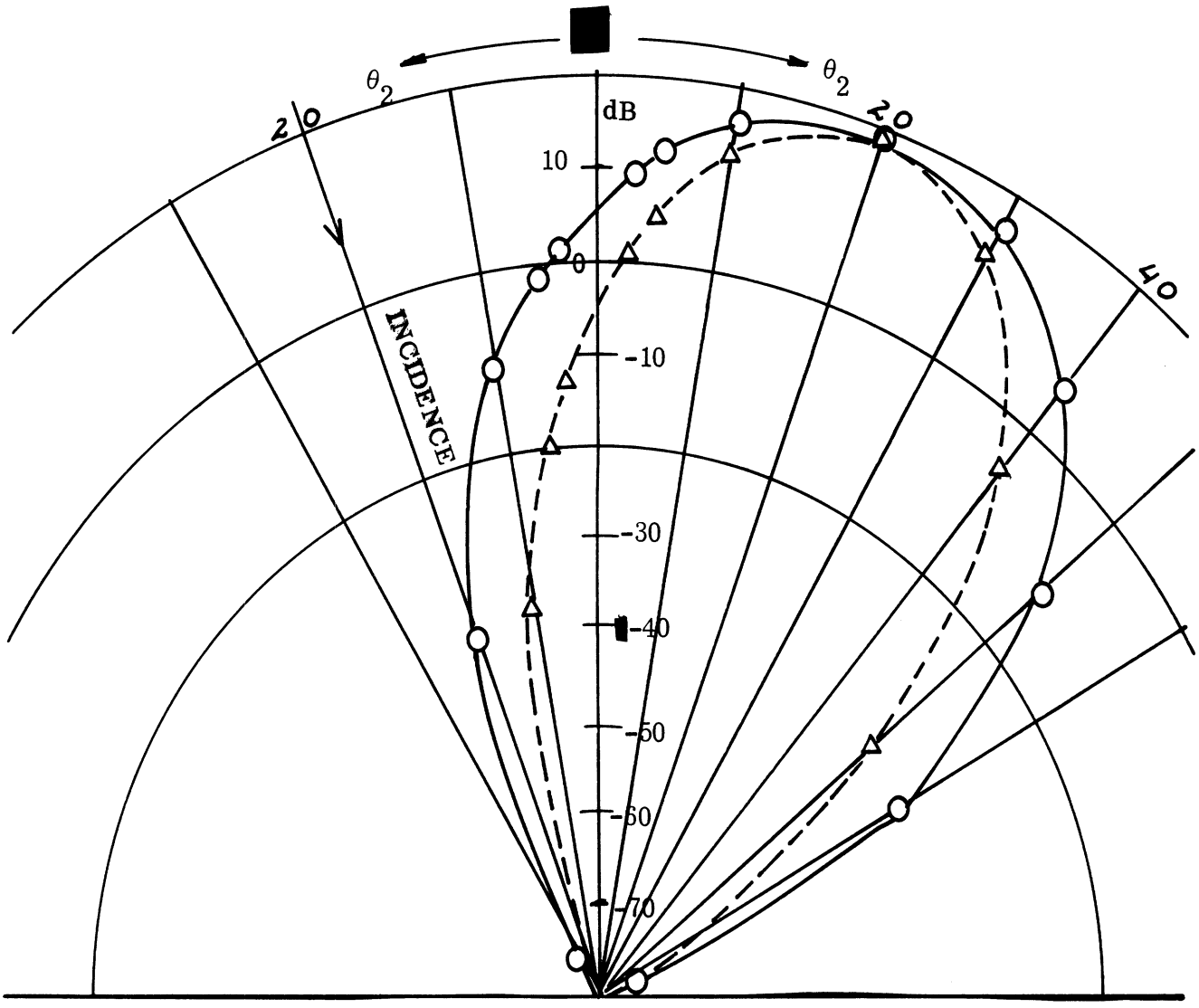

FIG. 2-9b: Variation of σ_h in Plane of Incidence (ϕ_1=180°) When Incident Latitude Angle θ_1=20° and Wind Speed = 1.5 m/sec.

—— Down Wind

----- Cross Wind

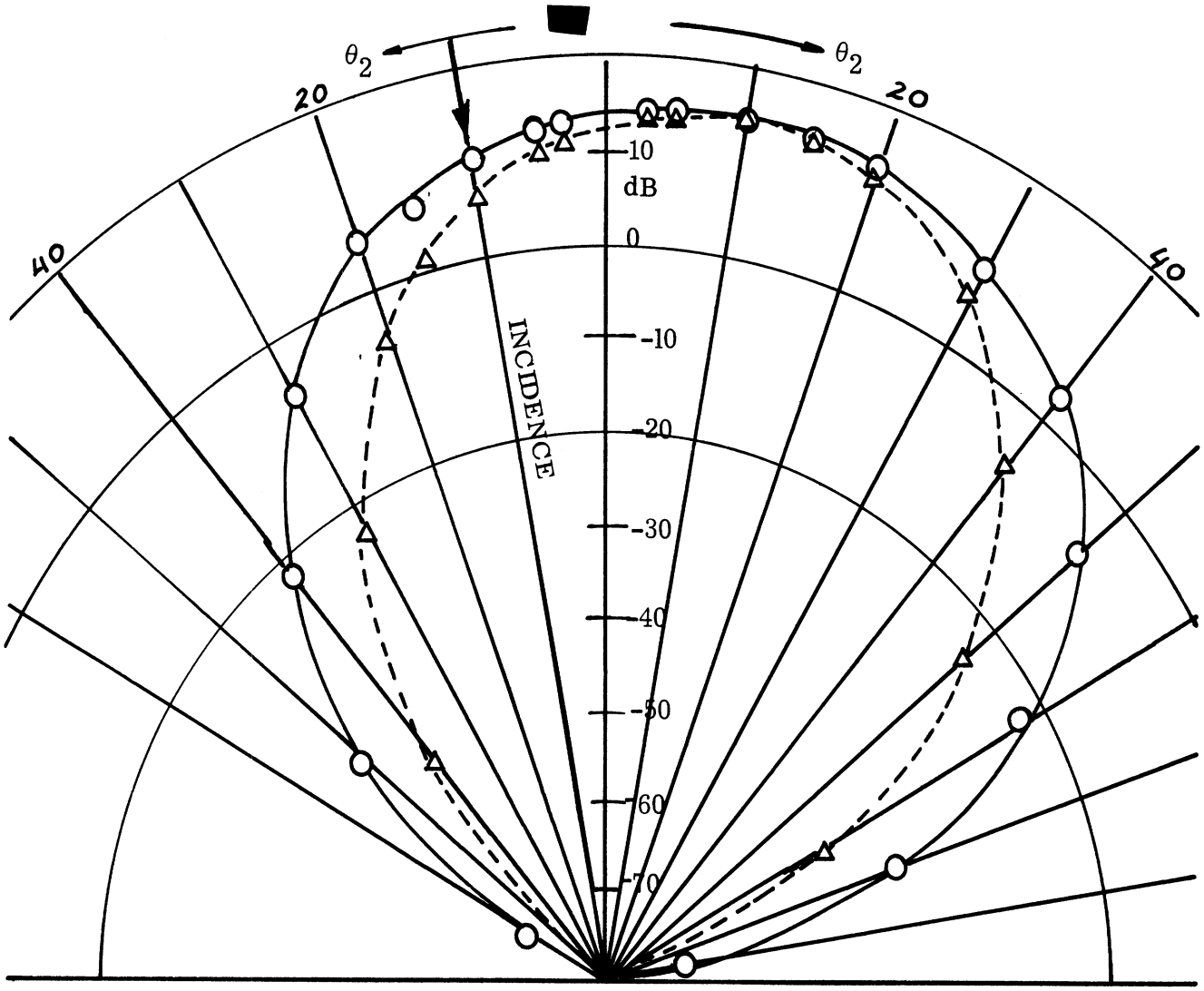

FIG. 2-10a: Variation of σ_h in Plane of Incidence ($\phi_1=180^o$) When Incident Angle $\theta_1=10^o$ and Wind Speed = 4 m/sec.

—— Down Wind

– – – Cross Wind

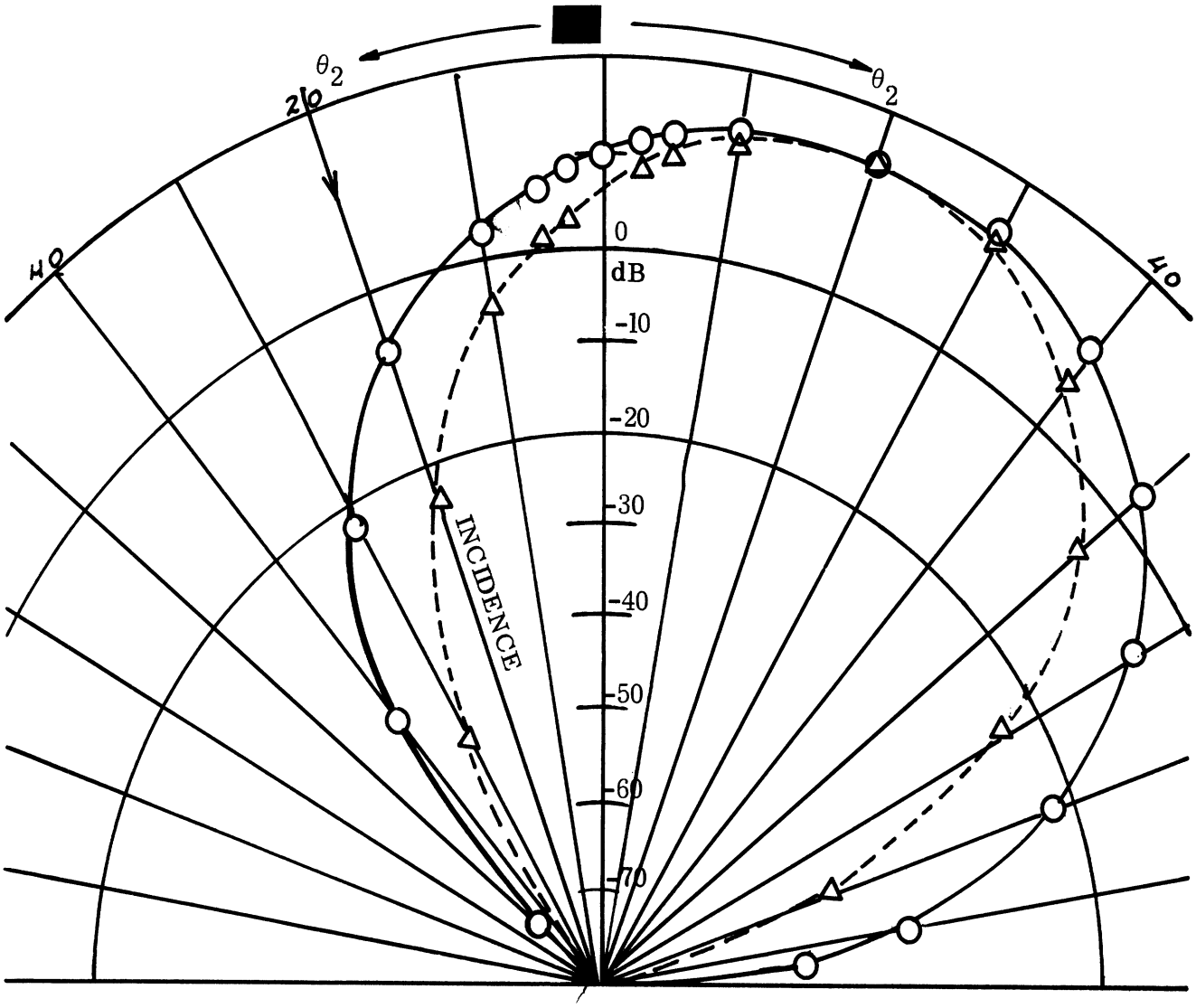

FIG. 2-10b: Variation of σ_h in Plane of Incidence (ϕ_1=180°) When Incident Angle θ_1=20° and Wind Speed = 4 m/sec.

—— Down Wind

---- Cross Wind

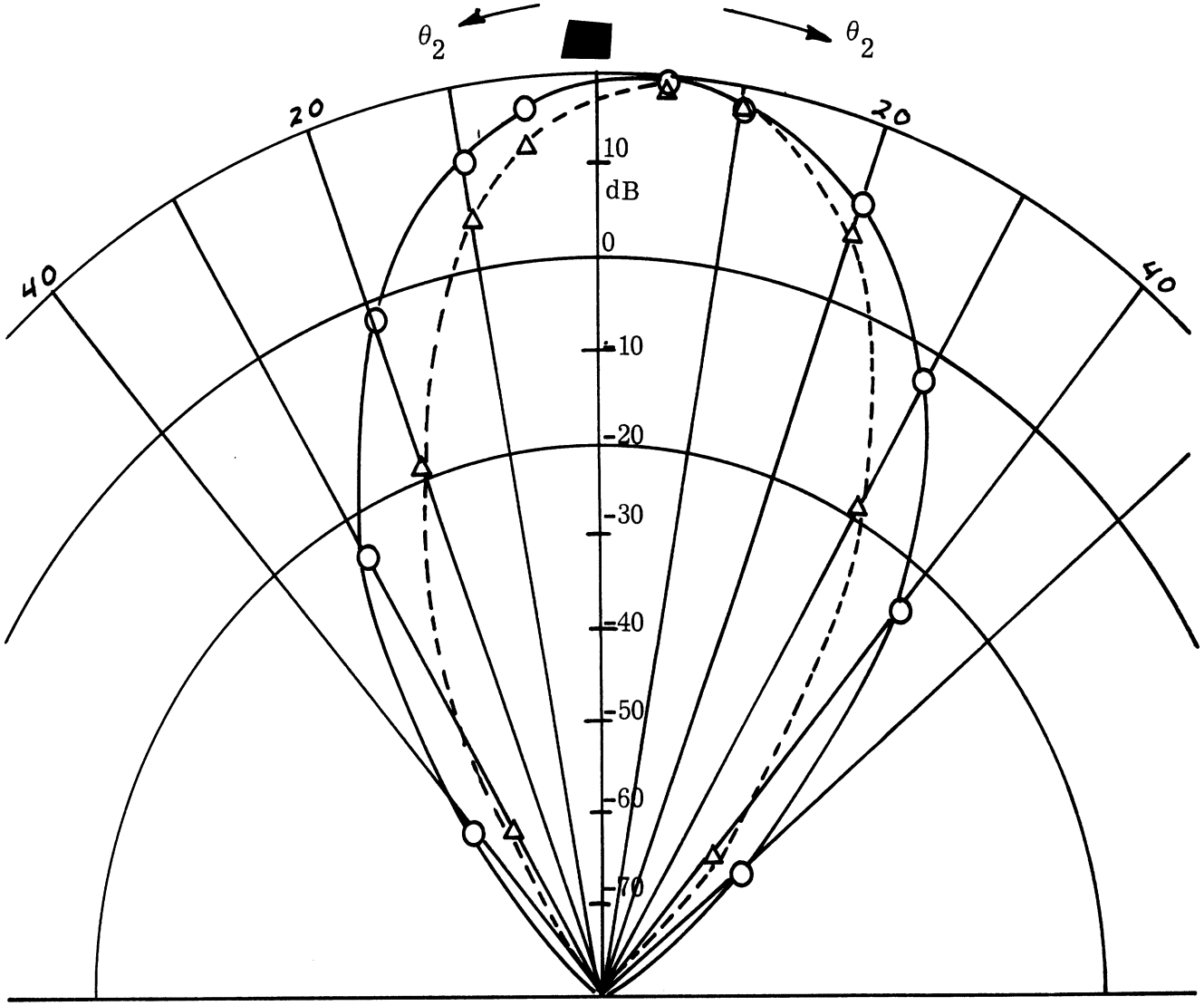

FIG. 2-11a: Variation of σ_h in Azimuth Plane (ϕ_2=10°) For Incident Latitude Angle θ_i = 5° and Wind Speed = 1.5 m/sec.

—— Down Wind

----- Cross Wind

For Figs. 2-11a through 2-14b, incident direction is not shown since it is not in the plane represented in the figures.

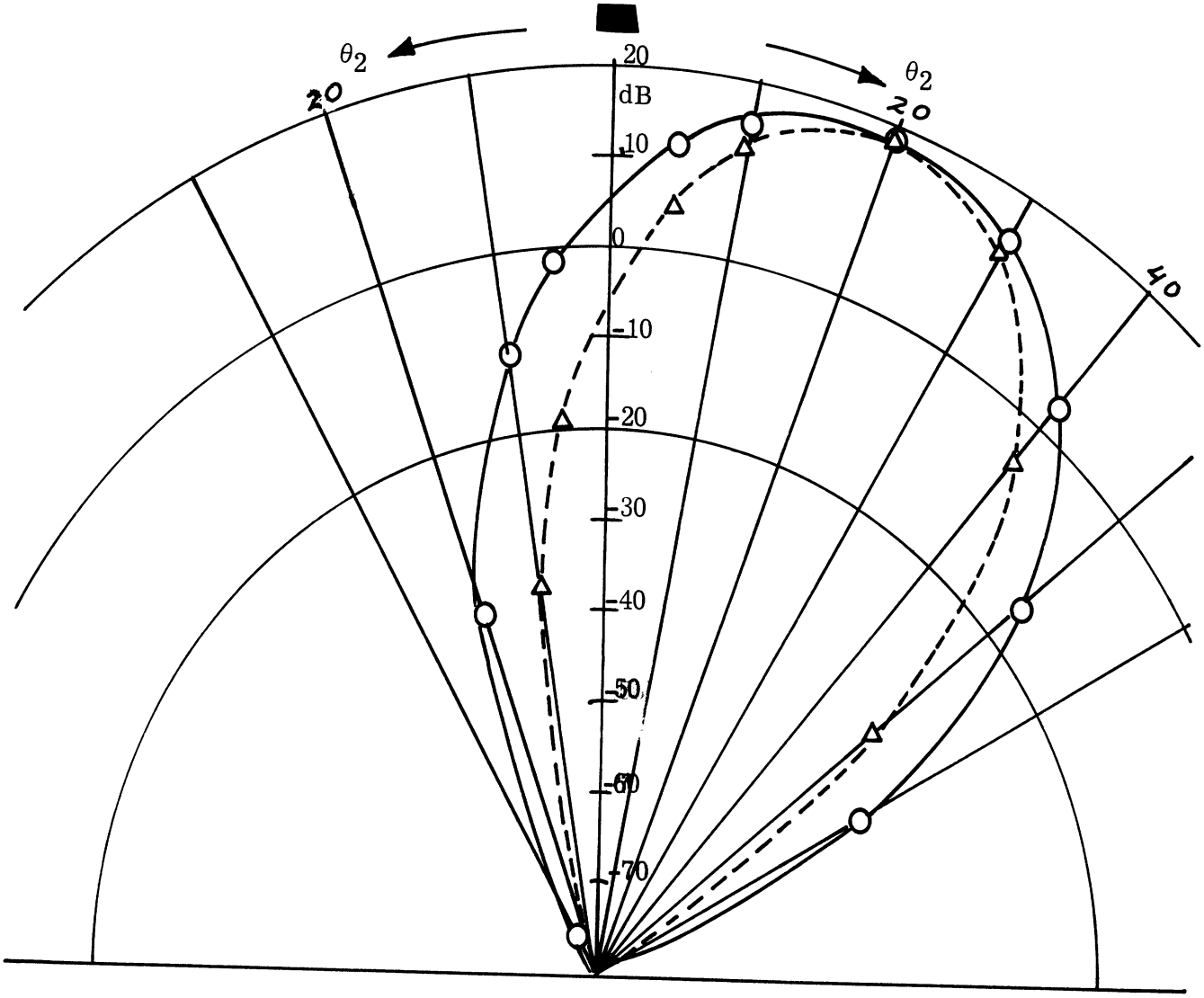

FIG. 2-11b: Variation of σ_h in Azimuth Plane (ϕ_2=10°) for Incident Latitude Angle θ_1 = 20° and Wind Speed = 1.5 m/sec.

——— Down Wind

----- Cross Wind

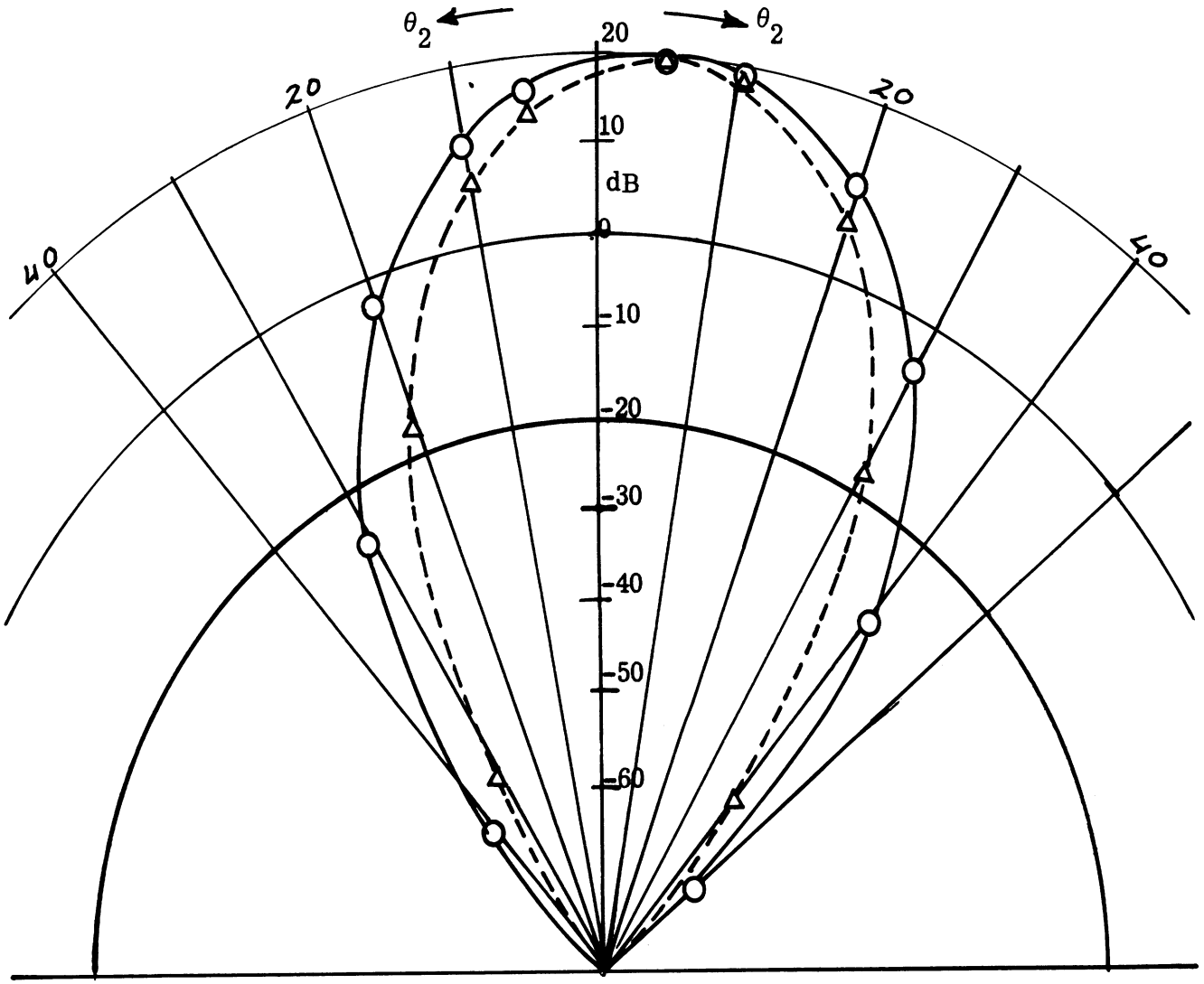

FIG. 2-12a: Variation of σ_h in Azimuth Plane ($\phi_2=20^o$) for Incident Latitude Angle $\theta_1= 5^o$ and Wind Speed = 1.5 m/sec.

——— Down Wind

----- Cross Wind

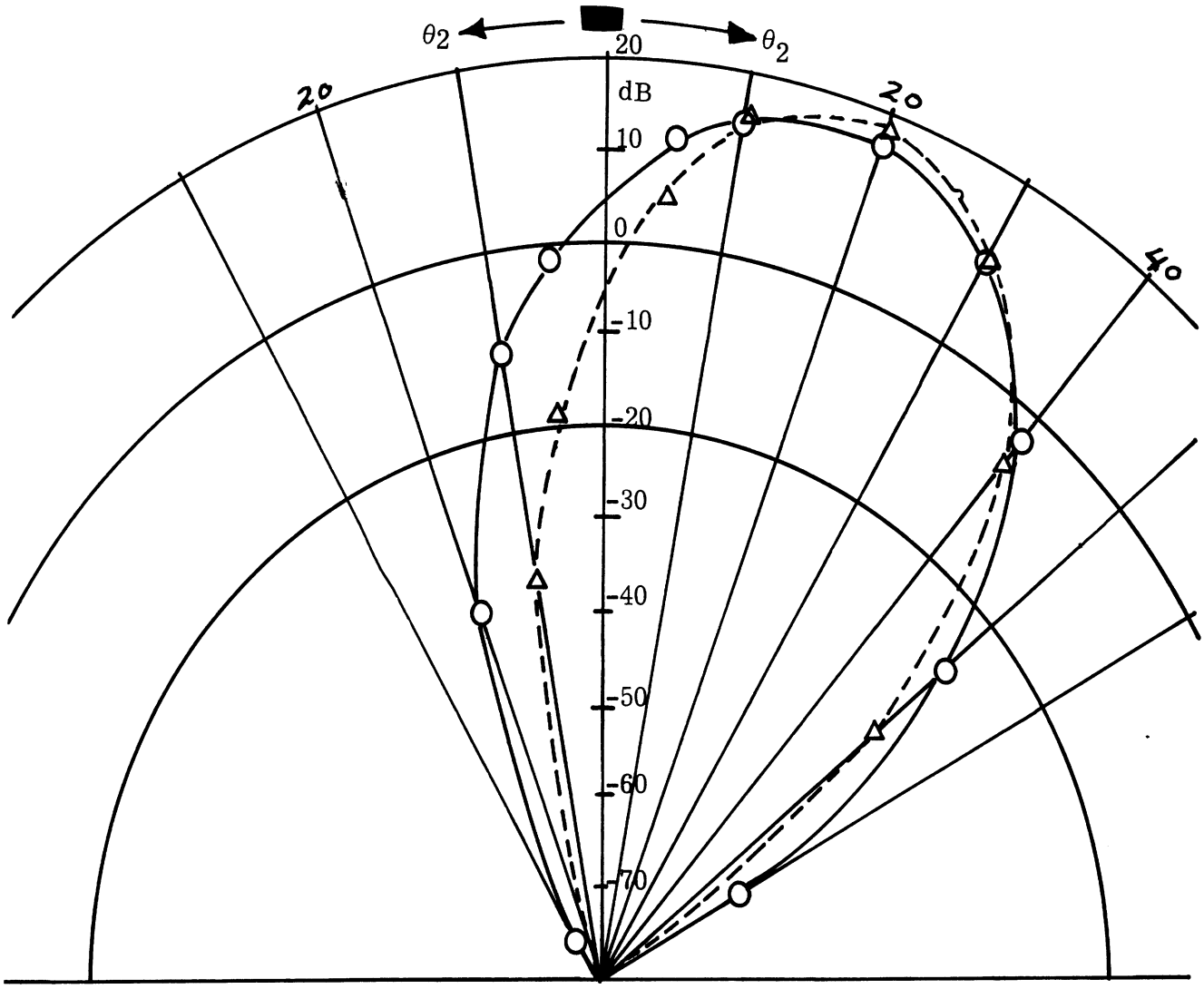

FIG. 2-12b: Variation of σ_h in Azimuth Plane ($\phi_2=20^o$) for Incident Latitude Angle $\theta_1=20^o$ and Wind Speed = 1.5 m/sec.

——— Down Wind

----- Cross Wind

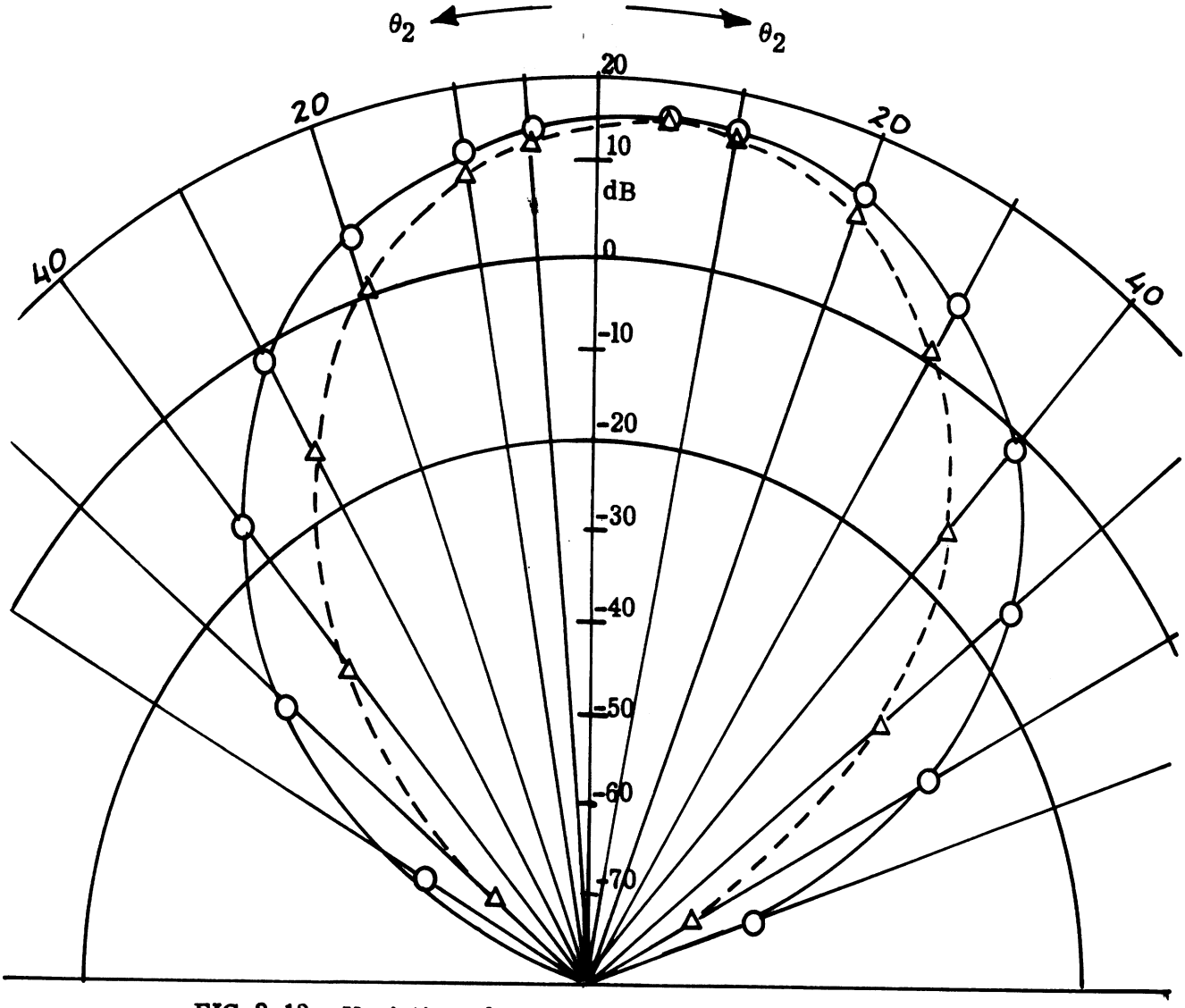

FIG. 2-13a: Variation of σ_h in Azimuth Plane (ϕ_2=10°) for Incident Latitude Angle θ_1=5° and Wind Speed = 4 m/sec.

——— Down Wind

----- Cross Wind

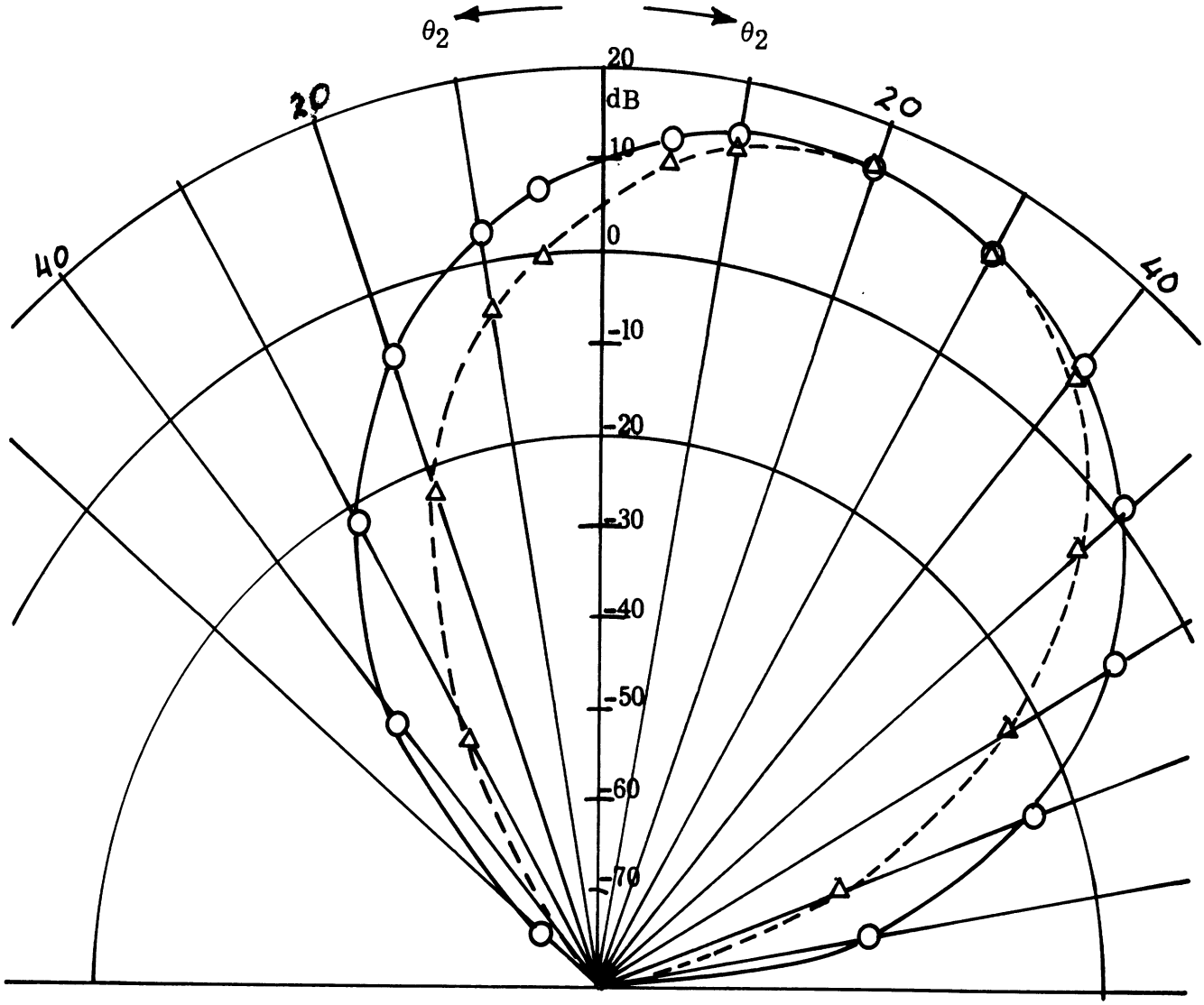

FIG. 2-13b: Variation of σ_h in Azimuth Plane (ϕ_2=10°) for Incident Latitude Angle θ_1=20° and Wind Speed = 4 m/sec.

——— Down Wind

------ Cross Wind

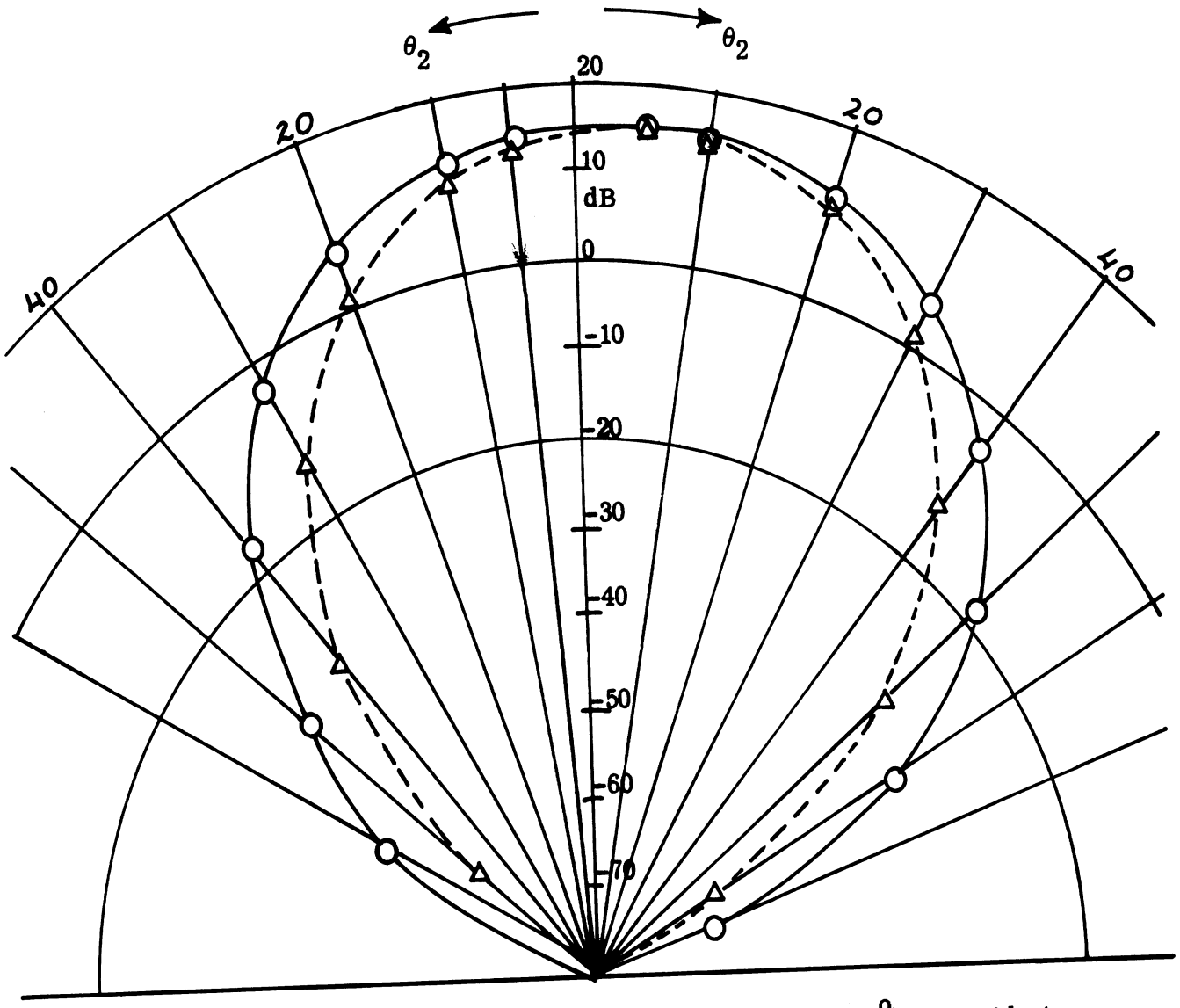

FIG. 2-14a: Variation of σ_h in Azimuth Plane ($\phi_2=20^\circ$) for Incident Latitude Angle $\theta_1=5^\circ$ and Wind Speed = 4 m/sec .

——— Down Wind

------ Cross Wind

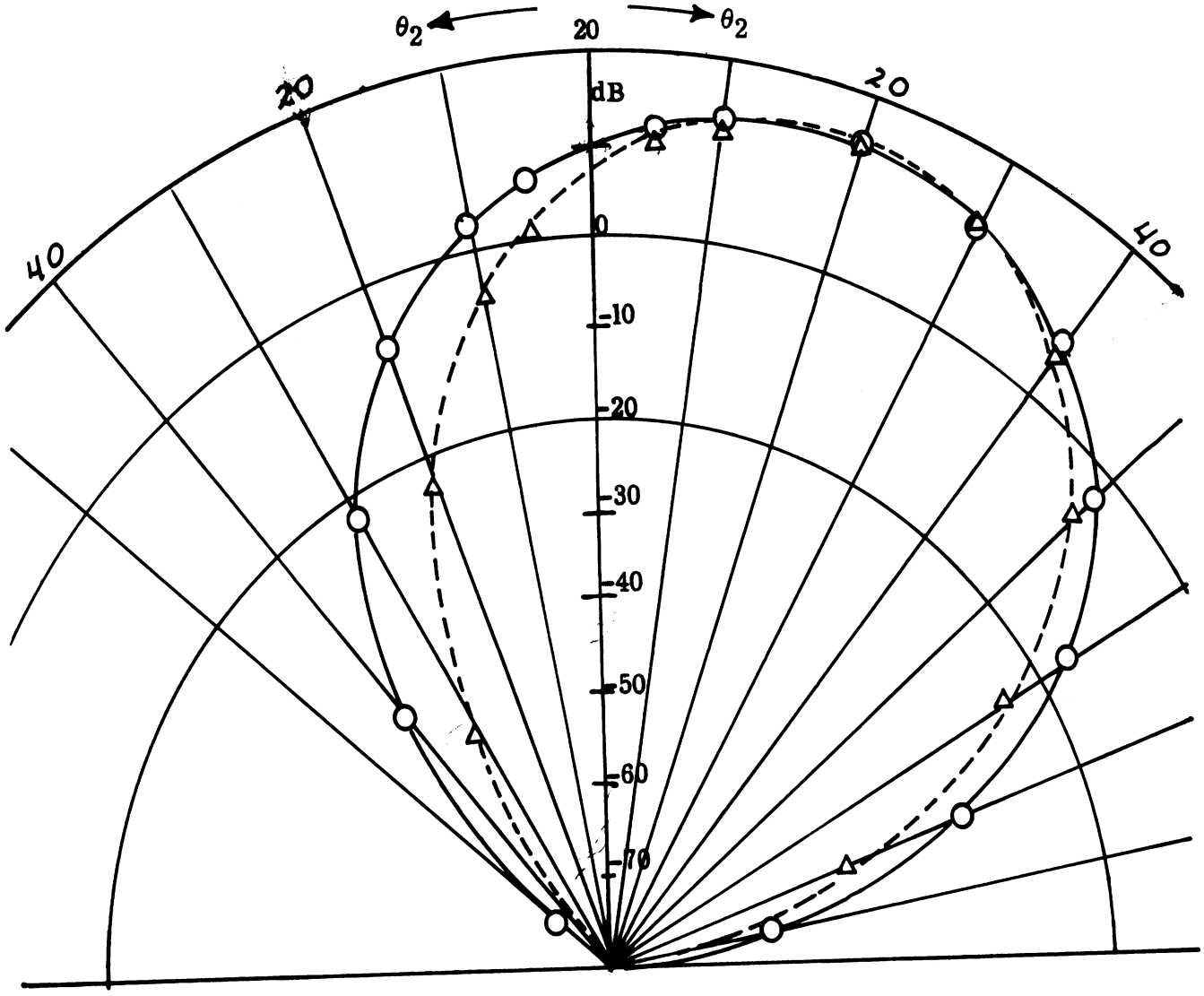

FIG. 2-14b: Variation of σ_h in Azimuth Plane ($\phi_2 = 20^\circ$)
for Incident Latitude Angle $\theta_1 = 20^\circ$ and Wind Speed = 4 m/sec.

——— Down Wind

------- Cross Wind

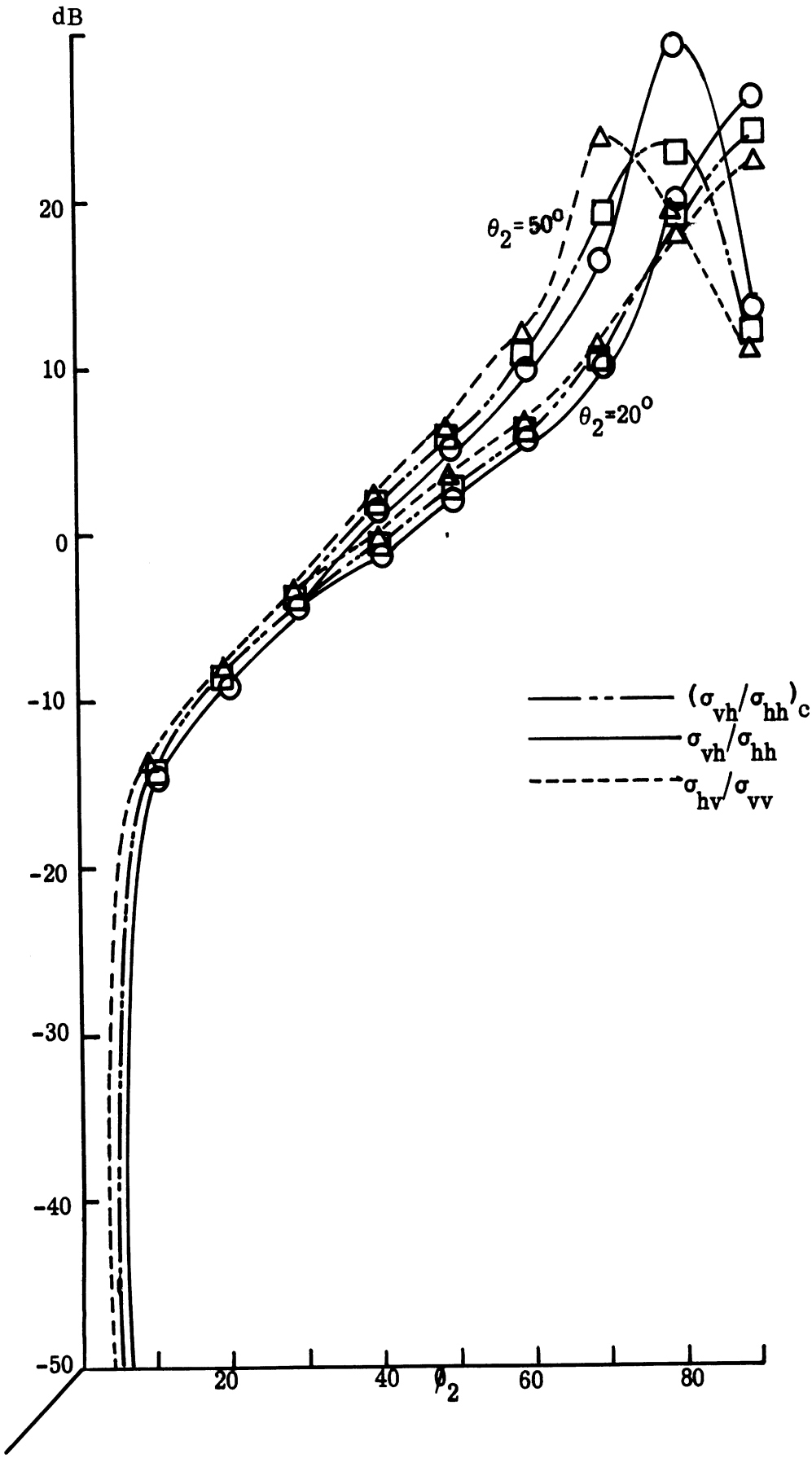

FIG. 2-15: σ_{vh}/σ_{hh}, σ_{hv}/σ_{vv} and $(\sigma_{vh}/\sigma_{hh})_c$ for Down Wind Speed = 4 m/sec; θ_1=20°.

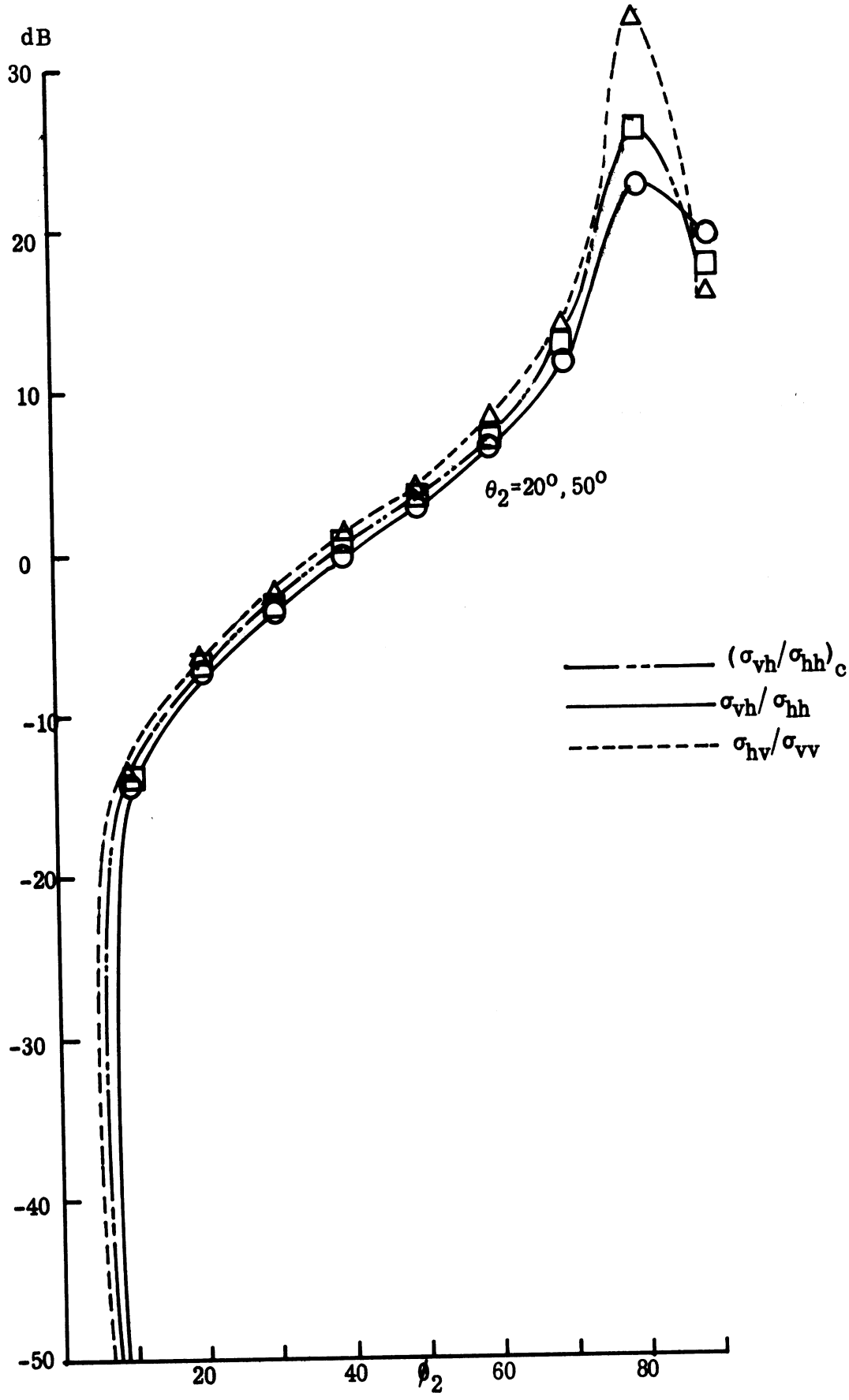

FIG. 2-16: σ_{vh}/σ_{hh}, σ_{hv}/σ_{vv} and $(\sigma_{vh}/\sigma_{hh})_c$ for Cross Wind Speed = 4m/sec; θ_1=20°.

III

MAXIMUM REFLECTED RADIATION INTENSITY AND ITS DIRECTION OF ARRIVAL

Based on the computed results of Chapter II for reflected radiation from the ocean surface, one could, in principle, predict (for the wind-generated open developed sea only) the order of magnitude of the reflected radiation intensity at any receiving point for a known plane wave incidence. In our case where the incidence is not the plane wave, but composed of a pair of particular non-uniform patterns (AN/APN-153), the task of predicting the reflected radiation intensity becomes many-fold more complicated. Despite the added complication due to the radiation pattern of the AN/APN-153 antenna, the observations summarized in Ch. II for the behavior of the sea surface reflection should be applicable for each indicent ray. By way of augmenting this viewpoint to aid in our understanding of the variation of the reflected radiation intensity at various receiving points, let us consider a hypothetical radiation pattern of a transmitting antenna shown in Fig. 3-1, where the patterns are projected on XY-planes.

X, Y denote the normalized coordinates defined by Eqs. (2.1) and (2.2) in Chu et al (December 1969, Vol. I):

$$X = \frac{x_r - x_a}{z_a} , \qquad Y = \frac{y_r - y_a}{z_a} ,$$

where x_r, x_a represent the x-coordinates of the receiver and the transmitting antenna; z_a represents the z-coordinate of the transmitting antenna. The normalized coordinate system (X, Y, z_r/z_a) was introduced so that the position of the receiver can be measured from the receiver in terms of the transmitter height. Note, also, that the z-coordinate of the transmitter is always 1 .

Let a receiver move on Y=0.5 line from X<0 toward X>0, maintaining a constant height z_r/z_a=0.5 i.e., on z_r/z_a=0.5 plane (see Fig. 3-1a). Suppose the

receiver is at X = -3, and denote this point by R(X=-3, Y=0.5, z_r/z_a=0.5). We wish to show how one could predict qualitatively from which part of the projected radiation pattern of the AN/APN-153 antenna the maximum reflected radiation intensity, F_{2M}, is likely to come at the receiver point R when the wind is blowing along the X-axis at the speed of 4m/sec.

Let us consider the Beam No. 2 (Fig. 3-1a). The point P, which is the peak point of this beam, has the coordinates (θ_1=29°, ϕ_1=140°). The corresponding normalized cartesian coordinates of these points are found by the formulas given in Chu et al (Dec.1969, Vol.I, Eq.2.11 and 2.12):

$$X = \frac{z_r}{z_a} \tan\theta_2\cos\phi_2 - \tan\theta_1\cos\phi_1,$$

$$Y = \frac{z_r}{z_a} \tan\theta_2\sin\phi_2 - \tan\theta_1\sin\phi_1 .$$

Thus, the cartesian coordinates of P is found to be (X=-0.42, Y=0.35) and the specular direction of the wave which is reflected at P intersects with z_r/z_a = 0.5 plane at X= -0.64, Y=0.54.

From the discussion on the variation of scattering cross section given in Chapter II, we know that the cross section is most significant on the plane of incidence with its maximum occurring in the specular direction; that the cross section decreases as one moves away from the plane of incidence (Fig. 2-1, for example). The rate of decrease in the cross section on various azimuth planes depends rather critically on the incident latitude angle given for a sea state. In specifying the wind direction, we have used terminology such as "down wind" and "cross wind" , which are so termed conventionally with reference to the direction of the incident wave. In the case of the backscattering with plane wave illumination, the use of these terminologies should not cause any confusion. However, in our present case where the transmitting antenna radiates laterly and fore and aft,

adherence to the usual definition of the terms down wind or cross wind becomes impossible. A convenient wave of specifying the wind direction is with reference to the fixed coordinate system, as was done in the Phase I report (Chu et al, 1969). It is realized that the use of these terms in such a manner is not meaningful physically in our case because 'down' and 'cross' are no longer referenced to the direction of incidence. The numerical results of F_{2M} and various scattering cross sections indicate (as shown in the Phase I report and in Ch. II of this present report) that the dependence of these quantities on the wind direction are relatively insignificant compared to the wind speed and the adaptation of the terminologies in a different way should not be of any great consequence.

The plane of incidence for the wave that corresponds to the peak point of Beam No. 2, P, is the azimuth plane $\phi_2 = 140^o$ (or $\phi_1 = 320^o$-plane), and the receiving point, R, lies on the azimuth plane $\phi_2 = 171.7^o$. The latitude angle of this receiving point with regard to P is computed by

$$\tan \theta_2 = \frac{X + \tan \theta_1 \cos \phi_1}{\frac{z_r}{z_a} \cos \phi_2} ,$$

to obtain $\theta_2 = 81.2^o$. Referring to Figs. 2-1 and 2-2 and recalling that the incident latitude angle of the wave which impinges on P is 29^o, one can see that the radiation intensity reflected at the peak point would be small at R because the azimuth plane of this receiving point is not only 31.7^o away from that of the incident wave (i.e. the plane of incidence for the wave that corresponds to the peak point **P** of the Beam No. 2) but also, more significantly the latitude angle of the receiving point R is $81.2^o - 29^o = 52.2^o$ away from the specular latitude angle. From this observation, one could conjecture that the maximum reflected radiation intensity at R is not likely to come from the peak point of Beam No. 2 .

Next, we look for the incident wave whose specular direction passes through R, for, if it exists, the maximum reflected radiation intensity will certainly come from that wave at R if the transmitter radiation pattern is uniform (plane wave). Even though, in our case, the antenna pattern is not uniform (see Fig. 3-1a), let us suppose, for the moment, that it is, in order to carry this argument further. Then, putting $\phi_2 = 171.7^o$, $\phi_1 = 351.7^o$, $z_r/z_a = 0.5$, $X = -3$ and $\theta_1 = \theta_2 \equiv \theta$ in

$$X + \tan\theta_1 \cos\phi_1 = \frac{z_r}{z_a} \tan\theta_2 \cos\phi_2 ,$$

we obtain $\theta = 63^o$. Thus, the incident wave having the spherical coordinates ($\theta_1 = 63^o$, $\phi_1 = 351.7^o$) has the specular direction through the receiver at R. The corresponding cartesian coordinates are ($X = -2$, $Y = 0.29$), which is denoted by Q in Fig. 3-1c). If the radiation pattern is uniform and extends wide enough to cover this reflection point, Q, the maximum F_{2M} at R would certainly come from Q. In the case of the AN/APN-153, Q falls far outside the pattern range as shown in Fig. 3-1c, and hence the maximum reflected radiation intensity at R cannot be a specularly reflected wave. Referring to Figs. 2-10a and b, on the other hand, it is observed that for an incidence with relatively small latitude angle θ_1, the cross section does not decrease so much even if θ_2 departs a little from the specular reflection latitude angle. This suggests that an incident wave whose plane of incidence corresponds to $\phi_2 = 171.2^o$ must have a relatively small latitude angle in order to have a relatively significant F_{2M} at R. One is thus led to conjecture that the point in the radiation pattern from which the maximum F_{2M} arrives at R should be somewhere in the region indicated by the hatched line in Fig. 3-1d. The computer result shows that, at the receiving point R ($X = -3$, $Y = 0.5$, $z_r/z_a = 0.5$), the maximum reflected radiation pattern comes from the point S($\theta_1 = 25^o$, $\phi_1 = 344^o$), indicated in Fig. 3-1d, which lies on the -5 dB contour of AN/APN-153. This corresponds to ($\theta_2 = 87.7^o$, $\phi_2 = 171.9^o$) shown in Fig. 3-5 .

The method of predicting the level and direction of the maximum reflected radiation intensity demonstrated above is less effective than the alternative procedure employed in the Phase I Report (Chu, et al 1969). The above discussion was intended to show only that one could predict the direction in which the reflected radiation intensity is significant from a knowledge of the reflection characteristics of the rough surface.

Thus, it seems that by drawing the segment of a sphere around the specular direction of the peak point of the radiation pattern for the given transmitting antenna, one could find the region in which the reflected radiation intensity is most significant.

Even though the findings in Section II indicate that the reflected radiation intensity is very slightly affected by the assumption of the perfect conductivity for the sea surface, we carried out the numerical computation anew based on the formula which retains the finite conductivity. The results show no significant change from the ones reported in the Phase I Report either in the variation of F_{2M}, or its direction of arrival. For completeness, they are presented in this section.

Figures 3-2 show the variations of latitude and azimuth angles versus the relative x-coordinate, X, for a down wind speed of 1.5 m/sec at the relative receiver height $z_r/z_a = 0.1$ and $Y = 0.5$. Upon comparison of these curves with the corresponding Figures 3-6 of Volume I of the Phase I Report, one recognizes that both θ_{2M} and ϕ_{2M} are almost identical throughout the interval $-3 \leq X \leq 3$, except for $-1 \leq X \leq 1$, where a rather significant deviation from the previous cases is observed for θ_{2M} and ϕ_{2M}. The similar curves shown in Figures 3-3 are at the relative receiver height of $z_r/z_a = 0.5$. At this relative receiver height, however, for both cases of the electric conductivities, the variations of θ_{2M}, ϕ_{2M} are identical (see Figures 3-4 of Vol. I, Phase I Report). Again, comparing Figures 3-3 with Figures 3-10 of Vol. I, Phase I Report, one notices a deviation of ϕ_{2M} in the range $-1 \leq X \leq 1$. This is the representative difference in the variation of the maximum direction of arrival throughout the cases investigated in this report. Figures 3-5 deal with the similar case at the different relative receiver height, $z_r/z_a = 0.5$. Figures 3-6 and 3-7 show the similar curves for the cross wind speed at 4m/sec. Figures 3-8 show the effect of the wind speed on the maximum direction of arrival for the down wind case at the relative receiver height $z_r/z_a = 0.1$ and $Y = 0.5$, with similar curves being shown in Figures 3-9 at the relative receiver height, $z_r/z_a = 0.5$. The effect of the wind directions at the velocity of 4m/sec are shown in Figures 3-10 and 3-11 at the relative receiver heights $z_r/z_a = 0.1$ and 0.5. As was the case in the Phase I Report, the variation of the maximum reflected radiation intensity along the given X axis is, to all practical purposes, insensitive to changes in the wind velocity.

As was mentioned in Section II, the infinite-conductivity assumption for the sea was found to have a minor effect on the cross sections. From this, one can expect no great change in the variations of F_{2M} from those reported in Vol. I of the Phase I Report. Indeed, the numerical results carried out with the finite conductivity supported this expectation.

Figures 3-12 through 3-15 show the variation of F_{2M} in dB versus X for various Y for the down wind cases at the two different relative receiver heights. Figures 3-16 and 3-17 deal with similar cases for the cross wind, the effects of the wind speed and its direction on dB F_{2M} being shown in Figures 3-18 through 3-21.

The present investigation of the problem of the reflection from the ocean surface is based on the physical optics method in which the scattering matrix is linearized on the slopes of the surface. This linear analysis precludes any possibility of incorporating non-linear effects which may not be insignificant in a rough surface scattering problem at our frequency level. In view of this, a modification of the conventional physical optics approach is being investigated in the current period by including terms up to the quadratic terms of the surface slopes in the scattering matrix. Time permitting, this phase of the work will be continued in the remaining period.

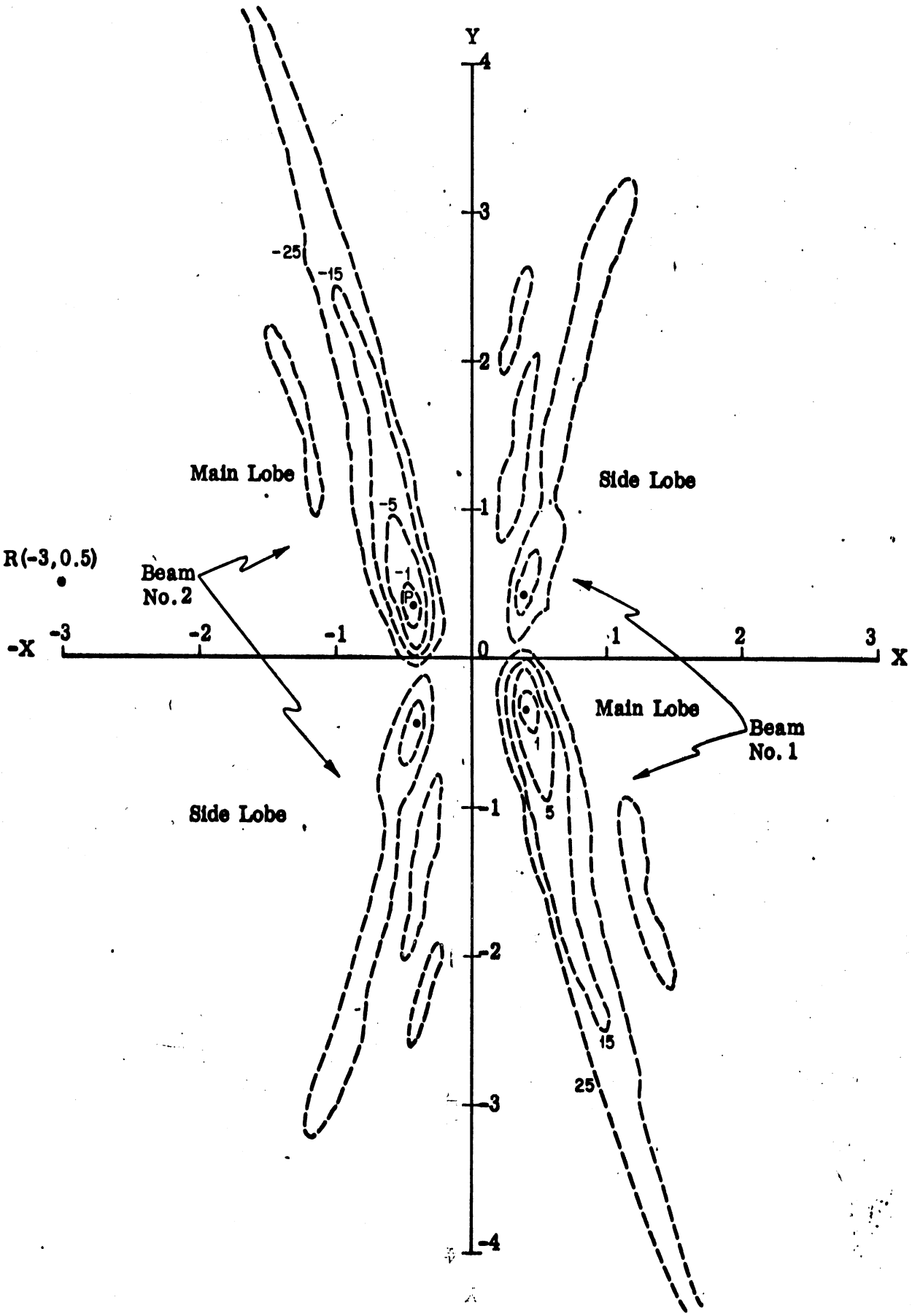

FIG. 3-1a: Projection of AN/APN-153 Radiation Pattern on XY-Plane (z_r/z_a = 0 plane).

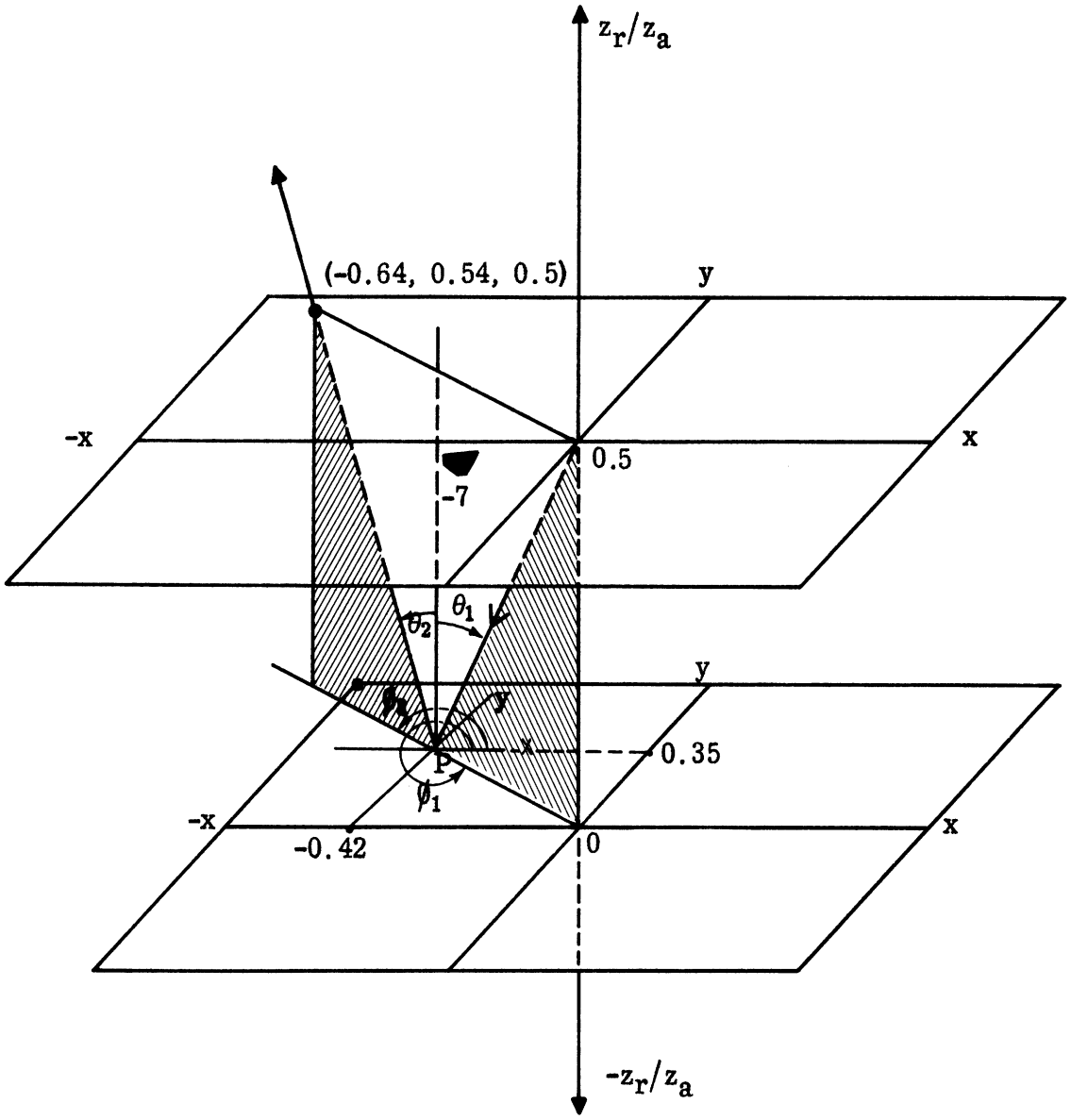

FIG. 3-1b: Geometry of Specular Reflection of the Incident Wave Which Impinges on the Point P, the Peak Point of Beam No. 2 of AN/APN-153. $\theta_1 = \theta_2 = 29^o$. $\phi_1 = 320^o$, $\phi_2 = 140^o$.

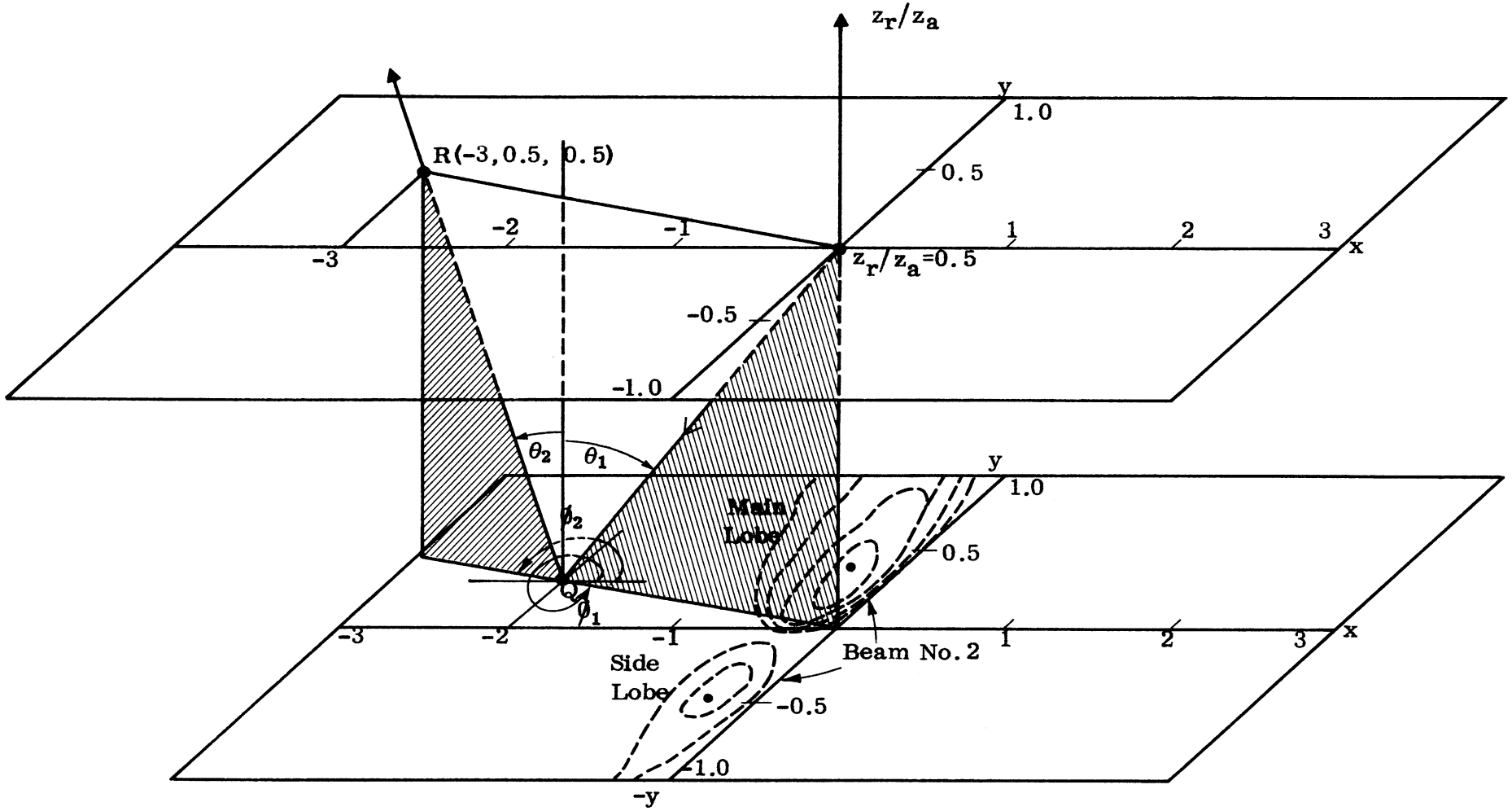

FIG. 3-1c: Geometry of the Specular Reflection Point Q (x=-2, y=0.29) for Receiver at R (x=-3, y=0.5, z_r/z_a=0.5). $\theta_1 = \theta_2 = 63^o$, $\phi_1 = 351.7^o$, $\phi_2 = 171.7^o$.

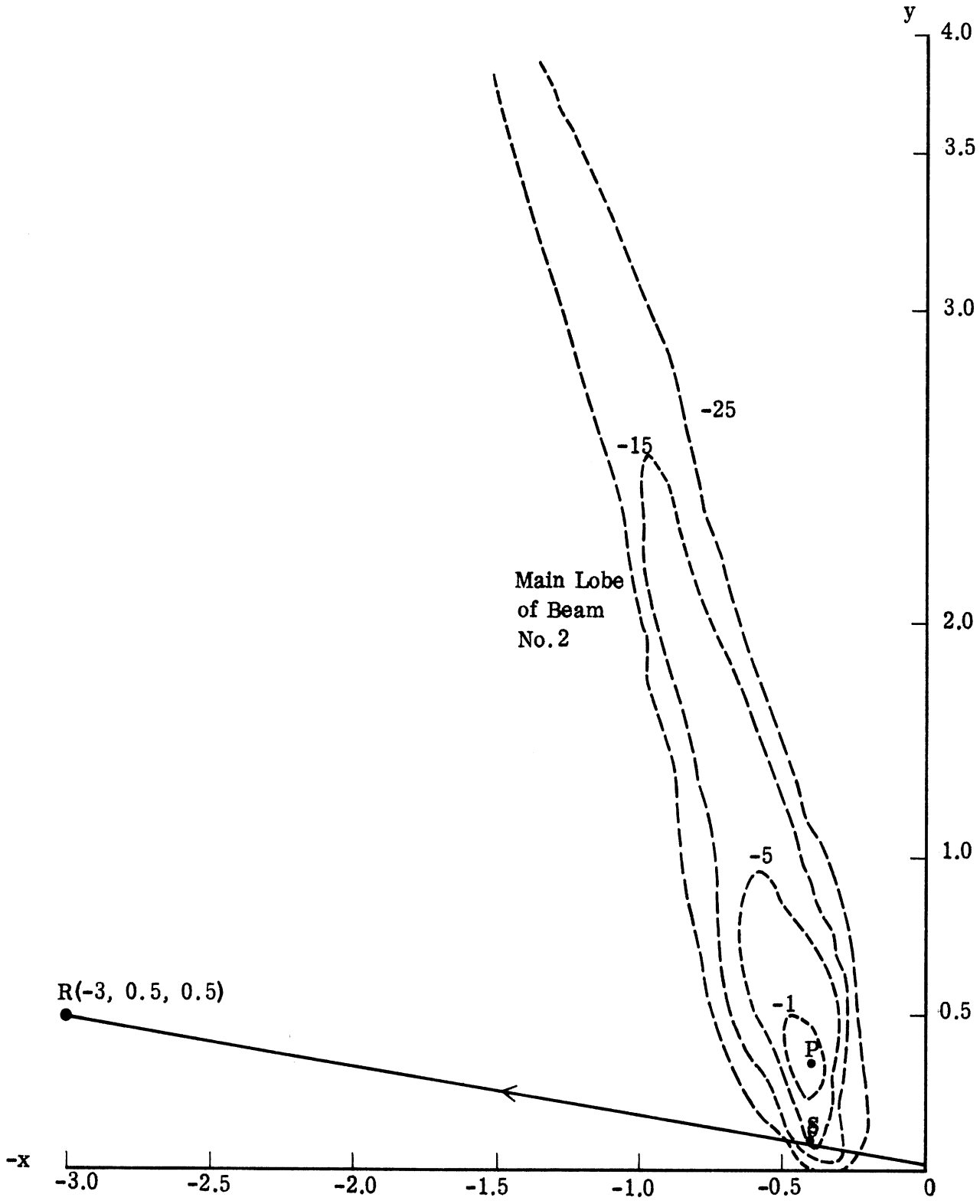

FIG. 3-1d: Position of Point S (x=-0.447, y=0.174) in AN/APN-153 Pattern from which Maximum Reflected Radiation Intensity F_{2M} Comes for Receiver Positioned at R (x=-3, y=0.5, z_r/z_a= 0.5).

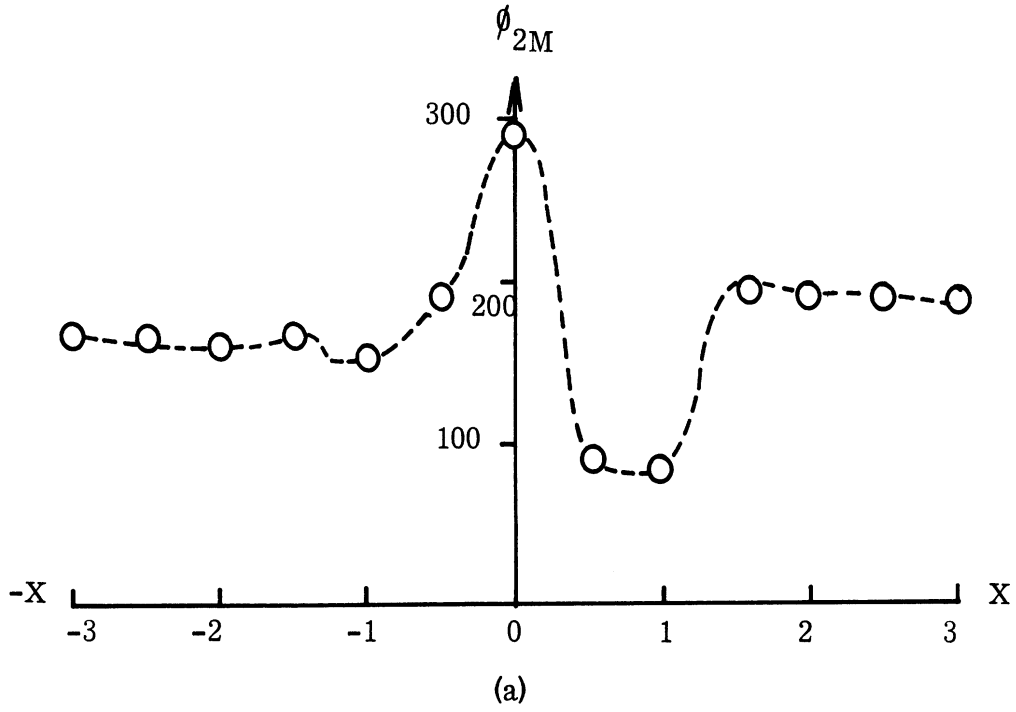

(a)

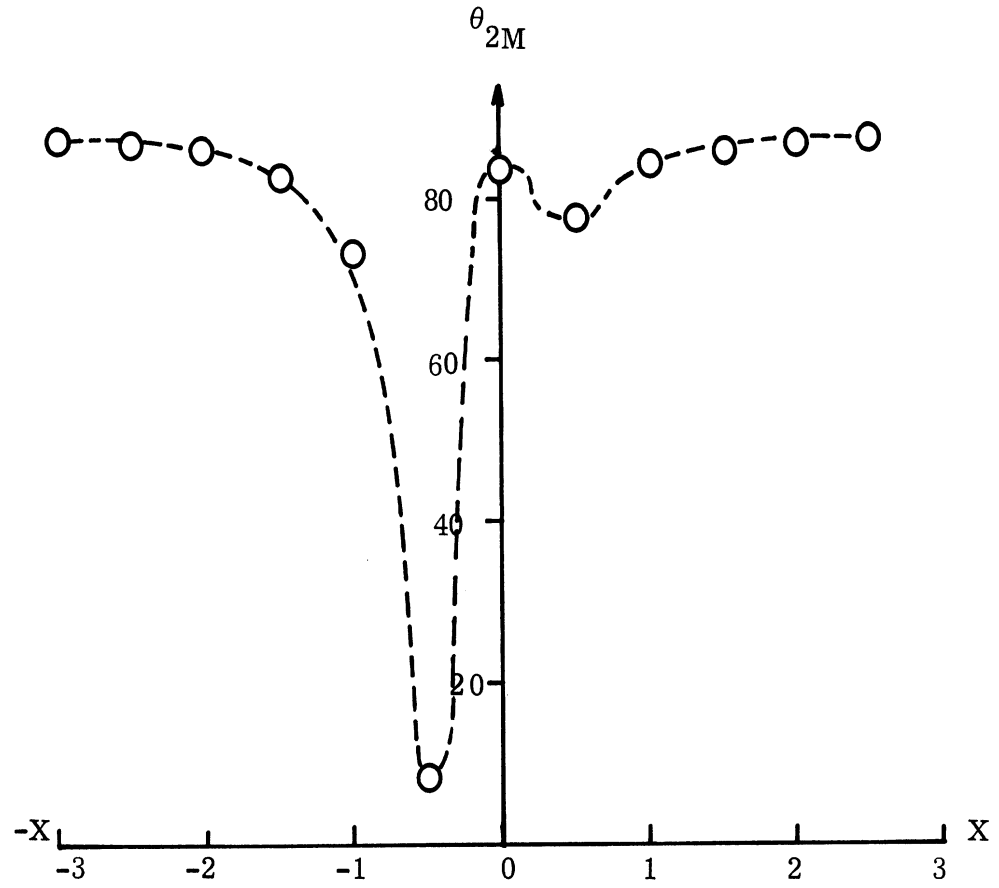

FIG. 3-2: Variation of Maximum Directions of Arrival (Latitude, Azimuth) vs X for Down Wind Speed = 1.5 m/sec; z_r/z_a = 0.1, Y=0.5.

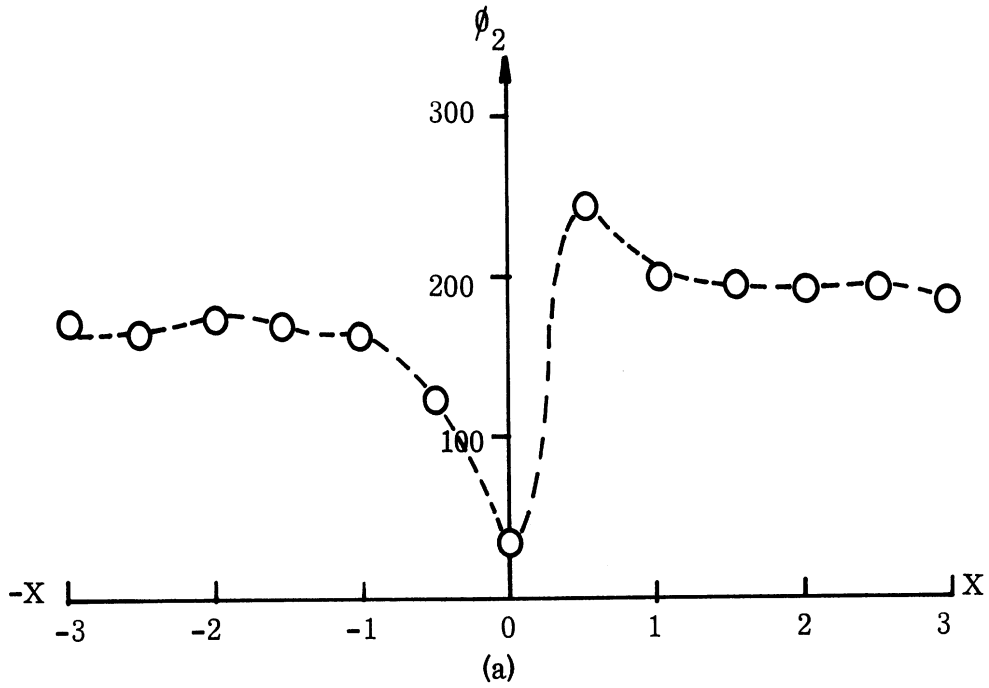

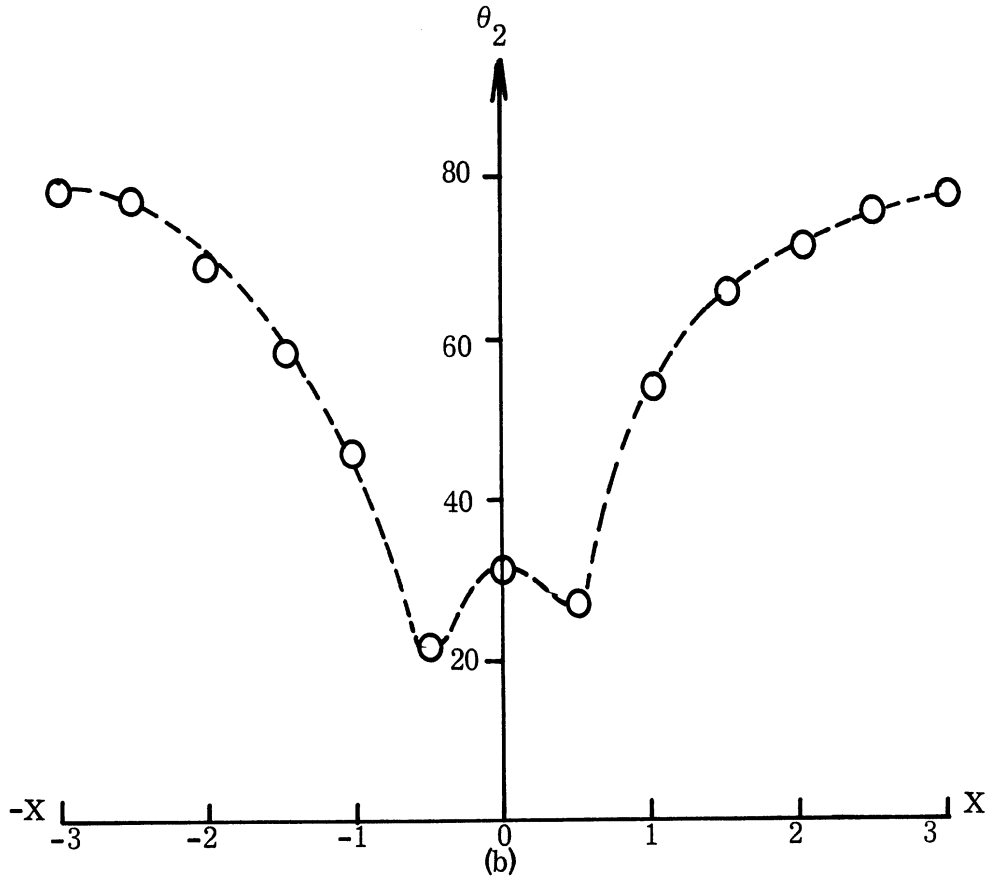

FIG. 3-3: Variation of Maximum Directions of Arrival (Latitude, Azimuth) vs X for Down Wind Speed = 1.5 m/sec; $z_r/z_a = 0.1$, $Y = 0.5$.

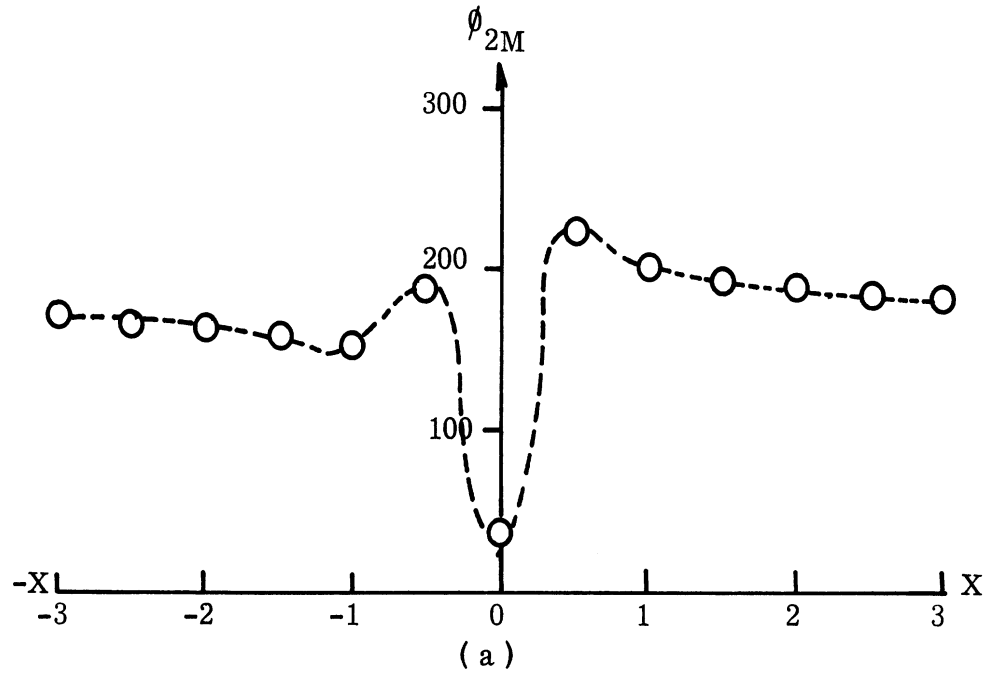

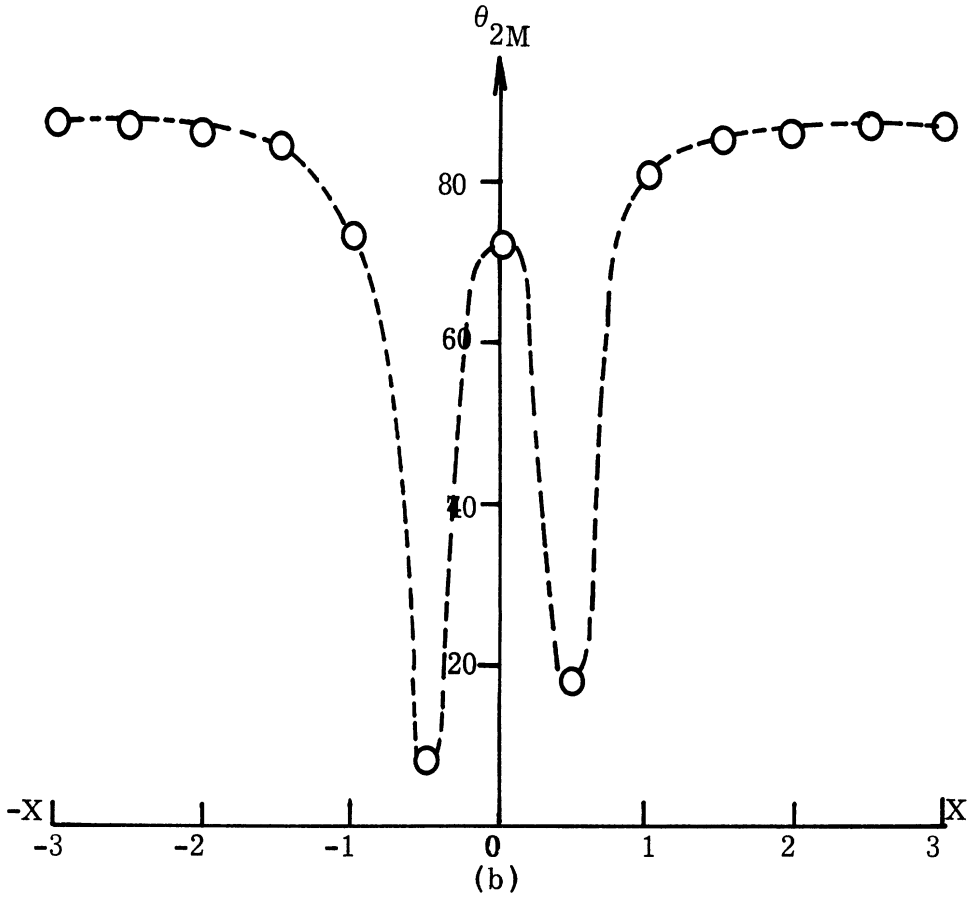

FIG. 3-4: Variation of Maximum Directions of Arrival (Latitude, Azimuth) vs X for Down Wind Speed = 4 m/sec; z_r/z_a=0.1, Y=0.1 .

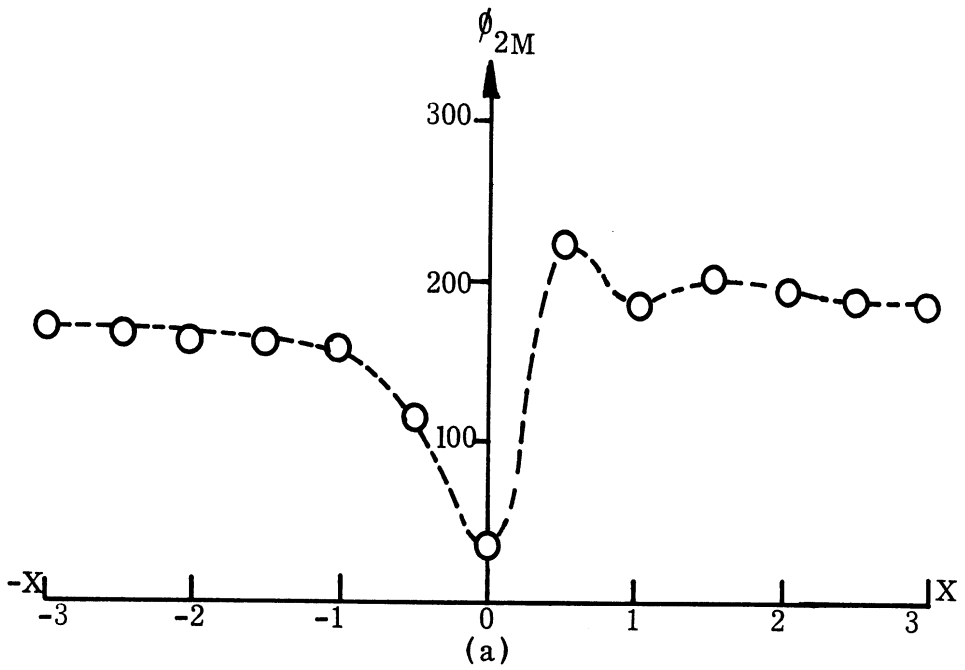

(a)

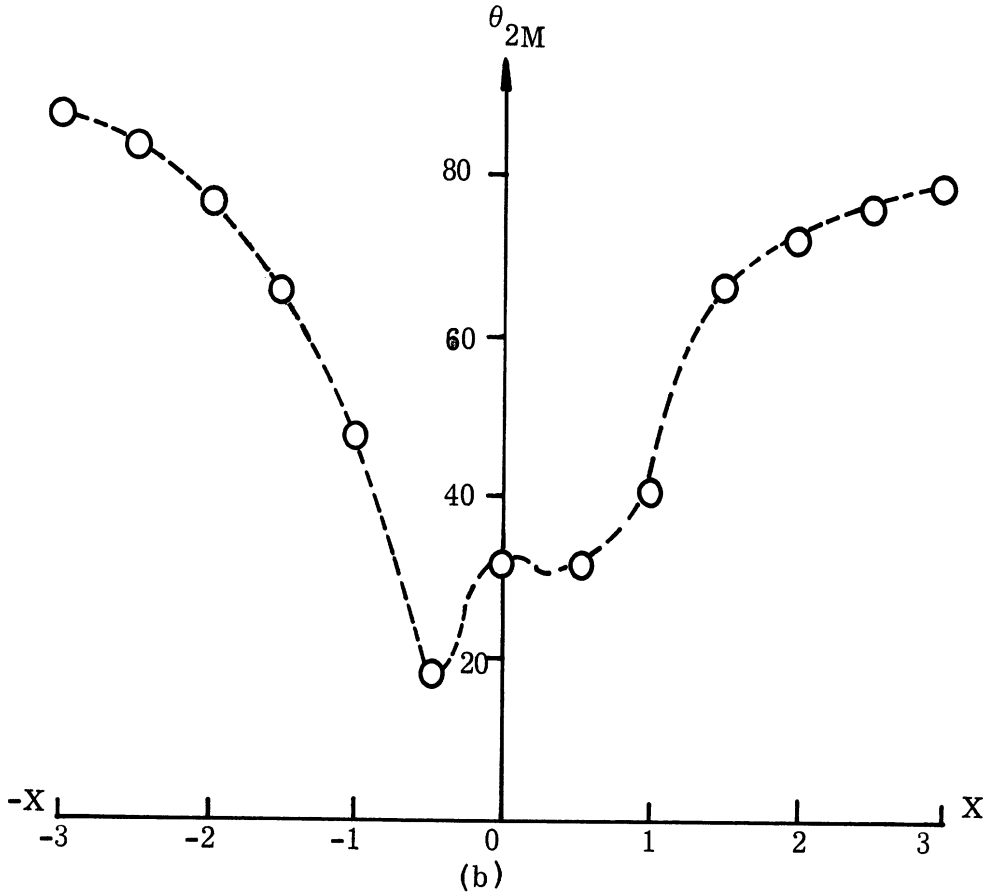

(b)

FIG. 3-5: Variation of Maximum Directions of Arrival (Latitude, Azimuth) vs X for Down Wind Speed = 4 m/sec; z_r/z_a=0.5, Y=0.5 .

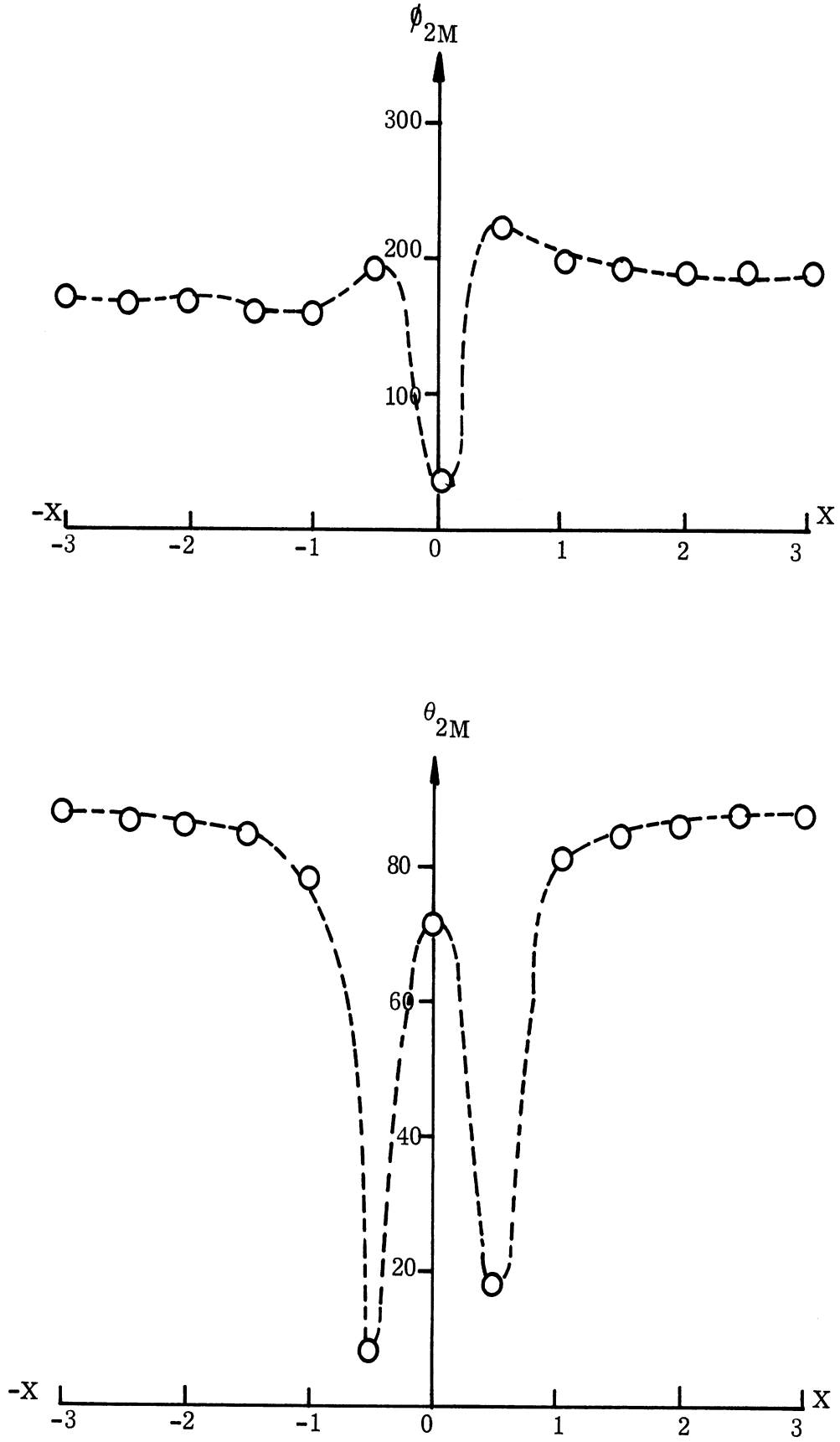

FIG. 3-6: Variation of Maximum Directions of Arrival (Latitude, Azimuth) vs X for Cross Wind Speed = 4 m/sec; z_r/z_a=0.1, Y=0.5 .

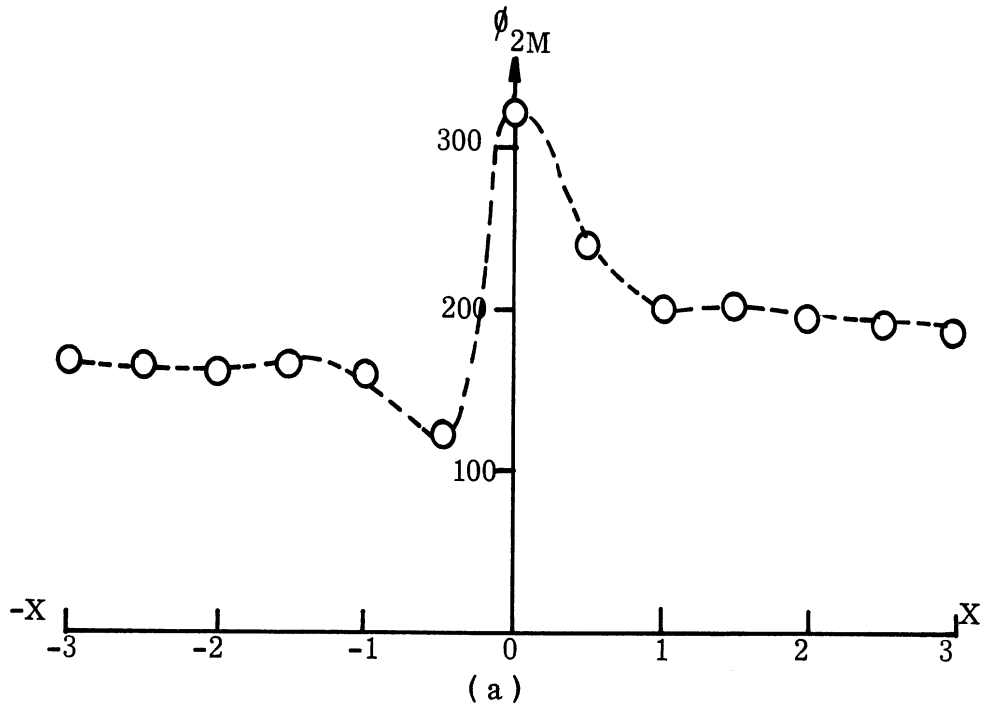

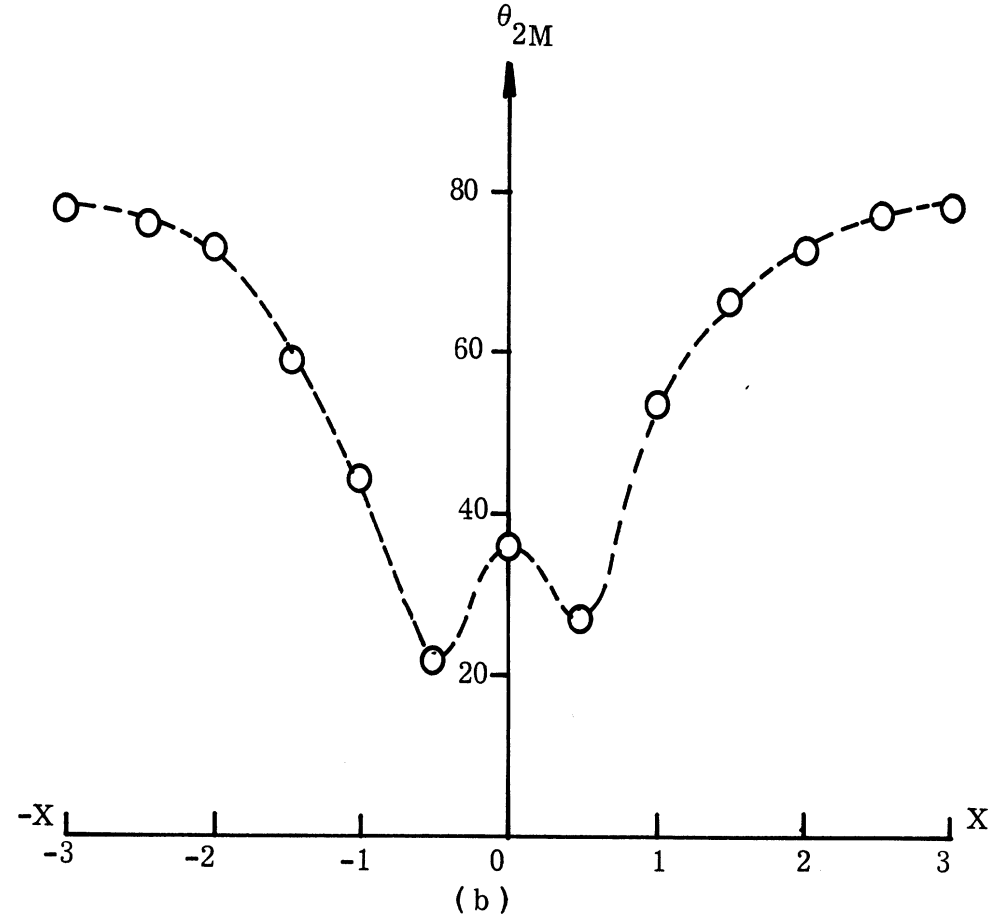

FIG. 3-7: Variation of Maximum Directions of Arrival (Latitude, Azimuth) vs X for Cross Wind Speed = 4 m/sec; z_r/z_a = 0.5, Y = 0.5 .

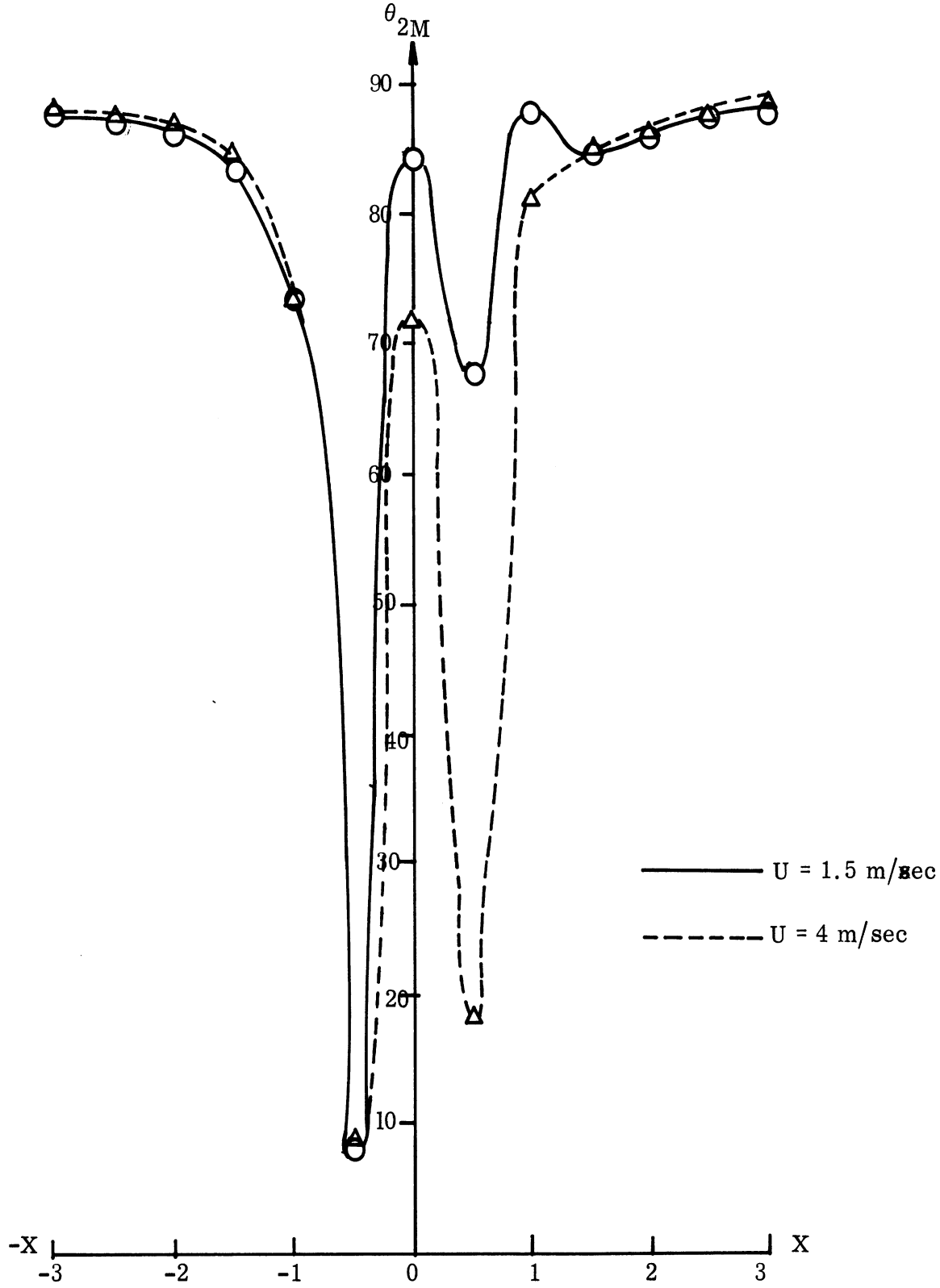

FIG. 3-8a: Effect of Wind Speed on Direction of Maximum Reflected Radition Intensity (Latitude) for Down Wind Case; $z_r/z_a = 0.1$, $Y = 0.5$.

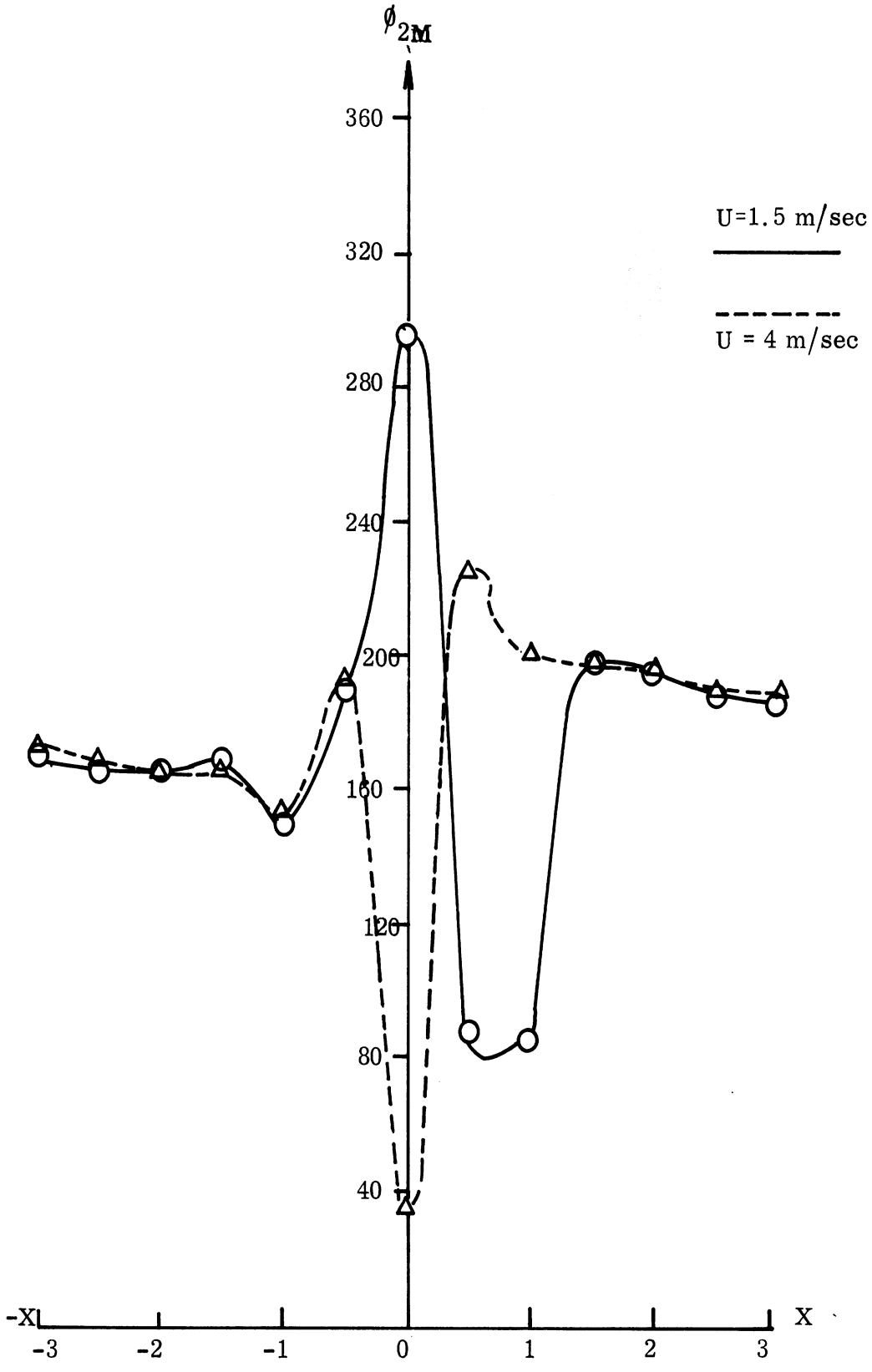

FIG. 3-8b: **Effect** of Wind Speed on Direction of Maximum Reflected Radiation Intensity (Azimuth) for Down Wind Case; $z_r/z_a = 0.1$, $Y = 0.5$.

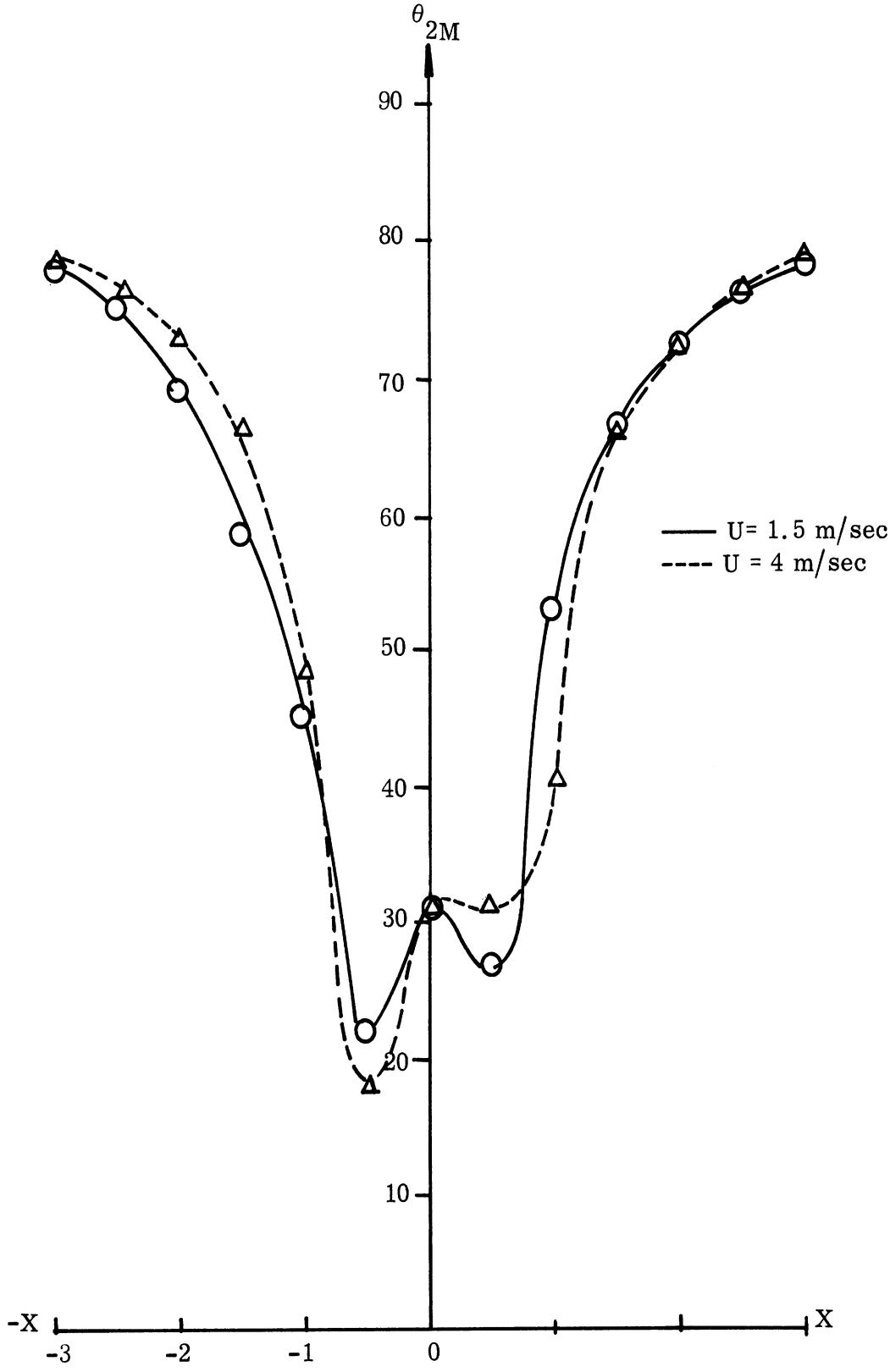

FIG. 3-9a: Effect of Wind Speed on Direction of Maximum Reflected Radiation Intensity (Latitude) for Down Wind Case; z_r/z_a=0.5, Y= 0.5 .

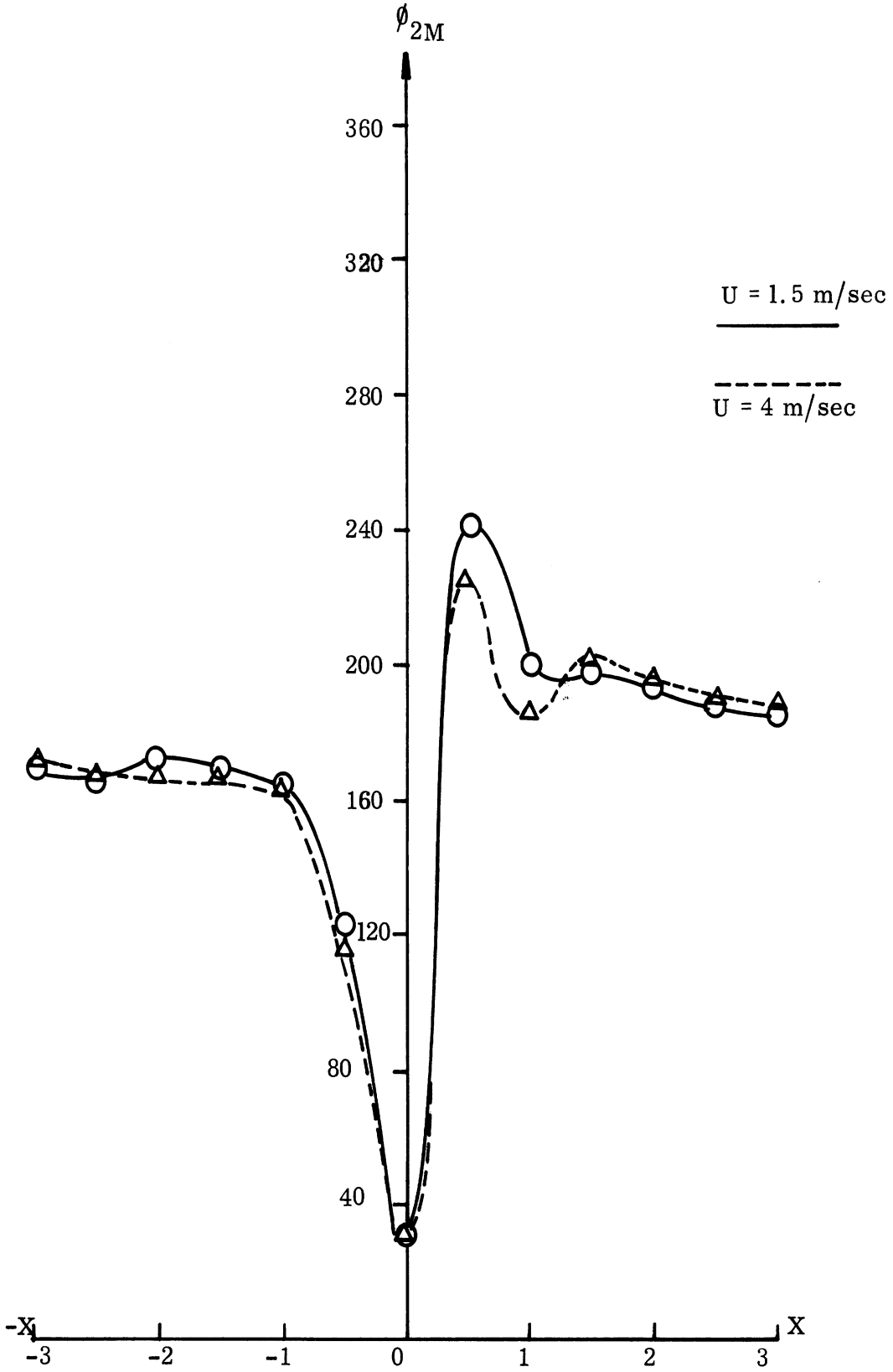

FIG. 3-9b: Effect of Wind Speed on Direction of Maximum Reflected Radiation Intensity (azimuth) for Down Wind Case; $z_r/z_a = 0.5$, $Y = 0.5$.

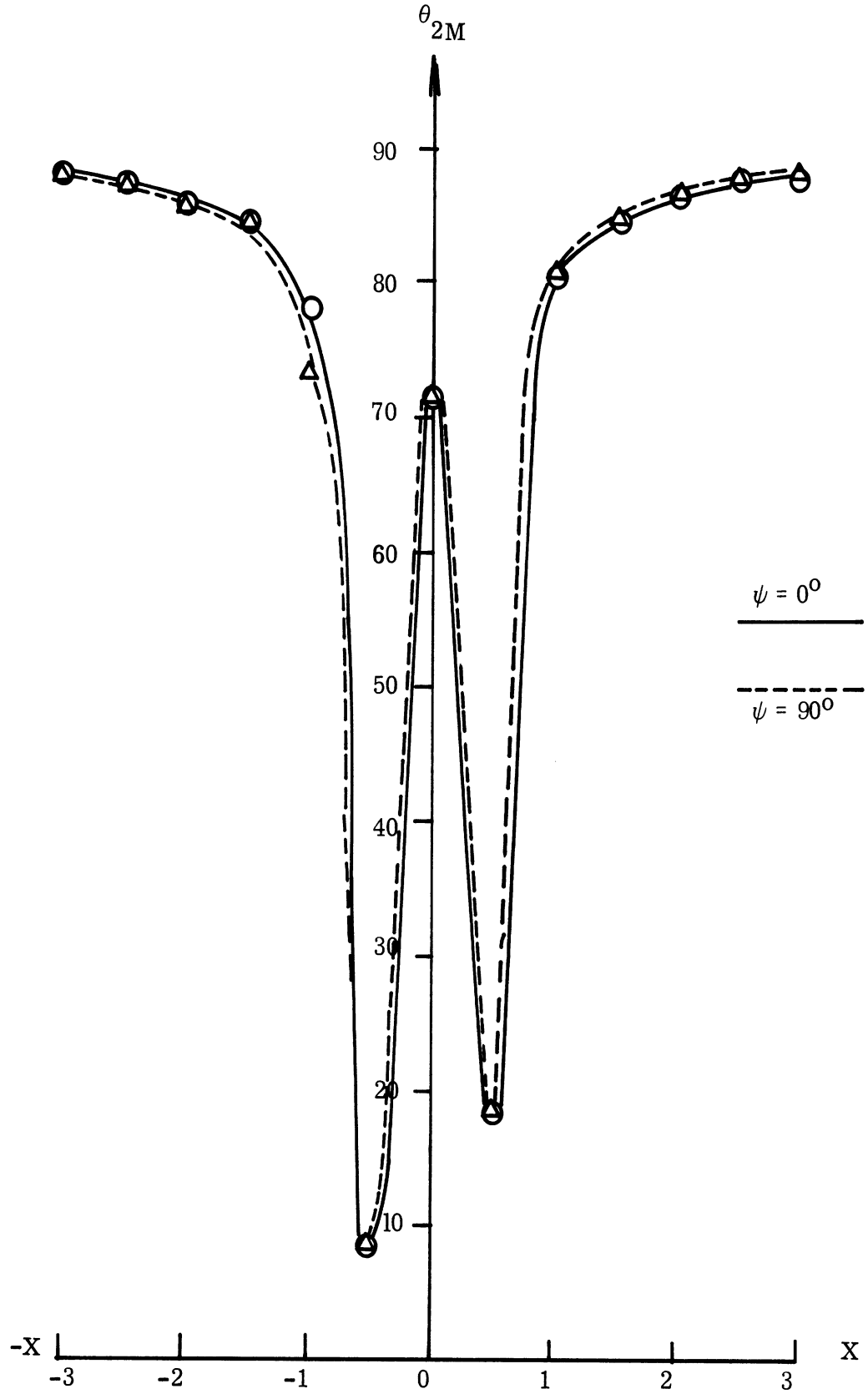

FIG. 3-10a: Effect of Wind Direction on Direction of Maximum Reflected Radiation Intensity (latitude) at Wind Speed = 4 m/sec; z_r/z_a=0.1, Y=0.5 .

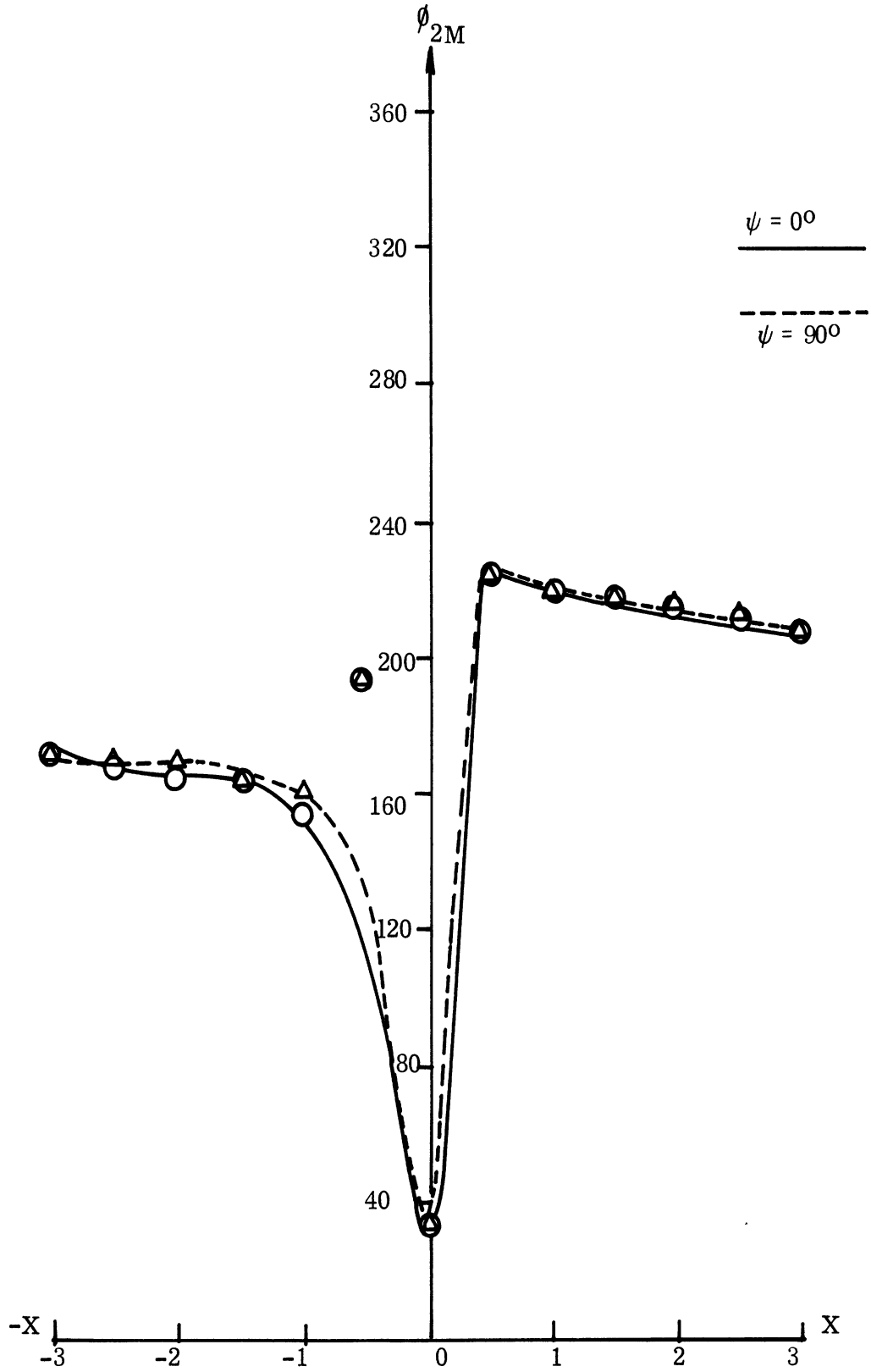

FIG. 3-10b: Effect of Wind Direction on Direction of Maximum Reflected Radiation Intensity (latitude) at Wind Speed = 4 m/sec; $z_r/z_a = 0.1$, $Y = 0.5$.

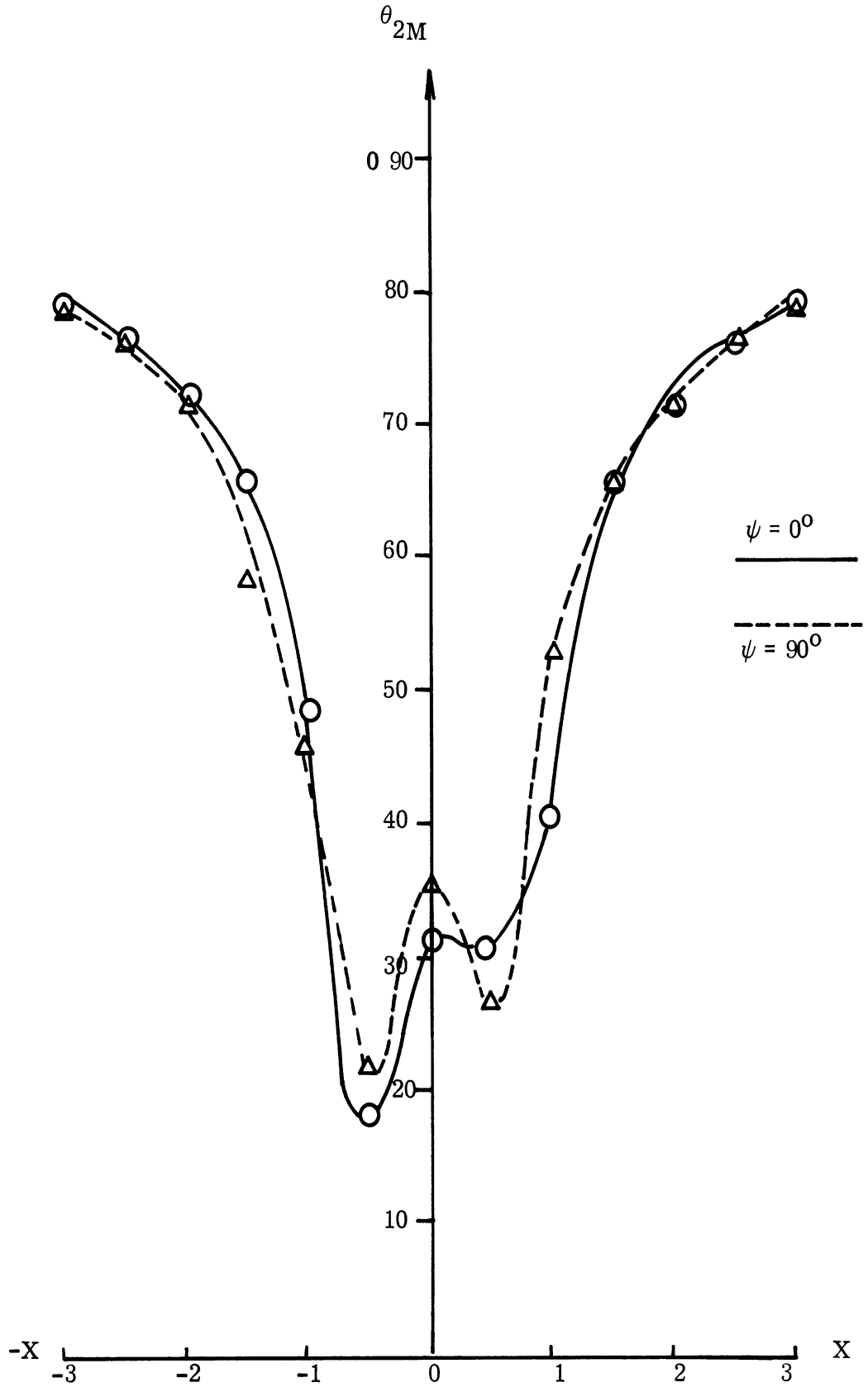

FIG. 3-11a: Effect of Wind Direction on Direction of Maximum Reflected Radiation Intensity (latitude) at Wind Speed = 4 m/sec; $z_r/z_a = 0.5$, Y= 0.5.

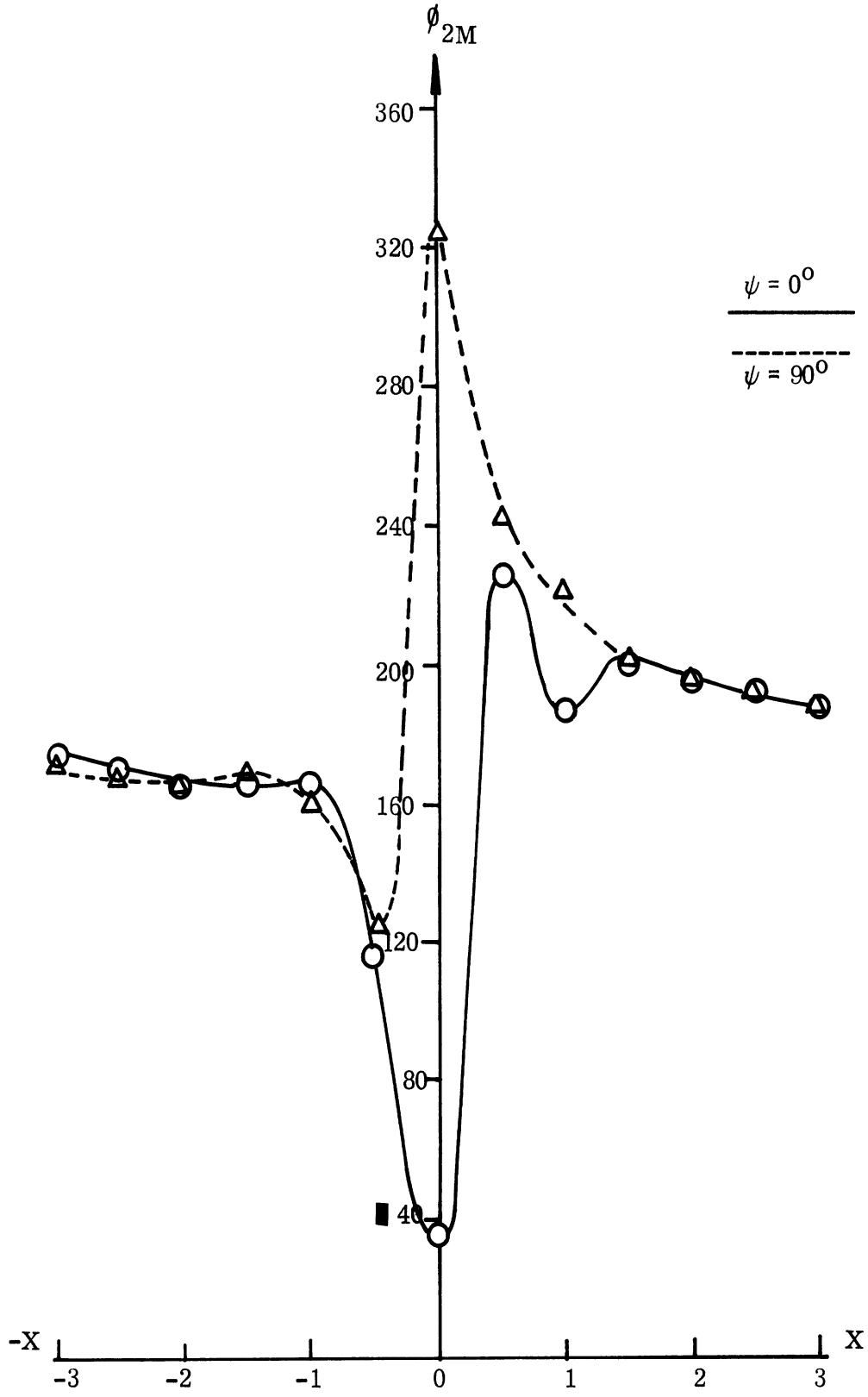

FIG. 3-11b: Effect of Wind Direction on Direction of Maximum Reflected Radiation Intensity (azimuth) at Wind Speed = 4 m/sec; $z_r/z_a = 0.5$, Y= 0.5 .

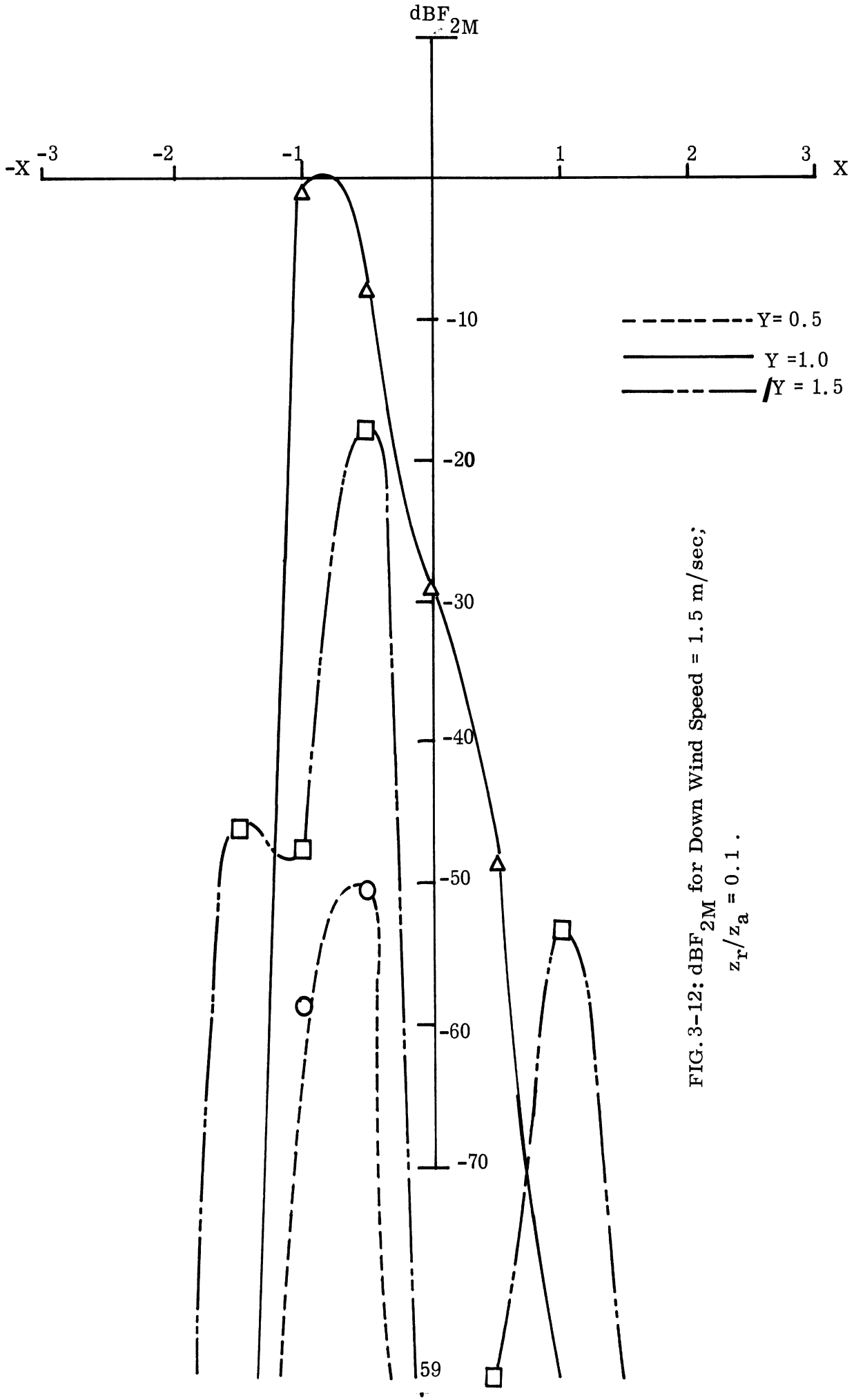

FIG. 3-12: dBF_{2M} for Down Wind Speed = 1.5 m/sec; $z_r/z_a = 0.1$.

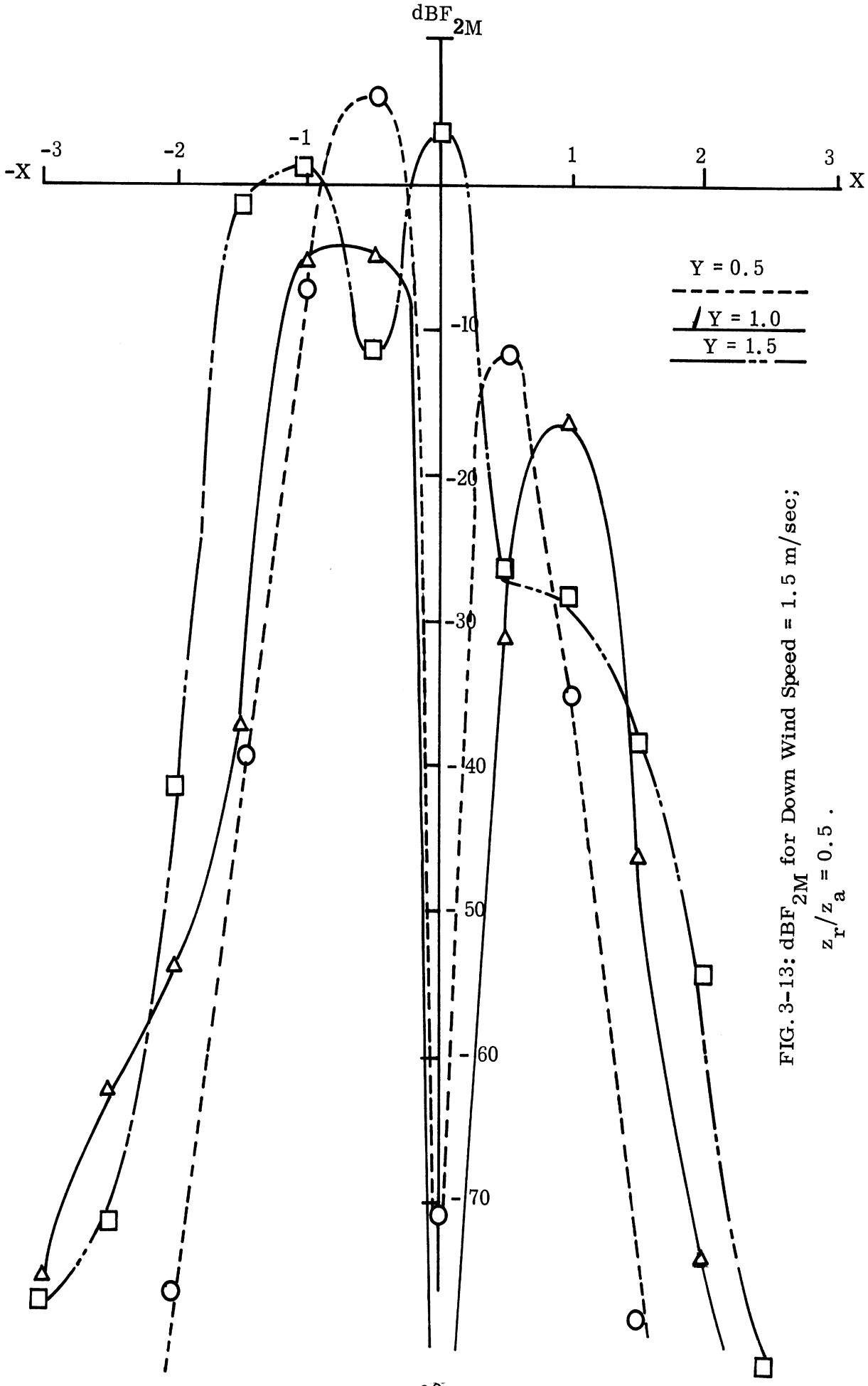

FIG. 3-13: dBF_{2M} for Down Wind Speed = 1.5 m/sec; $z_r/z_a = 0.5$.

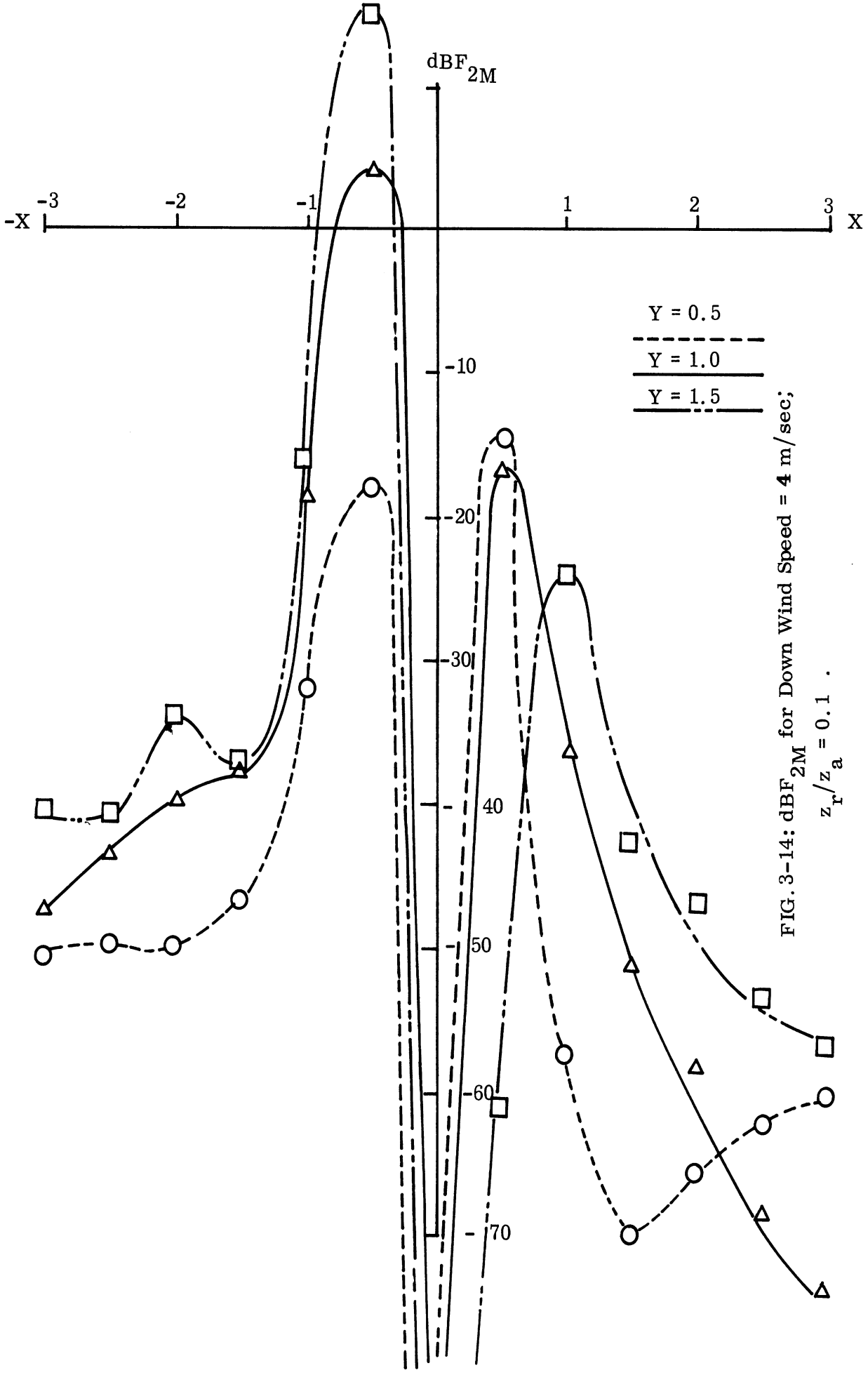

FIG. 3-14: dBF_{2M} for Down Wind Speed = 4 m/sec; $z_r/z_a = 0.1$.

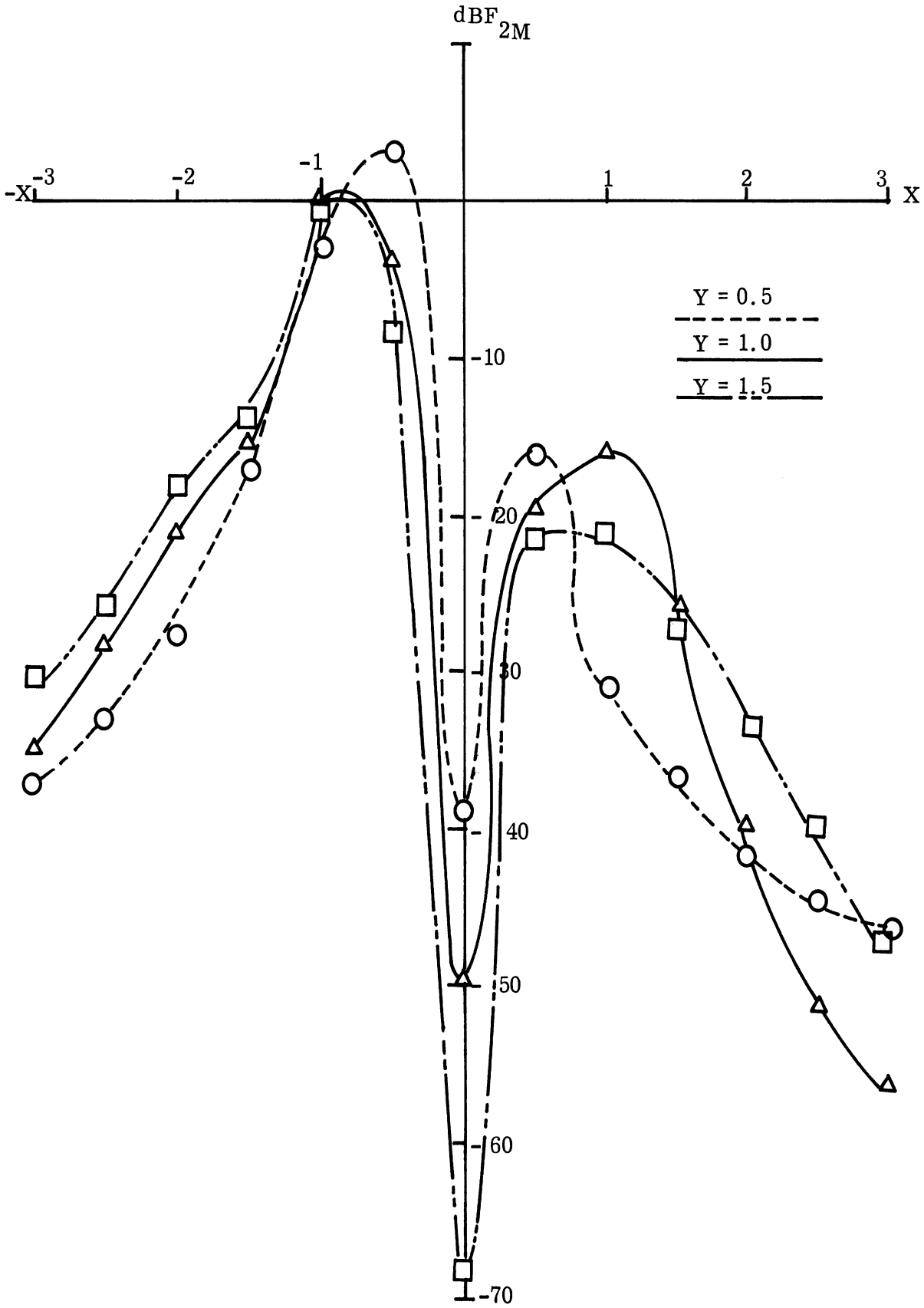

FIG. 3-15: dBF_{2M} for Down Wind Speed = 4 m/sec; $z_r/z_a = 0.5$.

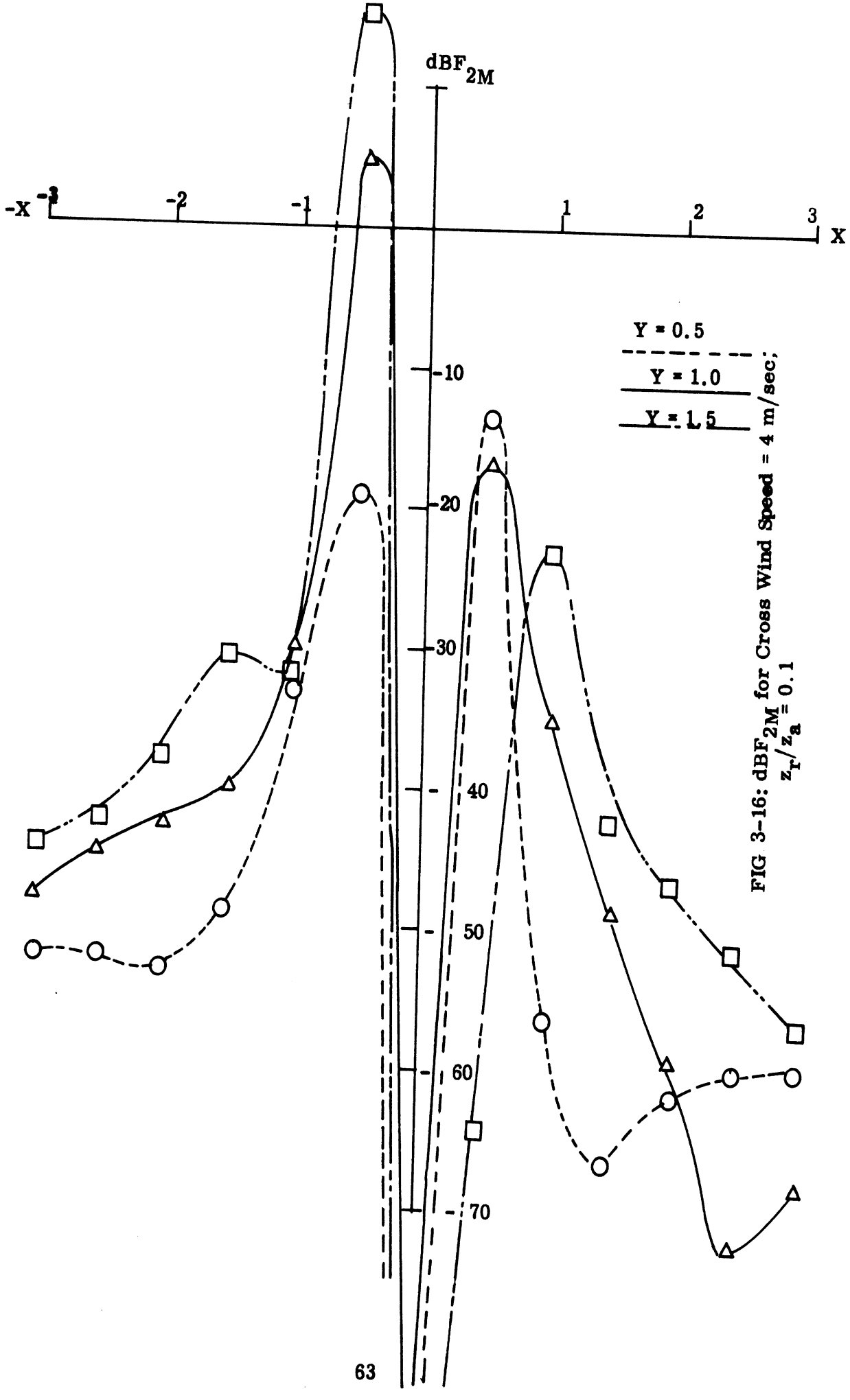

FIG 3-16: dBF_{2M} for Cross Wind Speed = 4 m/sec; $z_r/z_a = 0.1$

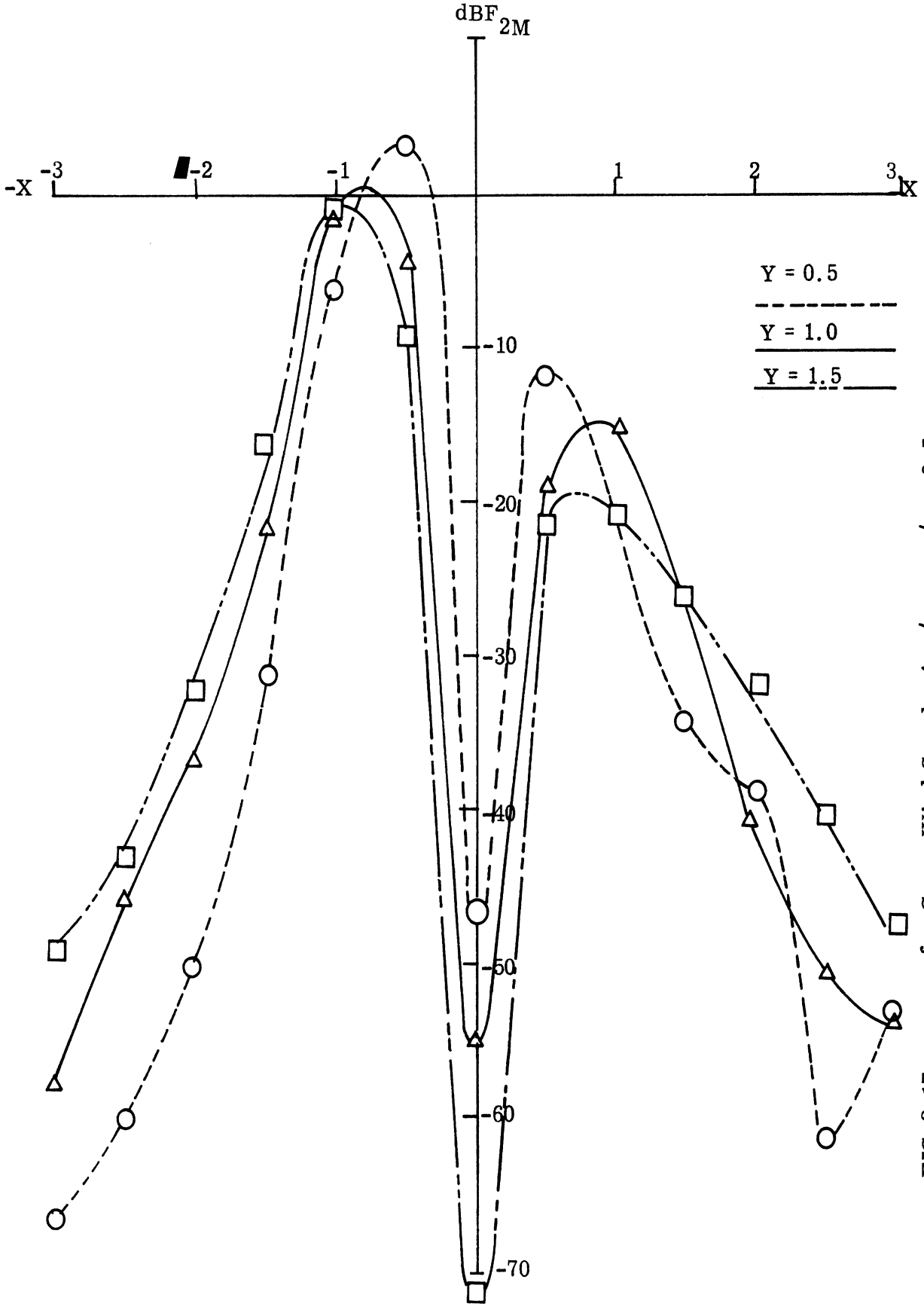

FIG. 3-17: dBF_{2M} for Cross Wind Speed = 4 m/sec; $z_r/z_a = 0.5$

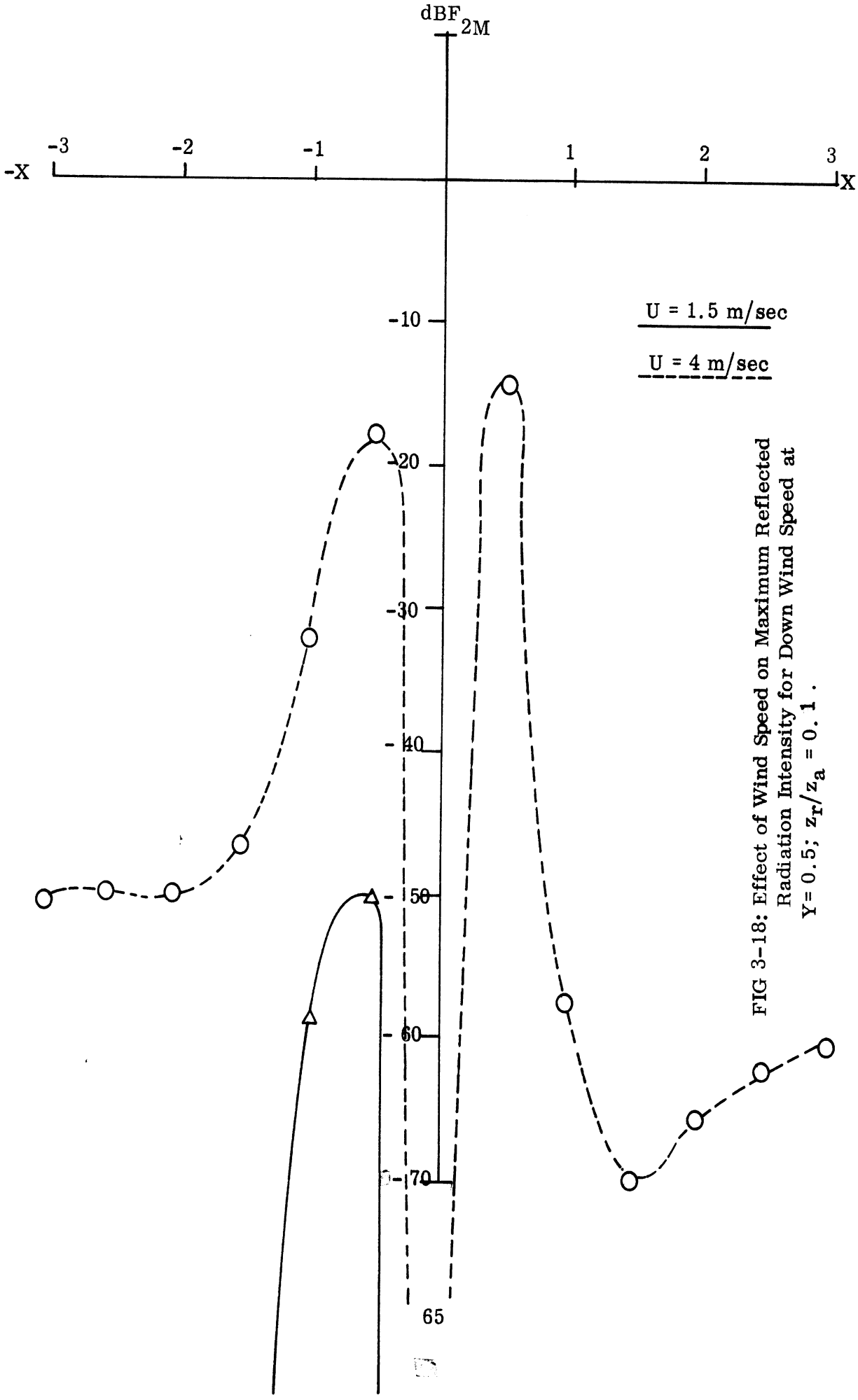

FIG 3-18: Effect of Wind Speed on Maximum Reflected Radiation Intensity for Down Wind Speed at Y= 0.5; $z_r/z_a = 0.1$.

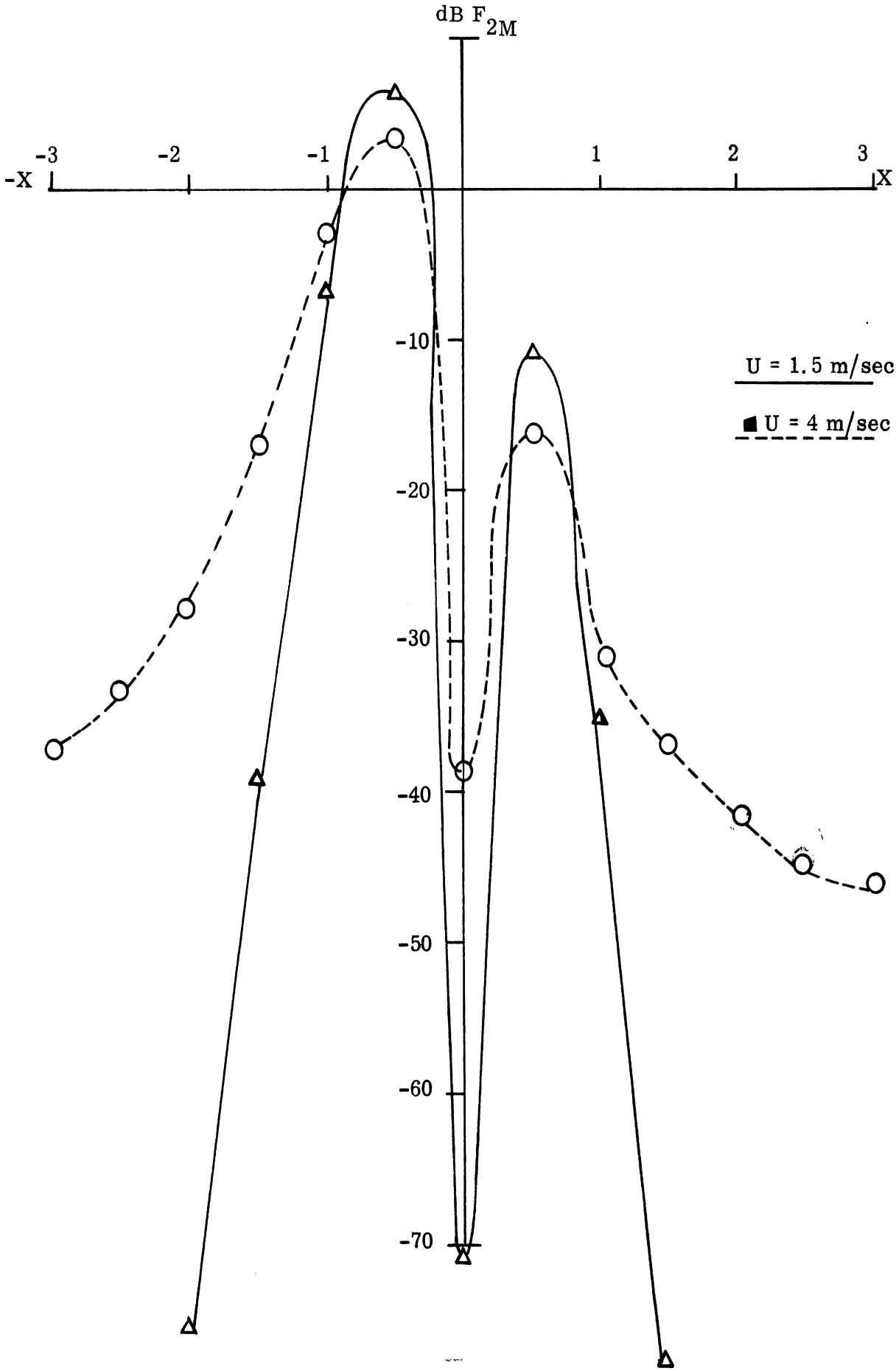

FIG. 3-19: Effect of Wind Speed on Maximum Reflected Radiation Intensity for Down Wind Speed at Y = 0.5; $z_r/z_a = 0.5$.

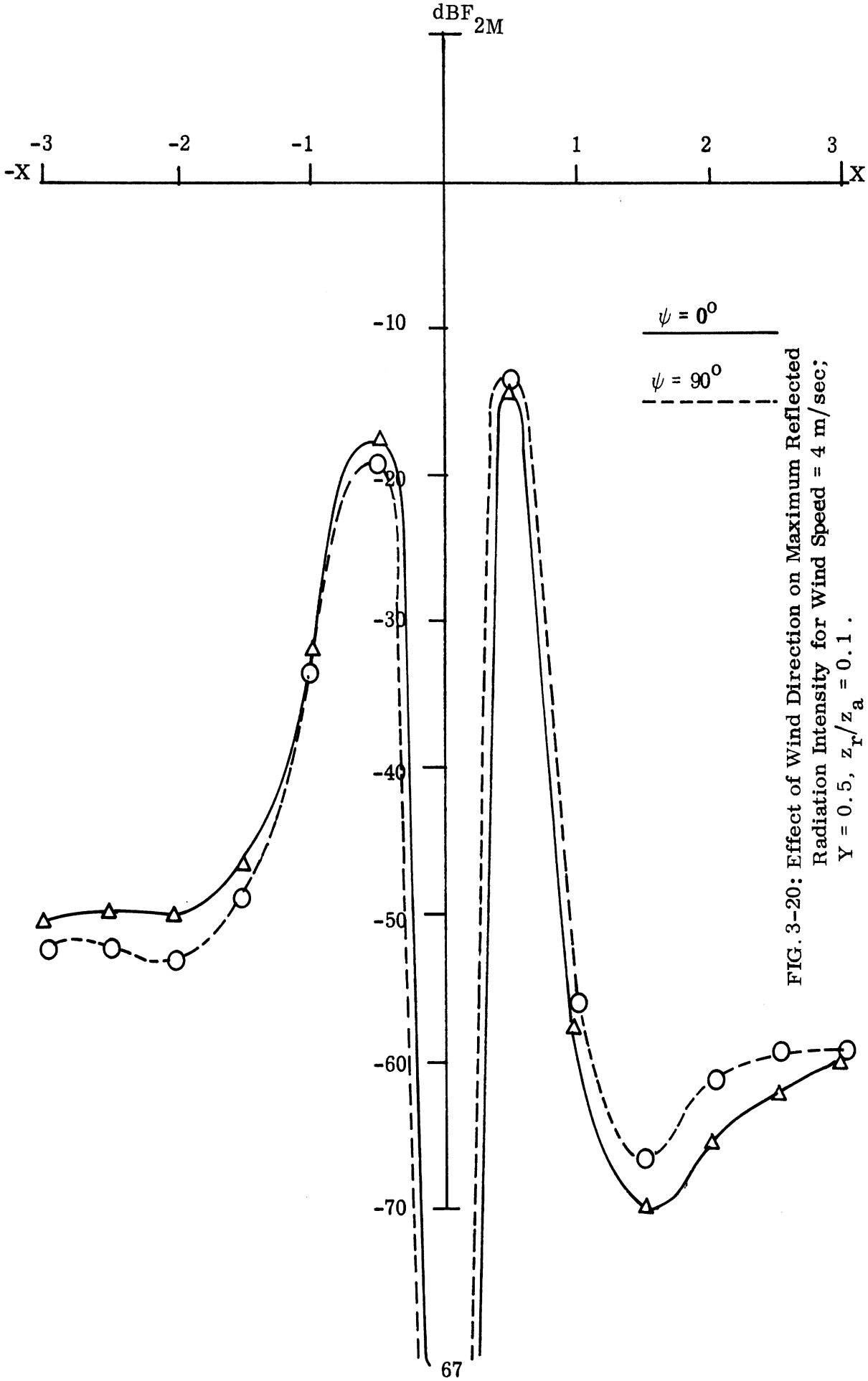

FIG. 3-20: Effect of Wind Direction on Maximum Reflected Radiation Intensity for Wind Speed = 4 m/sec; Y = 0.5, z_r/z_a = 0.1 .

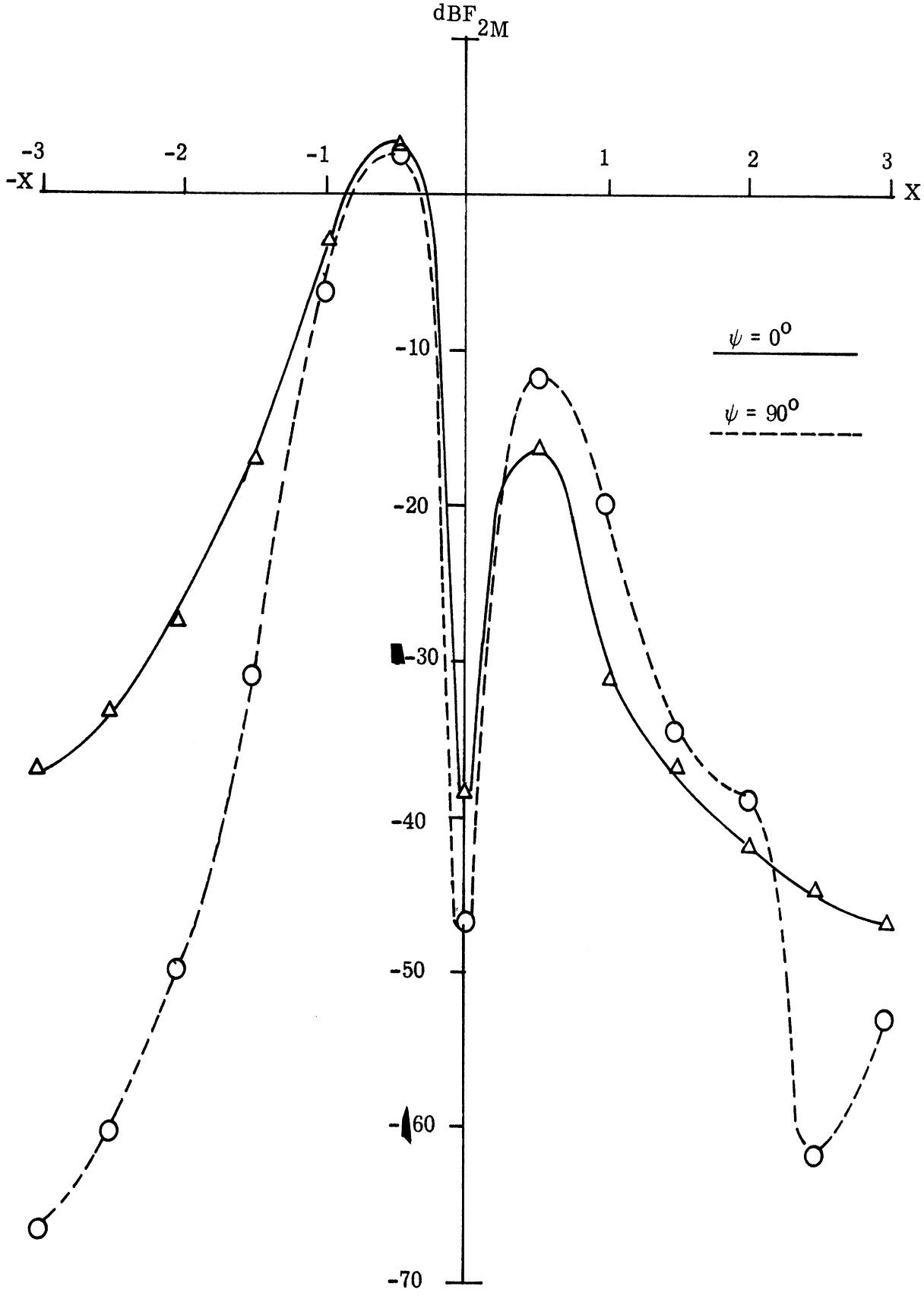

FIG. 3-21: Effect of Wind Direction on Maximum Reflected Radiation Intensity for Wind Speed = 4 m/sec; Y=0.5, $z_r/z_a = 0.5$

IV

EXPERIMENTAL EFFORT

This study was conducted in accordance with the change of scope of the Doppler Radiation Study Contract N62269-68-C-0715 (para. 3). To ensure a maximum of operating time, the fly-by tests were conducted at Key West, Florida. The test site was a battery-operated lighthouse located on a small island referred to as Sand Key. The focal point of the light at Sand Key is 109' above sea level and our equipment was operated at 100 ' above sea level. In addition to tests that were conducted at the top of the lighthouse, data were also collected with the test equipment located on the beach of Sand Key. An aerial photograph of the Sand Key lighthouse is shown in Figure 4-1.

One of the principal advantages of the Sand Key test site was the fact that it was located remotely from surrounding land obstructions and gave an excellent view of the water from any angle that one wished to direct the receiving antenna. However, a disadvantage associated with the Sand Key site was the relatively shallow water conditions in that area. The problem here being that when the seas became heavy, e.g. the waves being more than 1 or 2 feet in height, there was sufficient undertow near the surface of the water to cause the waves to break and have white-caps. This situation would not exist in the open sea in areas of typical depth where the water would tend to have more of a roll to it, and the wave motion would be more sinusoidal in nature. However, it is believed that the principal factor influencing the scattering of the doppler energy is the ripples (on the ocean surface) that are associated with the water motion. Such ripples will generally exist in relatively calm seas and will always be found in rough seas. Ripples were present at all times and in all areas involved in these tests except for a small area adjacent to the sand.

During this investigation data were collected from two doppler navigation systems; the first was a GPL system having a military designation of AN/APN-153. The second system was fabricated by the Teledyne Ryan Corporation of

San Diego and is designated as a 733 system. The differences between these two systems were primarily the fact that the GPL system radiates in the range of 10 watts of RF power and employs a gimballed low gain antenna system with the beams stabilized with respect to the vertical. The Ryan system, on the other hand, radiates approximately 800 milliwatts of RF power and employs a high gain antenna system fixed with respect to the aircraft. It should be noted that the GPL antenna radiates a relatively broad beam of energy cross-track to the aircraft and a narrow beam along the track of the aircraft. The Ryan system radiates a narrow beam both in the cross-track and along the track of the aircraft.

During this experimental effort, two aircraft were flown at three altitudes of 100', 300' and 3000' above sea level. The sea state varied from a relatively calm sea (with light ripples, perhaps 1 to 2 inches in height) to a relatively rough sea having waves 3' to 5' in height with 20' or so inbetween waves and with rippling on the surface of the waves from 2" to 5" in height. Two receiving antennas were used, however, only one at a time. The first antenna had a relatively narrow beam with a half-power beamwidth of 9^{o} and a gain of 25 dB above an isotropic source. The second antenna had a half-power beamwidth of 16^{o} and a gain of 20 dB.

Employing the above circularly polarized receiving horns, data were collected through the use of a laboratory type high frequency receiver (Micro-Tel, WR-200) . The output of the receiver was then fed to both a magnetic tape recorder (Sony Model 600) and an oscilloscope (Hewlett - Packard Model 130 C) . The magnetic tape recorder has a dual input such that on one channel we recorded the signal level scattered by the doppler system and on the second channel we inserted voice information to aid in later reduction of the data. A portable 6000 kva 60-cycle generator was employed to power the electronic equipment. To provide communication between the receiving site at Sand Key and the aircraft , a military ARC-27 transceiver was used.

Scheduling of aircraft was such that operations began each day at approximately 8:00 AM and continued to approximately 3:00 PM. A project flight schedule is shown in Table IV-1. This will provide insight into the hours that were flown and reasons for cancelled flights. The work day for the Sand Key personnel normally started at 7:30 AM and ended at 5:00 PM. These personnel departed from the Naval Ordnance Unit Dock at Key West sometime between 7:00 and 7:30 in the morning. It took approximately one hour to transit from Key West to Sand Key. It generally took an additional half hour to set up the equipment. The aircraft generally came on sight at 8:00 AM and until 9:00 AM it was used to conduct unrelated tests for the Naval Air Development Center personnel while the Sand Key receiving site was being set up. This is referred to in Table IV-1 as "Sea Drift".

Two aircraft were used; the first was a C-117-D equipped with the Ryan doppler system. The second aircraft was an S-2E supplyed by the Naval Air Facilities at Key West and this system employed the GPL-APN-153 doppler system. Generally the schedule was such that the C-117 aircraft flew in the morning and the S-2E in the afternoon. Each aircraft was scheduled to fly from two to three hours each day.

Data collected during the week and a half stay at Key West is now being reduced at The University of Michigan. We may make a few preliminary comments that have been observed to date. Data thus far collected appears to be pretty much in agreement with data that we collected during the initial portion of this study at the Lake Michigan test site (Report 1969-1-F). In the Key West tests, we have noted that the aircraft signal was detectible earlier than had been predicted from our analytical studies. For example, when the aircraft was flown at an altitude of 300', and with the receiving equipment located 100' above sea level, it was observed that the aircraft could be detected at range 1500' or so greater than predicted. This was also observed in the previous data collected on Lake Michigan and an explanation for this was given in that Phase I Report. We found also that if one employs a higher gain receiving

antenna the signal level detected is correspondingly greater and the aircraft can be detected over a greater range. A third observation made is that as the sea becomes rougher, it has little effect on the detectibility of the doppler system. Here we hypothesize that the ripple structure of the large waves has more effect on the detectibility of the aircraft than the large swells associated with the sea state.

During recent tests we observed that regardless of the pointing direction of the antenna with respect to the wave motion, and regardless of the direction of the wind and the motion of the large wave surface, scattered RF energy was always detected. This observation leads one to conclude that the rippling disturbance on the surface of the sea is the great contributor to the detection of doppler energy that is forward scattered from the sea.

To give the reader some insight into the weather conditions prior to, and during the week and a half that these tests were conducted, Table IV-2 is included. This information was acquired from the Coast Guard Station at Key West.

The data discussed above was collected with the aircraft in level flight with the surface of the sea, as in measuring the doppler scatter from the sea surface. As previously noted we had the aircraft fly from 100' to 3000' above the sea, and at all times were able to detect RF energy scattered from the sea surface. A limited amount of data were collected with the aircraft at an altitude of 300' above the sea while the receiving site was located on the beach of Sand Key. Again we were generally successful in detecting the aircraft as a result of energy being scattered from the sea. In a third test the aircraft was flown in a turning pattern (aircraft bank angle of 20^{o} - 30^{o}) similar to what may be employed in the launching of an aircraft from an aircraft carrier and then banking as it makes a turning maneuver. In a typical example of these tests, the C-117 (employing the fixed antenna system) did some banking maneuvers. During these maneuvers it was found that it was possible to detect the aircraft as a result of energy being scattered off from the sea as the aircraft crossed in front of the receiving antenna with the underside of the fuselage tilted toward the receiving site.

FIG. 4-1: Sand Key Lighthouse.

Table IV-1

Project Flight Time

Hours Scheduled C117	Hours Scheduled S2E	Date	Test	Hours Flown C117D-BuNo. 12431	Hours Flown S2E(VX-1 "Eyesight 14") and "Eyesight 12"	Test
		Mon.26 Jan.	Test Hop	0.3	0.0	
		Tues.27 Jan.	Transit	7.0	0.0	No Schedule
		Wed.28 Jan.	No Schedule	0.0	0.0	
2	3	Thur.29 Jan	Cancelled Scheduled Flight for S2E		2.5	Doppler ("Eyesight 14")
3	3	Fri.30 Jan.	Sea Drift	1.0	0.0	Cancelled IFR (Fog)
			Doppler	2.5		
			Sea Drift	1.0		
3	0	Sat.31 Jan.	Cancelled Scheduled Flight due to Hi-Winds	0.0	0.0	Not Scheduled
0	0	Sun.1 Feb.	No Schedule	0.0	0.0	Not Scheduled
4	3	Mon.2 Feb.	Sea Drift	1.0	2.25	Doppler ("Eyesight 14")
			Doppler	1.5		
			"	1.5		
3	3	Tues.3 Feb.	Cancelled Schedule due to Hi-Winds and Rain	0.0	0.0	Cancelled Weather
5	3	Wed.4 Feb.	Doppler	1.0	0.0	Cancelled due to Project Equipment Malfunction
			"	1.7		
5	3	Thurs.5 Feb.	Doppler (AM)	1.5	1.0	Doppler ("Eyesight 12")
			Sea Drift	1.0		
		Fri.6 Feb.	Transit	6.5	0.0	No Schedule

Total: 25 15 Transit Time 13.5

Total flight time Sea Drift 4.0 + 0 = 4 hours sea drift

Doppler 9.2 + 5.75 ≈ 15 hours total beam scat

19.0 Hours Flown

40 Hours Scheduled 48 Percent of Scheduled Time Flown

Lost 27 Percent of Scheduled Time to Weather

Lost 25 Percent Maintenance and Project Equipment.

Table IV-2

Mean Wind and Temps Sunrise to Sunset at NQX.

Jan. 1970	Wind	Temp.	Feb. 1970	Wind	Temp.
5	070°/10-18 kts	70°F	1	110/17-25 kts.	70°
6	210/10-15	76°	2	140/13-20	75°
7	340/14-22	64°	3	200/17-27(noon)	70°
				210/16-25	64°
8	010/10-20	54°			
9	360/10-15	52°	4	010/15-23	50°
10	030/08	49°	5	030/12-18	60°
11	090/06	54°			
12	230/07	73°			
13	020/08	62°			
14	070/07	64°			
15	180/10	73°			
16	Lgt. Variable	65°			
17	Lgt. Variable	72°			
18	260/08	74°			
19	250/08	75°			
20	200/05	70°			
21	350/10	64°			
22	340/10	61°			
23	Lgt. Variable	67°			
24	350/10-15	65°			
25	050/06	71°			
26	130/06	76°			
27	070/08	74°			
28	080/10	77°			
29	110/10-15	77°			
30	300/08	75°			
31	020/15-20	60°			

REFERENCES

Beckmann, P. and Spizzichino, A. (1963), The Scattering of Electromagnetic Waves from Rough Surfaces, Pergamon Press (Ch. 18, pp. 414).

Chu, Chiao-Min, Soon K. Cho and Joseph E. Ferris (December 1969), "Doppler Radiation Study - Final Report to Phase I" The University of Michigan Radiation Laboratory Report No. 1969-1-F, Vol. I, AD 864556L, 133pp. UNCLASSIFIED

Cost, S. (26 February 1965), "Bistatic Microwave Cross Section Measurements," Ohio State University Research Foundation Report on Contract AF33(615)1153, 23pp. UNCLASSIFIED.

Katzin, M. (1955), "Backscattering from the Sea Surface," IRE Convention Record, Vol. 3, Part 1, Antennas and Propagation.

MacDonald, F. (1965), "Correlation of Radar Sea Clutter on Vertical and Horizontal Polarization with Wave Height and Slope," IRE Convention Record, Vol. 4, Part 1, Telemetry, Antennas and Propagation.

Peake, W., R. Cosgriff and R. Taylor (May 1960), "Terrain Scattering Properties for Sensor System Design," Ohio State University Terrain Handbook II, Bulletin No. 181, Vol. XXIX, No. 3.

APPENDIX A

SCATTERING CROSS SECTION OF A FINITELY CONDUCTING SEA SURFACE

The essence of the bistatic cross section of a finitely conducting open developed sea was derived in the previous report (Chu, et al, 1969, Appendix A, Vol.I). Here, we will rearrange that expression both for computational ease and for consideration of special cases such as backscattering and specular reflections.

As reported in Appendix A of Chu et al (1969, Vol.I), the bistatic cross sections $\sigma_{\ell m}$ was found in the following form

$$\sigma_{\ell m} = \frac{\sqrt{A_o B_o}}{q_z^4}(a_{\ell m}q_z - b_{\ell m}q_x - c_{\ell m}q_y)^2 \exp\left[-A_o(\alpha\cos\psi+\beta\sin\psi)^2 - B_o(\beta\cos\psi-\alpha\sin\psi)^2\right],$$

$a_{\ell m}, b_{\ell m}$ and $c_{\ell m}$ being given by Eqs. (A.68) through (A.78) of that same report. After some manipulation, $(a_{\ell m}q_z - b_{\ell m}q_x - c_{\ell m}q_y)$ can be simplified to the forms shown below.

Define

$$L_1 \triangleq 2\sin\theta_1\sin\theta_2 + (1+\cos\theta_1\cos\theta_2)\cos(\phi_2-\phi_1) \tag{A.1a}$$

$$L_2 \triangleq (1+\cos\theta_1\cos\theta_2)\ 2\sin\theta_1\cos(\phi_2-\phi_1) - \sin\theta_2\sin^2(\phi_2-\phi_1) + 2\sin^2\theta_1\sin\theta_2 . \tag{A.1b}$$

$$L_3 \triangleq (1+\cos\theta_1\cos\theta_2)\sin\theta_2\sin^2(\phi_2-\phi_1) , \tag{A.1c}$$

$$M_1 \triangleq 2(\cos\theta_1+\cos\theta_2)\sin(\phi_2-\phi_1) \tag{A.2a}$$

$$M_2 \triangleq (\cos\theta_1+\cos\theta_2)\ 2\sin\theta_1+\sin\theta_2\cos(\phi_2-\phi_1)\ \sin(\phi_2-\phi_1) \tag{A.2b}$$

and

$$M_3 \triangleq (\cos\theta_1+\cos\theta_2)\sin\theta_2\sin(\phi_2-\phi_1)\cos(\phi_2-\phi_1) . \tag{A.2c}$$

Then

$$\begin{bmatrix} a_{hh}q_z - b_{hh}q_x - c_{hh}q_y \\ a_{vh}q_z - b_{vh}q_x - c_{vh}q_y \\ a_{hv}q_z - b_{hv}q_x - c_{hv}q_y \\ a_{vv}q_z - b_{vv}q_x - c_{vv}q_y \end{bmatrix} = \begin{bmatrix} -L_1 & L_2 & L_3 \\ M_1 & -M_2 & M_3 \\ M_1 & M_3 & -M_2 \\ L_1 & -L_3 & -L_2 \end{bmatrix} \begin{bmatrix} 1 \\ (1+R_\perp)/\sin\theta_1 \\ \\ (1-R_{\parallel})/\sin\theta_1 \end{bmatrix} . \qquad (A.3)$$

Now one can write down the cross sections for various polarizations. Thus,

a) for a horizontally polarized incidence,

$$\sigma_h \equiv \sigma_{hh} + \sigma_{vh}$$

$$= \frac{\sqrt{A_o B_o}}{q_z^4} \left[\left(-L_1 + \frac{(1+R_\perp)}{\sin\theta_1} L_2 + \frac{(1-R_{\parallel})}{\sin\theta_1} L_3\right)^2 + \left(M_1 - \frac{(1+R_\perp)}{\sin\theta_1} M_2 + \frac{(1-R_{\parallel})}{\sin\theta_1}\right)^2 \right]$$

$$\cdot \exp\left[-A_o(\alpha\cos\psi + \beta\sin\psi)^2 - B_o(\beta\cos\psi - \alpha\sin\psi)^2\right] , \qquad (A.4)$$

b) for a vertically polarized incidence,

$$\sigma_v \equiv \sigma_{hv} + \sigma_{vv}$$

$$= \frac{\sqrt{A_o B_o}}{q_z^4} \left[\left(M_1 + \frac{(1+R_\perp)}{\sin\theta_1} M_3 - \frac{(1-R_{\parallel})}{\sin\theta_1} M_2\right)^2 + \left(L_1 - \frac{(1+R_\perp)}{\sin\theta_1} L_3 + \frac{(1-R_{\parallel})}{\sin\theta_1} L_2\right)^2 \right]$$

$$\cdot \exp\left[-A_o(\alpha\cos\psi + \beta\sin\psi)^2 - B_o(\beta\cos\psi - \alpha\sin\psi)^2\right] . \qquad (A.5)$$

For a perfectly conducting surface, $R_\perp = -1$, $R_{\parallel} = 1$, so that (A.4) and (A.5) reduce to the identical expression:

$$(\sigma_h)_c = (\sigma_v)_c$$

$$= \sqrt{A_o B_o}\,(1+\alpha^2+\beta^2)^2 \exp\left[-A_o(\alpha\cos\psi + \beta\sin\psi)^2 - B_o(\beta\cos\psi - \alpha\sin\psi)^2\right] , \qquad (A.6)$$

the case used in the previous report (Chu, et al, 1969) for numerical computations for reflection radiation intensity. Also,

c) for depolarizations,

$$\frac{\sigma_{vh}}{\sigma_{hh}} = \frac{\left[M_1 - \frac{(1+R_\perp)}{\sin\theta_1} M_2 \mp \frac{(1-R_{||})}{\sin\theta_1} M_3\right]^2}{\left[-L_1 + \frac{(1+R_\perp)}{\sin\theta_1} L_2 + \frac{(1-R_{||})}{\sin\theta_1} L_3\right]^2} \tag{A.7}$$

$$\frac{\sigma_{hv}}{\sigma_{vv}} = \frac{\left[M_1 + \frac{(1+R_\perp)}{\sin\theta_1} M_3 - \frac{(1-R_{||})}{\sin\theta_1} M_2\right]^2}{\left[L_1 - \frac{(1+R_\perp)}{\sin\theta_1} L_3 + \frac{(1-R_{||})}{\sin\theta_1} L_2\right]^2} \tag{A.8}$$

and

$$(\sigma_{vh}/\sigma_{hh})_c = (\sigma_{hv}/\sigma_{vv})_c = \frac{M_1^2}{L_1^2} \ , \tag{A.9}$$

d) for backscattering, we let $\theta_1 = \theta_2 \equiv \theta$ and $\phi_1 = \phi_2 \equiv \phi$, or $\hat{\Omega}_2 = -\hat{\Omega}_1$. Then

$$\sigma_{hh}^{(b)} = \sqrt{A_o B_o}\, \sec^4\theta |R_\perp|^2 \exp\left\{-\tan^2\theta \left[A_o \cos^2(\phi-\psi) + B_o \sin^2(\phi-\psi)\right]\right\} \tag{A.10}$$

$$\sigma_{vv}^{(b)} = \sigma_{hh}^{(b)} \, |R_{||}|^2 / |R_\perp|^2 \tag{A.11}$$

and

$$\sigma_{vh}^{(b)} = \sigma_{hv}^{(b)} = 0 \ . \tag{A.12}$$

The Eq. (A. 12) indicates the absence of the depolarization in the backscattering direction.

e) for specular reflection, we set $\theta_1 = \theta_2 = \theta$ and $\phi_1 - \phi_2 = 180^o$ and, without jeopardizing the generality we let $\phi_1 = 180^o$ and $\phi_2 = 0^o$. Then, $\alpha = \beta = 0$, so that

$$\sigma_{hh}^{(s)} = \sqrt{A_o B_o}\, |R_\perp|^2 , \tag{A.13}$$

$$\sigma_{vv}^{(s)} = \sqrt{A_o B_o}\, |R_\parallel|^2 , \tag{A.14}$$

and

$$\sigma_{vh}^{(s)} = \sigma_{hv}^{(s)} = 0 , \tag{A.15}$$

indicating , again, the lack of the depolarization in the specular direction. It is also seen that the cross sections are maximum in the specular direction.

UNCLASSIFIED

Security Classification

DOCUMENT CONTROL DATA - R & D

(Security classification of title, body of abstract and indexing annotation must be entered when the overall report is classified)

1. ORIGINATING ACTIVITY (Corporate author) The University of Michigan Radiation Laboratory, Dept. of Electrical Engineering, 201 Catherine Street, Ann Arbor, Michigan 48108	2a. REPORT SECURITY CLASSIFICATION UNCLASSIFIED 2b. GROUP N/A

3. REPORT TITLE

Doppler Radiation Study

4. DESCRIPTIVE NOTES (Type of report and inclusive dates)

Interim Report 22 December 1969 - 22 March 1970 , Technical

5. AUTHOR(S) (First name, middle initial, last name)

Chiao-Min Chu, Soon K Cho and Joseph E. Ferris

6. REPORT DATE	7a. TOTAL NO. OF PAGES	7b. NO. OF REFS
May 1970	80	6

8a. CONTRACT OR GRANT NO.	9a. ORIGINATOR'S REPORT NUMBER(S)
N62269-68-C-0715 (Mod. No. 1) b. PROJECT NO. c. d.	1969-4-Q 9b. OTHER REPORT NO(S) (Any other numbers that may be assigned this report)

10. DISTRIBUTION STATEMENT

Each transmittal of this document outside the agencies of the U.S. Government must have prior approval of CO, NADC, Warminster, Penna., 18974 or CO, NASC, Wash. DC 20360

11. SUPPLEMENTARY NOTES	12. SPONSORING MILITARY ACTIVITY
	Naval Air Development Center Warminster, Penna., 18974

13. ABSTRACT

In order to extend our understanding of the reflection characteristics of the moderately rough ocean surface, the scattering cross section was computed and analyzed for various sea states with plane wave incidence. The use of the results of the cross section analysis makes it feasible, in principle, to predict qualitatively the order of the maximum reflected radiation intensity and its angular distribution for various receiving points for a given transmitting antenna pattern. The result of the cross section analysis also indicated that the assumption of the infinite conductivity for the sea water introduces errors no greater than about 2 dB for purely horizontally and vertically polarized incidences, indicating the relative fairness of the usual assumption of infinite conductivity for the sea water at 13 GHz.

DD FORM 1 NOV 68 1473

UNCLASSIFIED

Security Classification

14. KEY WORDS	LINK A		LINK B		LINK C	
	ROLE	WT	ROLE	WT	ROLE	WT
Doppler Radar						
Detectibility						
Radiation Characteristics						
Sea Return						
Terrain Return						